Numerical Modeling of a Ducted Rocket Combustor With Experimental Validation

Patrick W. Hewitt

Dissertation submitted to the faculty of the Virginia Polytechnic Institute and State University in partial fulfillment of the requirements for the degree of

Doctor of Philosophy

In

Aerospace Engineering

J. A. Schetz, Chair

W. F. O'Brien

B. Grossman

J. Marchman

J. Sparks

September 04, 2008

Blacksburg, Virginia

Keywords: Ducted Rocket, Ramjet, Combustion, Boron, Soot, Gas Generator

Numerical Modeling of a Ducted Rocket Combustor With Experimental Validation

Patrick W. Hewitt

(ABSTRACT)

The present work was conducted with the intent of developing a high-fidelity numerical model of a unique combustion flow problem combining multi-phase fuel injection with substantial momentum and temperature into a highly complex turbulent flow. This important problem is very different from typical and more widely known liquid fuel combustion problems and is found in practice in pulverized coal combustors and ducted rocket ramjets. As the ducted rocket engine cycle is only now finding widespread use, it has received little research attention and was selected as a representative problem for this research. Prior to this work, a method was lacking domestically and internationally to effectively model the ducted rocket engine cycle with confidence.

In the ducted rocket a solid fuel gas generator is used to deliver a fuel-rich multi-phase mixture to the combustion chamber. When a valve is used to vary the fuel generator pressure, and thereby the delivered fuel flowrate, the engine is known as a Variable Flow Ducted Rocket (VFDR). The Aerojet MARC-R282 ramjet engine represents the worlds first VFDR flown, and the first in operational use. Although performance requirements were met, improvements are sought in the understanding of the ramjet combustion process with a future aim of reducing the visible exhaust and correcting uneven combustor heating patterns. For this reason the MARC-R282 combustor was selected as the baseline geometry for the present research, serving to provide a documented baseline case for numerical modeling and also being a good candidate to benefit from an improved understanding of the combustion process.

In order to proceed with the present research, experiments were first carried out to characterize the gas generator particulate exhaust in terms of composition and particle

size. Equilibrium thermochemistry was used to supplement these data to develop a gas phase combustion model. The gas phase reactions and resulting particle definition were modeling using the FLUENT Computational Fluid Dynamics (CFD) code for the baseline GQM-163A Supersonic Sea Skimming Missile (SSST) operating conditions. These results were compared to direct-connect ramjet ground tests in order to validate the analysis tool.

Data were developed to understand the gas and solid phase fuel exhaust characteristics at the propellant surface, exiting the gas generator injector, and following secondary combustion with air. Particles were collected and analyzed from the fuel generator exhaust. While exhibiting some variation with time in the firing, they were roughly an average of 20 microns in diameter, in line with prior experience with pulverized coal combustion experiments. A computational model was developed based on coal combustion parameters using FLUENT. However, despite considerable effort, the CFD analysis was not able to predict effective burning of the carbon particles to the degree seen in testing. In addition, using equilibrium thermochemistry as a basis for determining the carbon particle content in the fuel exhaust, the CFD analysis resulted in trends in performance opposite to the test results. These facts led to a hypothesis that there was actually a significant fraction of small particles or much less carbon produced than equilibrium thermochemistry would predict. A parametric analysis was performed replacing the 20 micron soot particles with fine fraction particles, representing a fraction of the predicted equilibrium carbon soot being still in the gas phase as higher molecular weight hydrocarbons, or in the form of sub-micron particles. When almost all particles were replaced with fine fraction particles, the model was able to correctly predict absolute values of combustion efficiency as well as trends for different injector geometries. The presence of particles was apparent from the visible exhaust and collection data, however they were found not to play a significant role in the combustion process for this fuel and engine configuration.

The robustness of the computational model was also evaluated by examining the effects of turbulence model, order of discretization, and grid size. Comparable trends and results were seen for all cases examined.

With the successful development of this modeling tool and an improved understanding of the combustion process, future work is enabled to develop improved combustor flow management and fuel injection schemes to improve existing designs and develop new configurations. This research has served to advance the field of combustion modeling by providing: 1) a solid ducted rocket combustion modeling tool considering solid and gas phase combustion, 2) a correlation between primary combustion theory and particulate exhaust sampling, 3) low length/diameter ratio ducted rocket combustor modeling, and 4) combustor CFD coupled with solid particle tracking and combustion models.

Acknowledgements

As a lesson to those who believe that they have finally left the classroom behind, one should avoid casual dining in Munich with the person of Dr. Joseph A. Schetz. With a self-admitted cunning, I was lured into the current episode by this respected professor after a 25 year hiatus. Having served as my mentor in round one, I was equally treated for the second course with sound advice and encouragement, for which I will be eternally grateful.

I also owe thanks to the Aerojet-General Corporation for allowing me to pursue this goal while maintaining an active position with the company, although in a somewhat diminished capacity. Specifically, Rick Yezzi and Adam Siebenhaar deserve credit for enabling me to mix business and academic goals during this period, hopefully for the good of all.

I would like to also thank my committee for helping with this endeavor by providing guidance and useful inputs, and for tolerating the logistics associated with linking the University and Industry for study and research.

Invaluable advice and support with FLUENT modeling was provided by Aerojet's Thong Nguyen and Ted Smith, who were responsible for implementing the requested cases, and who responded faithfully to unreasonable schedule and technical demands.

And finally, none of this would have been possible without the understanding and support from my wife Diana, who has been with me through all phases of my career, and from Michelle, my daughter and fellow scholar.

Table of Contents

List of Figures

UNLESS OTHERWISE NOTED, ALL IMAGES ARE PROPERTY OF THE AUTHOR.

List of Tables

Nomenclature

Hv = Volumetric heating value

Hg = Gravimetric heating value

A/F = Air to fuel mass ratio

K = Reaction rate

q = Rate of removal of carbon per unit external surface

p_g = Partial pressure of gas

x = Particle diameter

c^* = Characteristic exhaust velocity

$ = Solid phase compound

* = Liquid phase compound

γ = Ratio of specific heats

V = Velocity

X = Mole fraction

Bi = Biot number

h = Convective heat transfer coefficient

k = Thermal conductivity

r = Radius

A = Area

T = Temperature

ρ = Density

C_p = Specific heat at constant pressure

Nu = Nusselt number

M = Mach number

D,d = Diameter

Re = Reynolds number

u = Flow speed

g_c = Gravitational constant

R = Gas constant

P = Pressure

$\dot{m}$ = Mass flowrate

W = Weight flowrate

X = X function

Y = Y function

Z = Z function

$\overline{F}$ = Specific stream thrust

η = Efficiency

F = Thrust

θ = Nozzle half angle

φ = Equivalence ratio

S_A^* = Air specific stream thrust

Subscripts

diff = Diffusion

g = Gas

s = Surface

vap = Vaporization

eff = Effective

PS = Polystyrene

∞ = Infinity

0 = Total, initial

d = Diameter

T = Total

CBE = Choke Block Entrance

*CB** = Choke Block Throat

1.5 = Diffuser

2 = Dump plane

3 = Fwd Combustor

4	= Aft Combustor
5	= Ramjet Nozzle Throat
6	= Ramjet Nozzle Exit
D	= Discharge
ΔT	= Temperature rise
$corr$	= Corrected
$meas$	= Measured
a	= Ambient
x	= Axial
atm	= Atmospheric
n	= Nozzle
a	= Air
f	= Fuel

CHAPTER 1 - INTRODUCTION

1.1 Baseline Ducted Rocket Combustor Flowfield

The ducted rocket is a ramjet engine cycle in which the fuel is delivered by combustion of a primary fuel propellant grain. The propellant contains mainly fuel ingredients, with only enough oxidizer as required to initiate combustion and expel fuel-rich products into the ramjet combustion chamber. The result of this marginal primary combustion is a large amount of particulate carbon and mildly warm gas phase combustion products, which must be efficiently burned in the ramburner.

Practical examples of the ducted rocket can be found in missile propulsion around the world, with the earliest implementation being the Soviet SA-6 in the late 1950's. Recent focus has been on a type of ducted rocket in which a variable-area fuel exhaust valve is used to vary the fuel output. This engine cycle has become known as the Variable Flow Ducted Rocket, or VFDR. The world's first flying example of this engine is the Supersonic Sea Skimming Target (SSST), with the ramjet supplied by Aerojet. The SSST propellant consists of a binder (hydroxyl-terminated polybutadiene) and oxidizer (ammonium perchlorate), with fuel additives including polystyrene, boron, and magnesium.

The SSST missile is intended to simulate threat anti-ship cruise missiles by operating at Mach 2.5 at near sea level for over 50 miles, while executing significant all-aspect maneuvers. The missile configuration is shown in Figure 1.1-1. The GQM-163A uses a first stage booster that provides sufficient impulse to achieve ramjet takeover speed, at which point it separates and ramjet operation commences. The significance of this staged operation is that there is no internal booster housed in the combustion chamber, as would be the case for an integral rocket ramjet weapon engine. This makes the addition of mixing and flame-holding devices in the combustor interior possible.

The ramjet engine was designated the MARC R282, and is shown schematically in Figure 1.1-2.

The MARC-R282 engine development activity took place from 2000 to 2003, with an emphasis on rapid development and low technical risk. As a result there was little

time available for combustor design optimization. Initial CFD work was performed to help determine the fuel injector geometry. The combustor inlet head end configuration was based on water flow visualization studies performed on a similar 4-inlet combustor by Virginia Research Associates[39]. Direct-connect testing demonstrated adequate delivered combustion efficiencies and adequate thermal margins during full duration mission simulations.

Although the delivered performance was consistent with the propulsion system specification, a large amount of unburned carbon was produced, resulting in a very visible exhaust trail (evidenced in Figure 1.1-1). This observation reinforces the need to develop a better understanding of the combustion process with an eventual aim of identifying hardware changes to be implemented.

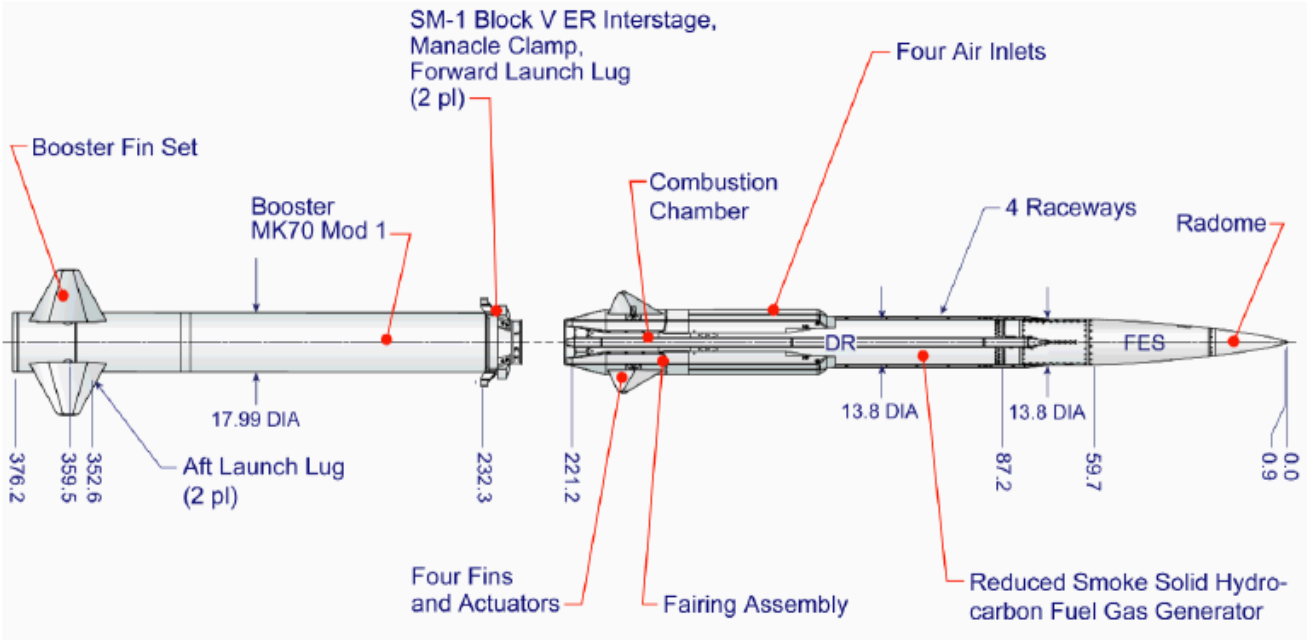

Image property of Orbital Sciences Corporation

Boost Phase

Image property of US Navy

Sustain Phase

Image property of US Navy

Figure 1.1-1 SSST Missile Configuration

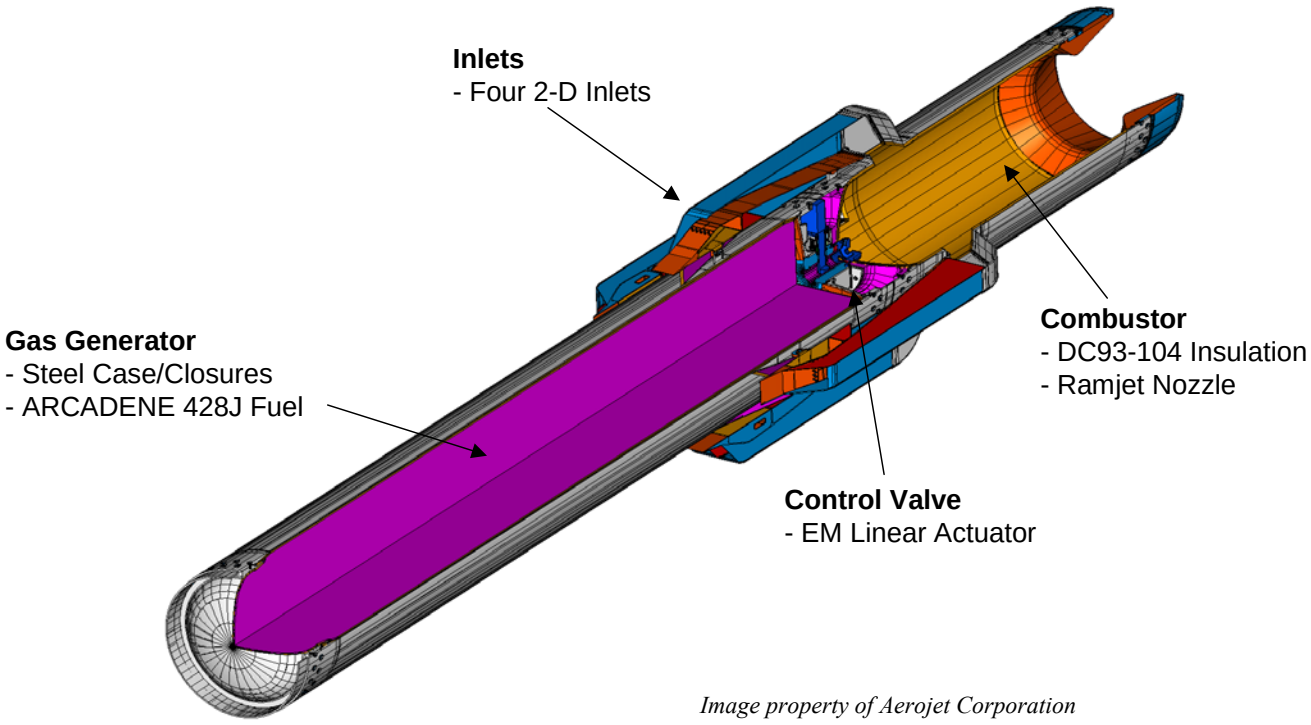

Figure 1.1-2 MARC-R282 Ramjet Engine

A second issue to be addressed in the SSST combustor is a region adjacent to the inlet dump station in which there is evidence of localized heating. This presents a risk of late flight case burn-throughs and heating of wiring harnesses that run through this region. Figure 1.1-3 shows the external combustor discoloration following a full-duration direct-connect test. Again, a suitable design tool is required to manage the

internal flow to reduce localized heating, yet maintain acceptable levels of engine performance.

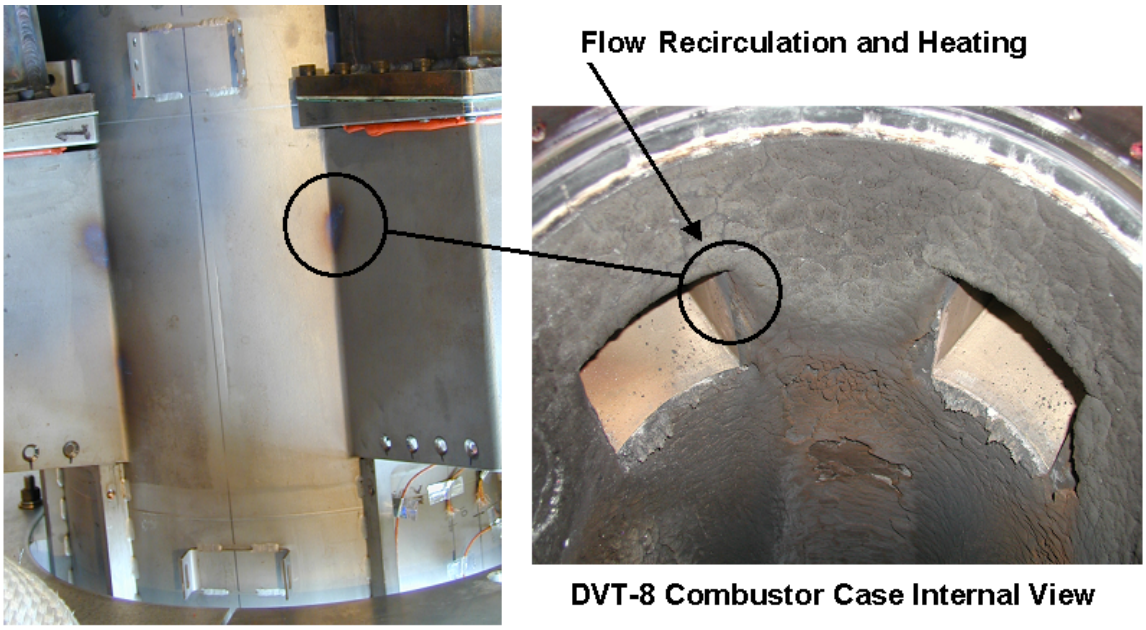

Image property of Aerojet Corporation

Figure 1.1-3 MARC-R282 Engine Heating

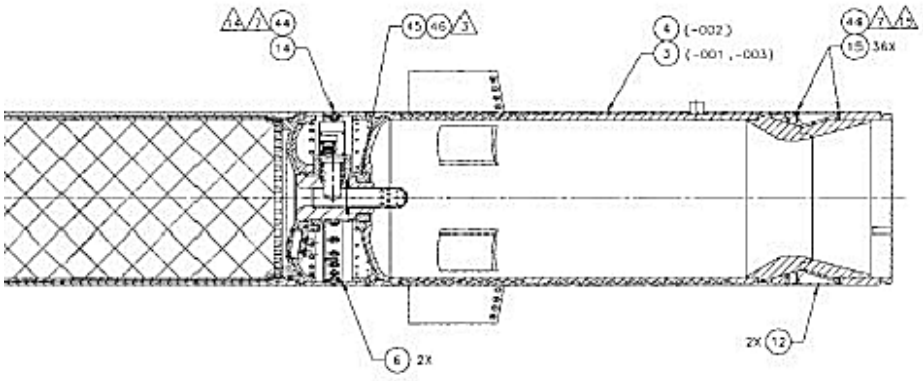

Image property of Aerojet Corporation

Figure 1.1-4 SSST Combustor Layout

The MARC-R282 combustor layout is shown in Figure 1.1-4. The length to diameter ratio, L/D, is only 2.5, which presents a challenge to reach a fully mixed state prior to the exit nozzle. The exit nozzle geometry and inlet dump location, angle, and area must remain fixed in order to avoid modifying qualified hardware. In attempting to improve the combustor performance the addition of flameholders, vanes, or other flow management devices is permissible. The injector diameter is fixed but the exit area and hole pattern may be modified. The injector length can be increased; however, structural considerations may prevent changes.

Preliminary CFD studies and post-test insulator mapping have provided a general indication of the internal combustor flowfield. Recirculation regions are established in the combustor head end, where higher fuel/air ratios are achieved and a favorable combustion environment is formed, as illustrated schematically in Figure 1.1-5. Outside of these regions the flow is much cooler and any carbon or boron not combusted in the primary recirculation zone is likely quenched and expelled as soot, contributing to the exhaust signature

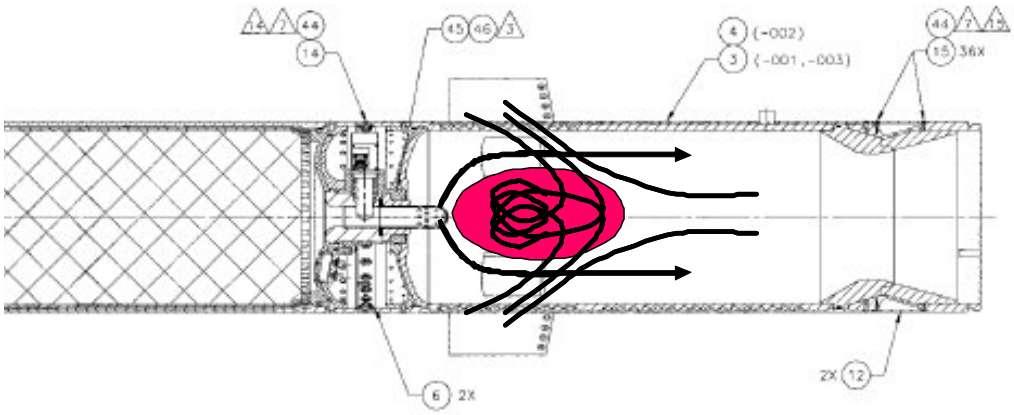

Figure 1.1-5 Combustor Flow Features

1.2 Research Objectives

The objective of this project is to develop an improved understanding of the combustion process in the ducted rocket combustor, and to develop a suitable engineering tool to guide future efforts. The ducted rocket engine cycle introduces multiple challenges to the engine designer, including particulate combustion in addition to a gas phase diffusion- and kinetically-controlled combusting flowfield. The experimental and analytical approach for the research includes:

- Modeling the primary equilibrium thermochemistry in the fuel gas generator and the associated fuel products injected into the combustor
- Experimentation to better quantify the composition and particle size of the particulates composing the solid fraction of the fuel exhaust
- The development of a CFD model of the current MARC-R282 internal fuel and air flowfield
- Model validation using ramjet direct-connect ground test data

1.3 Literature Review

A review of prior combustion research was performed to help devise a strategy for the current problem. The applicable prior work consisted primarily of carbon soot and boron particle combustion, and ducted rocket analytical modeling. An overview is provided here with detailed discussion to follow.

A large base of applicable combustion research was performed by G.M. Faeth[21,15,18] and associates. The majority concerned premixed laminar flames, with much focus on carbon soot formation, and to a lesser on oxidation of the resulting particles. Very little prior research exists on soot combustion in turbulent diffusion flames, as in all likelihood these problems are highly specific to individual geometries.

The diesel engine research area has also explored soot combustion; however, the bulk of work is primarily concentrated on soot formation and catalyst effects. The work is associated with very specific engine geometries and dynamics (timing).

The majority of rocket plume analysis and characterization has been aimed at Al_2O_3 formation, with a secondary focus on soot formation.

Applicable turbine engine research has been identified dealing with carbon slurry combustion models. The work describes two combustion stages: fuel vaporization and combustion followed by carbon particle heating and oxidation (which is of direct interest here).

Prior research on coal furnace combustion has yielded the most generally applicable results to the current problem and is discussed in detail in subsequent sections. In addition to combustion modeling, the broader subject of ramjet computational modeling is reviewed first, as this is the ultimate aim of the present research. Boron particle combustion is then considered.

1.3.1 Ramjet Combustor Modeling

Numerical modeling of ramjet combustion chambers can be a formidable task. High velocity flows are typically encountered, with complex flame-holding zones and high turbulence and strong flow gradients. In addition, fuel injection and chemical reactions must be treated. The ducted rocket adds additional degrees of complexity in which the fuel stream itself is a high temperature reacting multi-phase flow. For these reasons researchers would be well advised to seek mathematically straightforward models for each aspect of the problem. The benefit of an accurate numerical combustor tool is brought to focus by Ogerby[27], in which he states that "465 combustor modifications and 140 full-scale engine tests were carried out on the Pratt and Whitney JT8D fan engine to produce a smokeless combustor." This is a luxury unavailable to a tactical missile engine contractor.

Although the paper must be calibrated by significant recent advances in computational abilities, Edelman et al[7] discuss ramjet modeling techniques, and the conclusion is reached that it is difficult to impossible to provide sufficient resolution to adequately describe processes such as fuel injection that occurs on a much finer scale than overall the combustion chamber. They propose a modular model to break up the combustor into manageable regions. Similar views are expressed by Lilley[8], and doubt is cast that 3-D full simulations will prove practical to the designer. Special procedures

were devised for multi-path flows by Rodriguez[23] to model complete combustor configurations, which may be beyond the reach of even sophisticated CFD tools.

Harsha and Edelman[10] present a thorough treatment of combustor modeling, and put forth a modeling "hierarchy" from simple to detailed. Chemical reaction modeling types are also categorized from global to detailed. Again, a calibration must be made for present day capabilities and advances in CFD software packages.

Specific work undertaken in ducted rocket modeling is described by Stowe et al[13]. A one-stream approach was developed in which all of the fuel components were injected together and assumed to react instantaneously in the presence of the oxidizer. This method over-predicted combustion efficiency as one would expect. A more complicated two-stream model was also used in which the fuel was separated into gas components and 75 nanometer carbon particles, which exhibited better agreement with test data. Soot from the hydrocarbon fuel combustor was collected and measured from sub-micron to over 200 microns. The majority of the particles were near the 75 nm value. The average difference between test data and predicted temperature-rise combustion efficiency was 27% for the one-stream method, and 16% for the two-stream method.

Numerical predictions of ducted rocket performance were made by Lewis[17] using FLUENT gas phase and particle combustion algorithms. The model was exercised to evaluate trends in equivalence ratio, injector design, port covers, and inlet air conditions. Lacking experimental data, a 3 micron soot particle size was assumed for the studies, and the coal particle combustion models contained in FLUENT were utilized. Based on the present research it was found that larger particle sizes must be treated, and the reaction rates must be tailored to match the ducted rocket combustion environment.

Although the work was conducted for an Air-Turbo-Rocket, Thomas and Leonard[23] present work in which soot combustion is considered in a numerical model. The soot was modeled as solid carbon spheres of uniform diameter that react with the gas stream, converting carbon to CO and other products. Minimizing particle size to less than 100 microns results in increased combustion efficiency and reduced residence time requirements. The behavior of 50 micron and 100 micron particles was nearly identical.

A numerical simulation was performed by Ristori and Defour[25] for a hydrocarbon ducted rocket using a methodology based on a multi-species Reynolds Averaged Navier-

Stokes (RANS) approach associated with a turbulent combustion model. No particles were considered. Various combustion models are evaluated, with strengths and weaknesses of each identified. They were able to predict a global combustion efficiency with a precision better than 7 % and a global pressure recovery with a precision better than 5 %.

1.3.2 Boron Particle Combustion

As the ducted rocket engine cycle utilizes solid propellant combustion products as a fuel, it is relatively straightforward to add metals to the propellant composition. This is in direct contrast to liquid fuels, in which a slurry or gel must be prepared, along with the associated issues concerning settling, pumping, and atomization. Of the metals studied for application to the ducted rocket, boron is generally seen to be the most attractive fuel ingredient. Both the gravimetric and volumetric heating values of selected fuels are shown in Table 1.3.2-1. For volume limited applications like tactical missiles, the volumetric heating value proves the most attractive attribute, and illustrates why boron is the preferred choice.

Table 1.3.2-1 Metallic Ducted Rocket Fuel Additives

Fuel	Density (kg/m3)	Gravimetric Heating Value - Hg (MJ/Kg)	Volumetric Heating Value - Hv (MJ/m3)	Stoichiometric A/F
Aluminum	2.70	31.07	83.88	3.84
Beryllium	1.85	66.49	122.97	7.67
Boron	2.22	59.28	131.60	9.59
Lithium	0.53	42.96	22.77	4.98
Magnesium	1.74	24.74	43.05	2.84
Titanium	4.50	19.74	88.85	2.88

As a result of the benefits offered by boron, a great deal of research on single particle boron combustion has been performed. This has lead to a reasonable understanding of the conditions required to efficiently burn them in a ramjet combustor. Although the understanding exists, it is difficult in practice to achieve efficient combustion. One of the most effective methods is to employ combustion aids such as a propellant additive or

boron particle coatings. The aim of the present research, however, is not to promote efficient combustion through propellant tailoring, but rather through an improved understanding of the combustor flowfield and boron particle history. The following historical research is presented in order to summarize the body of knowledge on boron combustion.

The boron used in the validation motor firings uses a small percentage of amorphous boron with a maximum average particle size of 1 micron, and a boron purity of 95%, with the major impurity being oxygen. The accepted practice has been to model the particles for combustion studies as 95% B and 5% B2O3 using the as-received particle size. Mellor[12] studied the particulate exhaust properties of sample boron propellants and found that the particle sizes were relatively unchanged, however an allowance must be made for the formation of ammonium pentaborate ($NH_4B_5O_8*4H_2O$) on the particle surface by reaction with ammonium perchlorate or its decomposition products. The recommendation is made to characterize the particulate exhaust in cases where motor data are compared to theory.

A landmark paper was contributed by Komar and King[28] for single particle boron combustion. Laser based diagnostics were used for the determination of particle-size, velocity, temperature, and times-to-ignition for complete combustion of single boron particles. The particle combustion process is described in general terms as initially the heating and vaporization of an oxide layer which inhibits combustion and must be removed before "full-fledged" combustion can begin; considerable time may be consumed during this "ignition" stage. In addition, boron has a very high boiling point, necessitating relatively slow surface burning even after the oxide has been removed. Also pointed out is that the use of a particle burning law based on diffusion-limited combustion must become erroneous for sufficiently small particle diameters. Since the diffusional transport rates are predicted to approach infinity as particle size approaches zero, the kinetic process rates do not increase with decreasing particle size. Thus, at some finite diameter, the rate-limited particle burning processes must become kinetic rather than diffusional, with a resultant shift from the burning mass flux being inversely proportional to being independent of particle radius. This was found to be in the 30-40 micron particle size range. Thus, the one micron boron utilized in the verification case

places it well in the range of kinetic rate control. Although a detailed combustion model is alluded to, only limited data are presented for the diameters of interest here. Data are provided for one micron particle combustion times of less than one millisecond for a gas temperature of 4050°R and an oxygen mole fraction of 0.19, closely resembling stoichiometric conditions for the present research case.

Ignition delay was studied for small particles at 8.5 atm and 4050°R by Rood[30] for pure oxygen. At 1 micron particle sizes the ignition delays approach 10 microseconds. Odawara et al[31] present data showing ignition delay times account for roughly 80% of the combustion time, and that delay times drop dramatically above 2160 °R. Heating of the particles in the primary gas generator of a ducted rocket was shown to also reduce ignition delay times.

Schadow[33] also was able to show the effect of primary gas temperature on the combustion efficiency of boron. A non-equilibrium chamber temperature T* was calculated by treating the boron as a heat sink only, and not contributing to the reaction. A gradual increase in secondary combustion efficiency was seen over a T* range of 1260-3600°R, with no apparent jump near the 2160°R mark discussed in Reference 31. Additional research by Schadow[38] showed that efficient boron combustion is dependent on ignition and combustion of the gas phase, regardless of combustor operating pressure. This is a significant finding with regard to high altitude engine operation where combustor pressures below one atmosphere can be encountered. Mitani[37] conducted strand bomb experiments where it was shown that burning of boron is relatively easy in the primary chambers of ducted rockets if fine B powders are used. However, this result would be anticipated based on other research presented herein, as the equilibrium temperatures for most propellants tested exceeded 3780°R.

Abbott, et al[20] investigated boron combustion in a combustor. It was stated that a gas temperature of 3510°R is required for rapid boron combustion. Based on experiments, the statement is made that "When ignition of the gases occurs in farther aft regions of the duct, the mixture is too diluted in air to reach 3510°R. This result implies that rapid, early mixing can be disadvantageous to promotion of high combustion efficiency". This fact must be considered as the SSST combustor is examined. Vigot[29] demonstrated a technique using impinging injector jets to "scrub" the oxide layer in preparation for

injection into the combustion chamber, as well as dispersing agglomerates. A compromise was necessary in practice between injector efficiency and durability in withstanding the boron particle stream. Up to 50% improvement in combustion efficiency was shown, but this was limited to the range of 25% for practical injectors for missile applications.

A somewhat skeptical review of boron combustion is presented by Gany[32]. He also gives an ignition temperature of 3420°R-3600°R to begin removal of the oxide layer and initiation of boron surface reactions. Also presented is a novel theory in which the gaseous B_2O_3 partial pressure may reach a point in which further vaporization of the oxide layer is inhibited, termed "Thermodynamic Blocking". This effect was stated to prevent combustion of boron propellants at certain flight conditions. However, it is felt that through proper flow management encouraging near stoichiometric conditions in recirculation zones and the appropriate use of combustion aids this effect may not be a significant effect in practice. Natan and Gany[36] also show through modeling that at 3420°R the oxide removal rate increases and ignition times drop.

The preceding discussion illustrates that efficient burning of boron is rather difficult to accomplish in a ramjet engine. The ducted rocket has the advantage that the boron can be heated in the primary gas generator, thus beginning the process of oxide removal even before injection into the combustion chamber. Perhaps the most usefully elegant statement is made by Schadow[34]: "The present results indicate that, so long as the gaseous fuel component from the primary combustor can be made to react with the air in the secondary chamber before excessive mixing occurs, the resulting temperatures will be high enough to initiate high boron reaction rate."

King's recommendations for future boron combustion modeling remain largely unaddressed to date. These consist of:

- Development of a kinetics-limited model for the "full-fledged" combustion stage of boron burning. For such modeling to be successful, experimental identification of reaction paths and determination of kinetic data for limiting reaction steps are required.
- Definition of the nature of boron particles entering combustors should be addressed, (single unit particles, loosely bound porous conglomerates, tightly bound low porosity

conglomerates) and ignition/combustion models should be modified as needed to treat conglomerates as well as single particles.

1.3.3 Carbon Particle Combustion

A great deal of prior work has been undertaken to understand the formation of carbon soot in combustors, the heating, oxidation mechanisms, and reaction rates. Much of this work has been directed at gas turbine combustors, which has provided a solid basis for the chemical processes; however, the particle sizes are in the nanometer range, far smaller than those encountered in the present research. Another general area of fundamental research has been coal particle combustion. This research has proven to be most applicable to the current ducted rocket combustion problem, as the emphasis is primarily on decomposition verses formation, and the particle sizes are much more in line with those seen in the ducted rocket. The following discussion provides an overview of important carbon particle research, and summarizes the pertinent data employed in the current research.

1.3.3.1 Diffusion Flame Soot Combustion

Several sources exist in which soot formation and reaction rates are presented (Kim et. al.[14], Rodionov, et. al.[19], and Blevins[26]). An excellent review of the subject with comments on current understanding is provided by Urban and Faeth[21]. However, their usefulness for this research is limited to a broader view of the particle combustion mechanism rather than insight into applicable reaction rates.

1.3.3.2 Carbon Particle Combustion

Turns and Faeth[18] present results of combustion research aimed at carbon black slurries for use in airbreathing engines. The carbon black particle diameters range from 10 to 100 μm, and are thus of interest for the ducted rocket. The observation is made that particle burning rates are quite low until the particle temperature reaches 2700-3060 °R. This is slightly higher than the stated values for onset of combustion for coal particles but still in reasonable agreement.

Dempsey, et al[41] present data for carbon black particle agglomerates in the 45-66 μm size range, and states ignition times on the order of 1.2 to 1.6 milliseconds, and combustion times of nominally 0.9 milliseconds in a methane flat flame burner.

1.3.3.3 Coal Combustion Research

Baum and Street[1] investigated the burning of pulverized coal particles in the range of 60 μm in diameter. They relied on a large base of research that observed the process of coal particle combustion in which hollow spheres are formed upon rapid heating and the combustion process takes place at nearly constant diameter as oxidizing gases permeate the sphere and burning takes place internal to the shell. Fragmentation takes place as the shell is eroded away at the completion of the reaction. A mathematical model was developed based on observations in a laboratory furnace burning size-graded coal. A "swelling coefficient" is used to account for the increase seen in diameter as volatiles begin reacting and a hollow sphere is formed with large holes in its surface. In this state the remaining carbon burns at a rate determined by the diffusion of oxygen to the surface of the char (physical control), and the reaction of carbon and oxygen to CO and CO_2 (chemical control). Typical swelling coefficients were stated to be from 1.0 to 4.0. Cangialosi et al[16] reports maximum oxidation rates for coal fly ash to be at approximately 1620 °R through thermo-gravimetric analysis.

Peters and Weber[6] constructed a mathematical model for nominally 45 μm coal and compared predictions to actual data from a coal furnace. In the model they found that good accuracies were seen when a standard k-epsilon model for turbulence was employed. Magnussen and Hjertager[4] also were able to demonstrate good agreement between their combustion model and experiment by using the k-epsilon turbulence model. Soot combustion rates for a C_2H_2 diffusion flame were stated to be approximately 200 g/(m^3s) at stoichiometric conditions, where the rate was maximized. For a spherical particle of 20 μm with an assumed O_2 partial pressure of 0.2 in air, this value can be expressed in terms of surface area as .667 g/cm^2s atm for comparison with the much lower reaction rates shown below. This effect is likely due to the much smaller soot particle sizes for the acetylene flame.

Reaction rates for size-graded coal are reported by Field[5] for gas temperatures between 2160 °R and 3600 °R, and particle size diameters from 20 μm to 100 μm. Oxygen concentrations were tested at 0,5, and 10 percent. For large particle sizes the overall reaction rate was determined by diffusion of CO from the particle surface. For particles smaller than 80 μm it was found that the surface reaction rate coefficient was smaller, and independent of oxygen concentration and particle size. Photographs of the raw coal particles are shown, exhibiting irregular angular surfaces closely similar to the ducted rocket particulate samples obtained in the present research.

The overall reaction rate K (g/cm^{2}s atm) is defined as the rate of removal of carbon per unit external surface q (g/cm^{2}s) per unit atmosphere partial pressure of oxygen in the gas p_g (atm), and

$$K = q / p_g$$

The maximum limiting value for diffusion, K_{diff} assuming CO transport is

$$K_{Diff} = 0.00128\left(\frac{T_g}{1600}\right)^{0.75} / x \ \text{(g/cm}^2\text{s atm)}$$

where T_g is the gas temperature (°K), and x is the particle diameter (cm).

A surface reaction rate K_s is calculated from the relation

$$K_s = \frac{K * K_{Diff}}{K_{Diff} - K} \ \text{(g/cm}^2\text{s atm)}$$

Values of K_s were found to be independent of oxygen concentration in the range from 0 to 10%, and depends only on the particle surface temperature. No effect of size was detected in the range of 28 μm to 105μm. The relationship given for coal particles within the surface temperature range of 1400 °K to 2000 °K is

$$K_S = -0.49 + 3.85 \times 10^{-4} T_S$$

A method is presented to numerically calculate particle surface temperature by performing a heat balance assuming combustion of CO.

The data presented by Field are tabulated in Table 1.3.3-1 for 28 μm and 38 μm particles. These data were used to construct a simplified relationship neglecting the effects of oxygen concentration and particle size to approximate the reaction rates as shown in Figure 1.3.3-1. A simplified relationship based on a linear curve fit of the data presented is

$K = .0003 * T_g - 0.3993$ where T_g is the gas temperature (°K), and K has units g/cm^{2}s atm

The data clearly illustrate a critical gas temperature to be 1200°K (2160°R), below which reaction rates approach zero.

Table 1.3.3-1 Coal Particle Reaction Rates (Field Data)

28 Micron Sample 1			**28 Micron Sample 2**			**38 Micron Sample**		
Gas temp °K	K (5% O2)	K (10% O2)	gas temp	K (5% O2)	K (10% O2)	gas temp	K (5% O2)	K (10% O2)
1420	0.037	0.074	1320	0.019	0.053	1220	0.000	0.017
1520	0.087	0.144	1420	0.042	0.098	1320	0.026	0.025
1620	0.097	0.165	1520	0.106	0.126	1420	0.053	0.068
1720	0.140	0.167	1620	0.145	0.150	1520	0.103	0.120
						1620	0.139	0.145
						1720	0.158	0.165

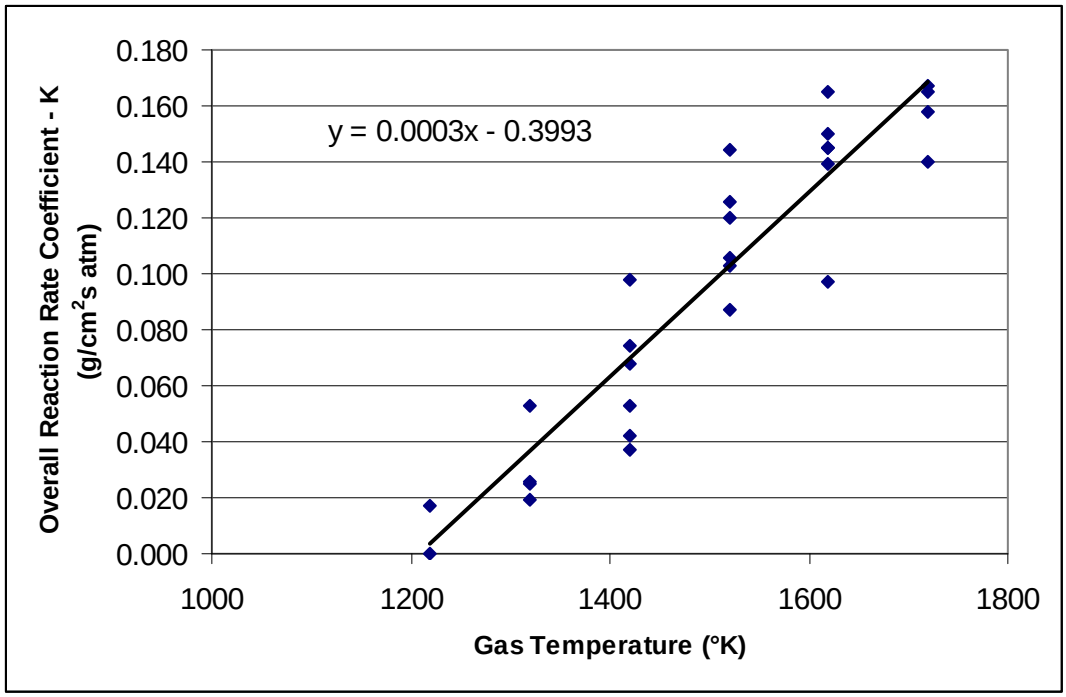

Figure 1.3.3-1 Coal Particle Reaction Rate Curve Fit

The preceding research forms the basis of the pulverized coal combustion modeling implemented in the FLUENT code[42]. FLUENT provides a choice of four heterogeneous surface reaction rate models for combusting particles:

- the diffusion-limited rate model (the default model)
- the kinetics/diffusion-limited rate model
- the intrinsic model (first-order kinetics/diffusion-limited rate model more effectively modeling pore diffusion)
- the multiple surface reactions model

Both the diffusion-limited rate model and the kinetics/diffusion-limited rate model were used in the present analysis.

CHAPTER 2 – Fuel Exhaust Characterization

2.1 Thermochemistry

2.1.1 Gas generator Exhaust Composition

2.1.1.1 Equilibrium Calculations

Table 2.1.1-1 provides the theoretical equilibrium thermochemical calculations using the ARCISP equilibrium thermochemistry program for the gas generator exhaust – prior to mixing with air in the combustion chamber. In practice, fuel rich propellants typically rarely reach the theoretical characteristic exhaust velocity, c*, or total temperature so these values must be used only as a guide. Further, the non-equilibrium combustion is time-dependent as the grain burns back and the free volume and fuel residence time increase.

Of primary interest in the predicted products is the value of particulate carbon produced, on the order of 40% by mass. Since combustion efficiencies up to 95% are achieved in operation, it is apparent that the majority of the carbon is being combusted. Any remaining carbon is believed to be responsible for the sooty exhaust. The other major constituents of the fuel output are combustible gases that provide a heat source in the initial phases of secondary combustion for particle burning.

The thermochemistry analysis also shows that the boron has been reacted to solid boron nitride and liquid boron oxide. Based on numerous models developed for boron combustion as discussed in Section 1.3.2, complete combustion in the primary chamber is not likely, and elemental boron particles will be present in the combustor as well. The following section discusses these non-equilibrium combustion situations.

Table 2.1.1-1 ARCADENE 428J Gas Generator Exhaust Properties

MASS FRACTIONS AT EQUILIBRIUM CONDITIONS ($=solid, *=liquid)

	CHAMBER	THROAT
CH4	.01817	.01555
CO	.20932	.19988
FECL2	.01017	.01229
H2	.05381	.05427
HCL	.06038	.06833
MGCL2	.04823	.03728
BN$	.06220	.05867
C$	.39085	.39696
MGO$	.02826	.03337
B2O3*	.08645	.09270
FE3C*	.01017	.00917
TOTAL MOLES:	7.52482	7.57053
MOLES GAS:	3.82018	3.80817
MOLES $,*:	3.70463	3.76237

	PRESSURE PSIA	TEMP. DEG R	HT. CAP CAL / K*100GM	MOLS GAS MOLES / 100GM	VELOC FT / SEC	C* FT / SEC
CHAMBER	1000.0000	3134.3	60.282	3.8202		
THROAT	580.1835	2963.2	59.802	3.8082	2508.6	3854.7

AIR/FUEL RATIO FOR STOICHIOMETRIC MIXTURE = 7.4488

	ACOUS VEL FT/SEC	GAMMA (BSD ON HT CAP)	PROCESS GAMMA
CHAMBER	2585.4	1.1441	
THROAT	2508.6	1.1449	1.1151

2.1.1.2 Non-Equilibrium Calculations

The SSST propellant uses a significant amount of polystyrene beads as a fuel ingredient (34% of the propellant mass). They are nearly spherical beads with a nominal diameter of 220 microns, as shown in Figure 2.1.1-1.

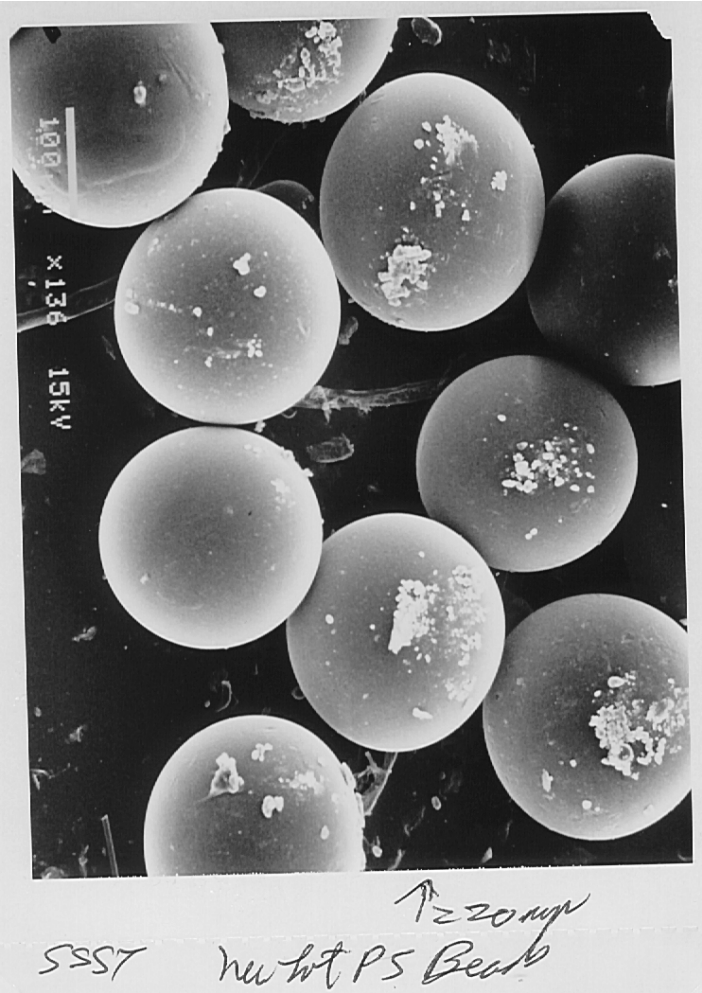

Figure 2.1.1-1 Polystyrene Beads (136X)

As the polystyrene beads are fairly large particles that require a finite time to heat up and begin contributing to the combustion process, it has been postulated that they are a primary source for the delay in gas generator characteristic velocity for the first several seconds of the motor firing. For this reason, a series of thermochemistry calculations were made to investigate the effects of non-reacting polystyrene on the gas generator exhaust. For these calculations the boron was modeled as non-reacting particles heated to the gas generator chamber temperature.

Figure 2.1.1-2 shows the effect on combustion products as the level of non-reacting polystyrene increases. It is apparent that the majority of carbon produced is derived from the combustion of the polystyrene beads, as this is the primary effect seen.

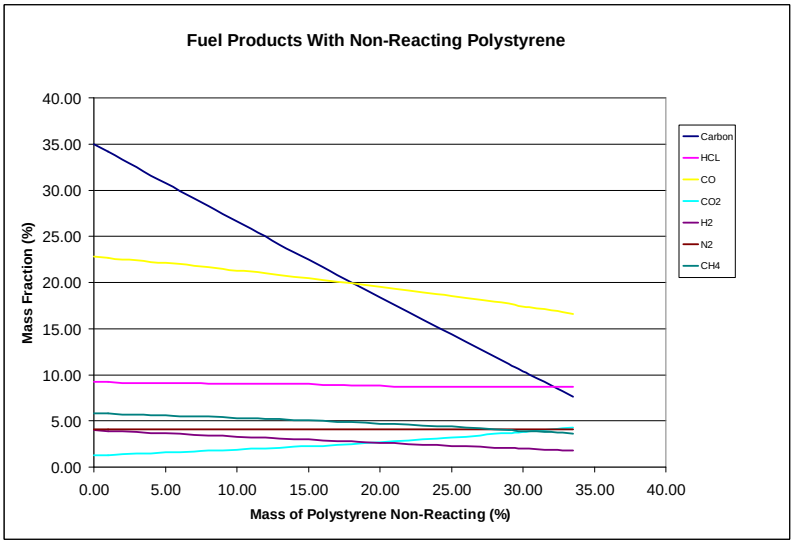

Figure 2.1.1-2 Fuel Products With Non-Reacting Polystyrene

This is an important fact when considering solutions for improving ramjet combustion efficiency and reducing signature, especially in light of the conclusions reached in Chapter 4 computational modeling. Figure 2.1.1-3 presents the effects of non-reacting polystyrene on chamber temperature and characteristic exhaust velocity c*. Although not as dramatic as the effect on carbon produced, the net result seen is a decrease in temperature and c* with an increased fraction of polystyrene unreacted, as one might expect.

The preceding results are not entirely rigorous, in that the polystyrene in actuality is actually only heated to the decomposition temperature before it begins reacting. Therefore a manual temperature and c* correction is required to reverse a portion of the enthalpy change occurring from the decomposition temperature to chamber temperature for the non-reacted polystyrene. This effect is bracketed in Figure 2.1.1-4, where calculations are shown for the two cases of zero heating of the beads, and the beads allowed to be heated beyond the vaporization temperature to the gas temperature.

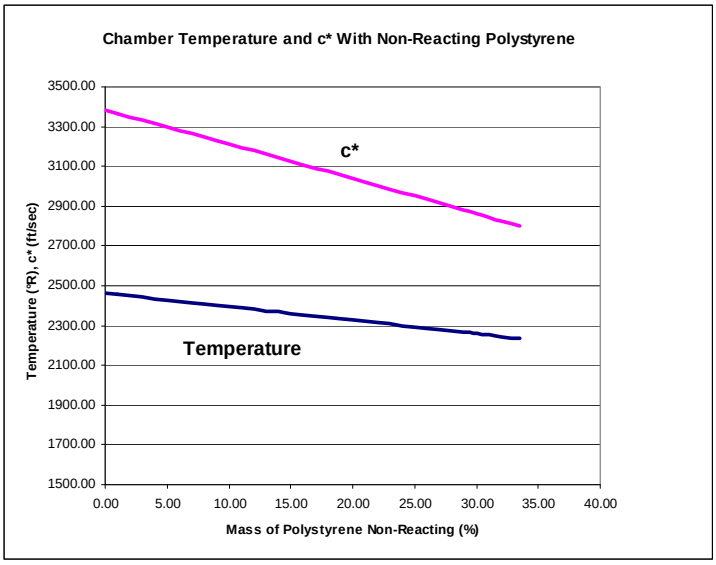

Figure 2.1.1-3 Chamber Temperature and c* With Non-Reacting Polystyrene

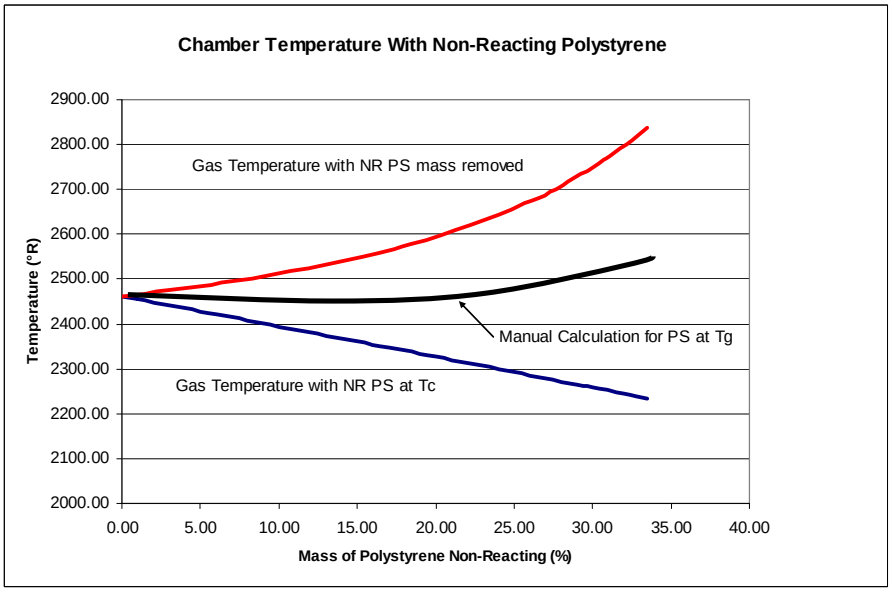

Figure 2.1.1-4 Chamber Temperature and c* With Non-Reacting Polystyrene and Different Assumptions for Polystyrene Heating

The polystyrene decomposition process was investigated in 1981 by Dr. Merril King[2], and modeled for a boron/polystyrene fuel by the author in 1994. Early in the firing, residence time is short in the gas generator, and there is little time for heat-transfer limited vaporization of spherical polystyrene to occur. Particles remain in the flow through nozzle with resultant two-phase flow losses. A model was developed to describe the process but only limited comparisons between theory and data were made. For the present research initial calculations were made in the event that the phenomenon was shown to be significant, and worth implementing in the CFD model. The polystyrene decomposition process is shown schematically in Figure 2.1.1-5.

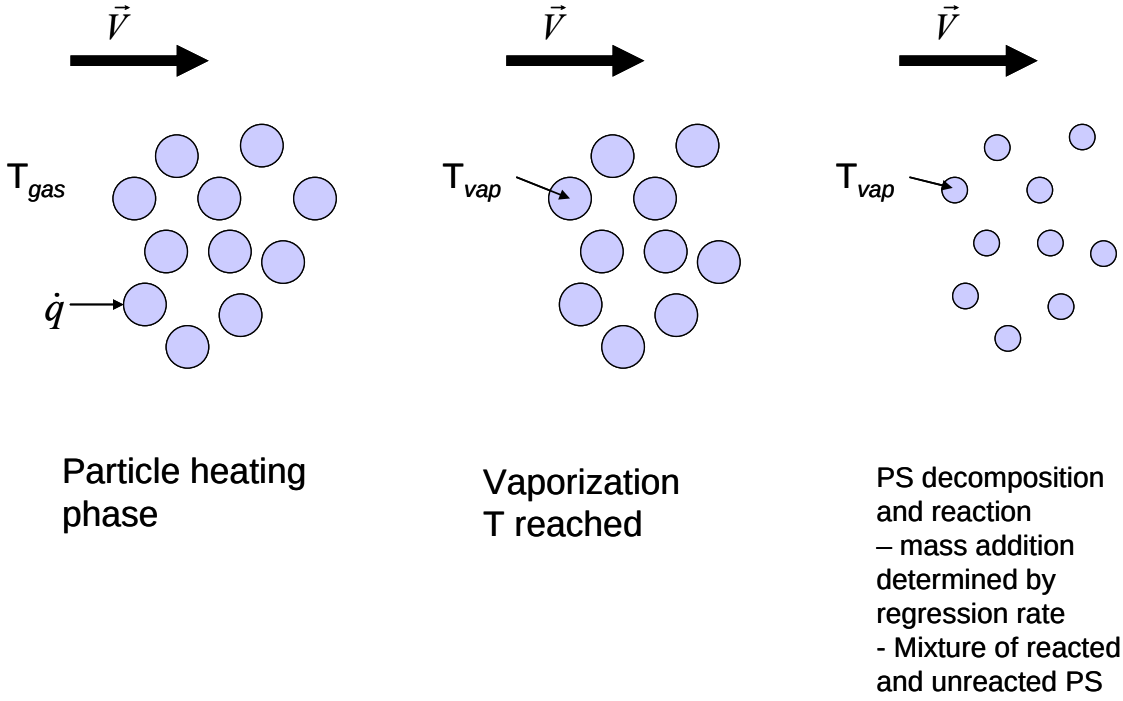

Figure 2.1.1-5 Polystyrene Decomposition Process

The King model assumes 100% thermal and velocity lags of particles in the nozzle, i.e. $c^*_{eff} = c^*_{gas}\, X_g$. Any unvaporized polystyrene passes through the nozzle at the vaporization temperature. Carbon formation is either allowed or suppressed from PS (allowed for fuel binder) to form limits for the analysis. A heat-up time (theta) is calculated, and if theta is greater than the particle residence time, the fraction of

polystyrene burned is zero, otherwise the particle size is determined from a burning rate equation.

The Biot number compares the relative magnitudes of surface convection and internal conduction resistances to heat transfer. When the Biot number is small, Bi<0.1, T(R,t)=T(t) and the sphere responds as a lumped mass.

$$Bi = \frac{h\left(\frac{V}{A}\right)}{k} = \frac{h\left(\frac{r}{3}\right)}{k}$$

For the polystyrene used in the SSST fuel and representative chamber conditions, h is likely less than 200 W/m^2°C, R ~ 150E-06 m, k (PS) = .08 W/m°K, the Bi is less than 0.125, so lumped heat capacity is assumed for the polystyrene beads.

The change in internal energy of bead is then set equal to the heat transfer from convection and integrated to determine the time to heat to the de-polymerization temperature:

$$q = hA(T - T_\infty) = -Cp_{PS}\rho_{PS}V\frac{dT}{dt}$$

$$\int_0^t \frac{-hA}{\rho CpV}dt = \int_0^t \frac{1}{T - T_\infty}$$

$$e^{\left(\frac{-hA}{\rho CpV}\right)t} = \frac{T - T_\infty}{T_0 - T_\infty}$$

$$t_{heatup} = \frac{-\rho_{PS}Cp_{PS}r_{0_{PS}}}{3h}\ln\left[\frac{T_{vap} - T_\infty}{T_0 - T_\infty}\right]$$

Expressing the equation in terms of Nusselt number, the expression becomes;

$$Nu = \frac{hD}{k_{gas}}$$

$$t_{heatup} = \frac{-\rho_{PS} Cp_{PS} r_{0_{PS}}^2}{1.5 k_{gas} Nu} \ln\left[\frac{T_{vap} - T_\infty}{T_0 - T_\infty}\right]$$

Using the expression provided by McAdams[43] for Nusselt number:

$$Nu = 0.37\left(\frac{u_\infty d}{\nu_f}\right)^{0.6} \quad ; 17 < \mathrm{Re}_D < 70,000$$

$$Nu \approx 1.5$$

The vaporization temperature for polystyrene derived from thermo-gravimetric analysis results presented in Figure 2.1.1-6 was taken as 425°C (1256°R). Additional

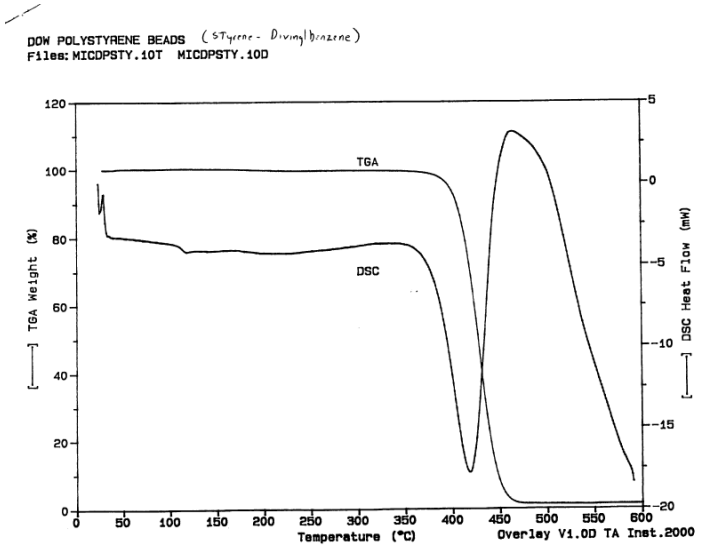

Figure 2.1.1-6 Thermo-Gravimetric Analysis Results For Polystyrene

required parameters were approximated as:

$$Cp_{PS} = 750\frac{cal}{kg\,°K}$$

$$r_0 = 220x10^{-6}\,m$$

$$k_{gas} = 20000\frac{cal}{\sec m\,°K}$$

$$T_0 = 25°C$$

$$T_\infty = 1500°C$$

The resulting heat-up time is found to be less than 0.2 milliseconds to raise the polystyrene particle to 425 °C (1256°R). Since gas generator residence times are much longer than this, even in the initial transient period for SSST, this is too quick to have an effect on ballistics. Particle collection results also later verified no unreacted polystyrene was found at the exit for the sample collection times. For these reasons all subsequent calculations assumed that the polystyrene beads are reacted completely in the gas generator. Supporting this conclusion, sub-micron soot and no evidence of partially decomposed polystyrene was found as reported in a workshop summary prepared by Waesche[22].

2.1.2 Gas Generator Exhaust Temperature

In order to set initial conditions for the FLUENT fuel inflow condition, the gas phase temperature must be estimated. Since the RT product is proportional to the characteristic velocity squared;

$R*T \sim (c*)^2$ taken from $$c*_{theo} = \sqrt{g_c \frac{1}{\gamma}\left(\frac{\gamma+1}{2}\right)^{\frac{\gamma+1}{\gamma-1}} RT}$$

the characteristic velocity was determined for the DC-1 gas generator. The inherent difficulty associated with this calculation, assuming the fuel flow determination is accurate, is that the gas generator throat area must be known. As the firing proceeds this value becomes less precise due to deposits that form on the interior surfaces, and thermal growth of the valve components. By restricting the analysis to the early portion of the

test, errors associated with deposits can be minimized. In order to estimate geometrical effects due to thermal growth, an analysis was performed to estimate the valve plunger dimensional variations with time. These data were used to calculate the area reduction experienced with time for the first twenty seconds in which the valve throttle position is fixed. With the area now known, c* can be determined from;

$$c^* = \frac{P_t * A_t * g_c}{\dot{m}}$$

And the RT product can be determined from the relationship

$$c^* = \sqrt{\frac{1}{\gamma}\left(\frac{\gamma+1}{2}\right)^{\frac{(\gamma+1)}{(\gamma-1)}} \frac{\bar{R}T_0}{\bar{M}}}$$

As seen in Figure 2.1.2-1, it is important to account for thermal growth as the valve heats and reduces the effective flow area. Using an approximate value of c* ratio equal to 0.89 for the first twenty seconds of the test results in a ratio of 0.79 for the RT product. This indicates a situation in which the degree of reaction is less complete than the equilibrium calculation, with a corresponding decrease in gas temperature, and the presence of higher molecular weight hydrocarbon compounds.

As a limiting case, if the molecular weight of the exhaust products is taken to be close to the theoretical value, the gas temperature is reduced to 1944 °R from 2462 °R (non-reacting boron). In reality, the gas temperature is somewhere between these values; however, to remain consistent with the gas phase chemistry chosen for the FLUENT model, the conservative value of 1944 °R was used.

The fact that the c* remains essentially constant during a time when the gas generator residence time is increasing considerably supports the assumption that molecular weight is not changing, otherwise the additional combustion time should result in a more complete reaction and an increase in calculated c*.

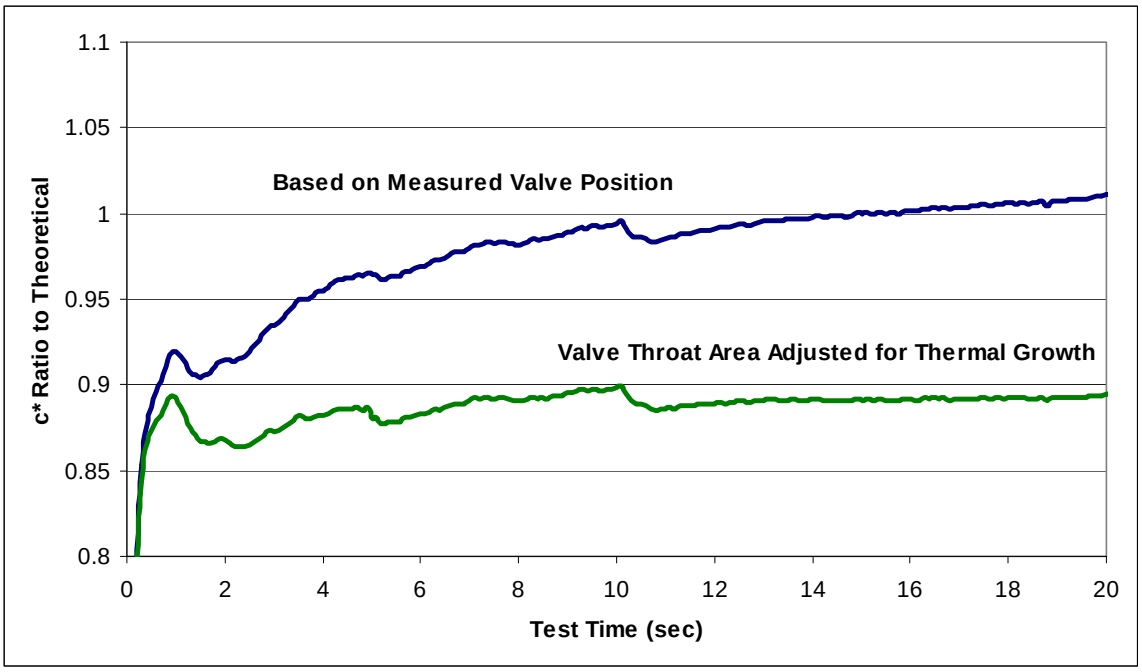

Figure 2.1.2-1 Calculated Characteristic Velocity, Test DC-1

2.1.3 Combustor Thermochemistry

The previous section dealt with the fuel gas generator prior to mixing with air. For ramjet combustor analysis, a second set of calculations must be performed using the fuel ingredients and air to determine theoretical combustor flow conditions. Air is modeled using standard atmospheric standards for analysis of flight operating conditions. For ground testing, the Aerojet test facility uses propane combustion to heat the air, with make-up oxygen added to return the mixture to the correct mole fraction of atmospheric oxygen. As a result, the air mixture, referred to as vitiated air, is modeled as nitrogen, oxygen, carbon dioxide, and water. A table of equilibrium values for process gamma, combustor total temperature, and gas molecular weight are developed as a function of inlet air temperature, operating pressure, and fuel/air ratio. The input parameters used to create the test data thermochemistry matrix are tabulated in Table 2.1.3-1.

Table 2.1.3-1 Equilibrium Thermochemistry Input Parameters

Inlet Air Temp (°R)	Combustion Pressure (psia)	Air/Fuel Ratio
1140.0	50.0	4000.0
1150.0	100.0	400.0
1160.0	125.0	100.0
1170.0	140.0	50.0
1190.0	160.0	27.0
		25.0
		23.0
		20.0
		15.0

In the test data analysis process if any individual data point falls outside the values used to create the thermochemistry matrix the calculations are halted to allow the matrix to be expanded.

The theoretical combustor total temperature for operation at near nominal flight conditions (T_{T0}=1200R, P_{T4}=150 psia) is shown in Figure 2.1.3-1. The engine typically operates at a fuel/air ratio of .05 to .06 during acceleration and cruise. Thus a well-mixed combustor equilibrium total temperature should be less than 3000 °R at 93% temperature-rise combustion efficiency. At this temperature the combustion gases are below the generally accepted 3500°R required to burn boron, and marginally above the 2160°R required to burn carbon. Therefore, a hotter flame-holding recirculation zone with combustion temperatures closer to stoichiometric values is required to achieve acceptable levels of combustion efficiency.

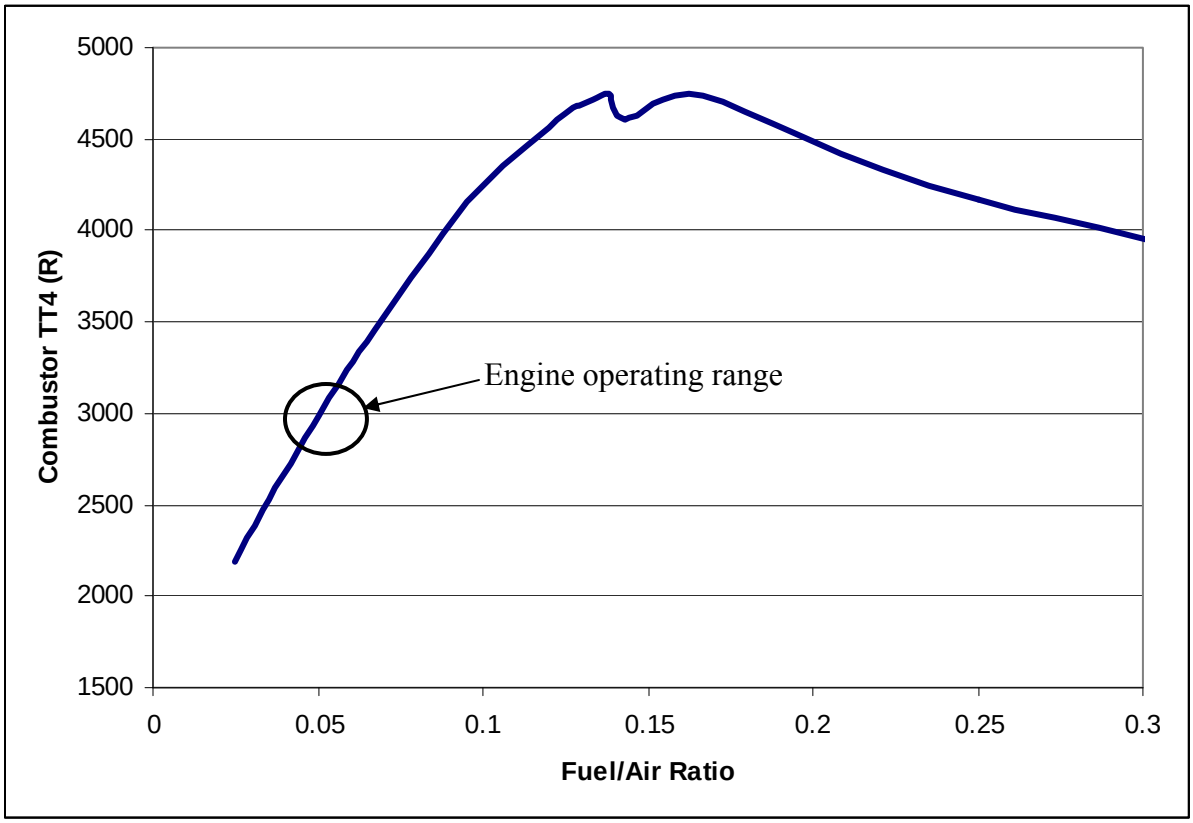

Figure 2.1.3-1 Typical Engine Operating Temperature

2.2 Particle Collection

Examination of the equilibrium thermochemical exhaust species for the SSST gas generator fuel shows that a significant fraction is predicted to be composed of solids, primarily carbon. Additionally, lacking conclusive evidence, the assumption is made that the boron does not react in the primary combustor and enters the combustion chamber as a solid. Therefore, when contemplating a method for numerical simulation of the process, it becomes of primary importance to understand the composition and particle sizes being injected with the fuel gas phase. Attempts were made experimentally to characterize the particulate exhaust at each step in the process:

- At the propellant surface; the flame front and products ejected from propellant surface in gas generator
- As the fuel is injected into the combustion chamber; gas / particulate flow exiting fuel injector
- At the ramjet exhaust after mixing with air

2.2.1 Propellant Surface Particle Testing

Two methods were used to examine the flow properties at the propellant surface - window bomb testing and particle bomb testing. Although not directly applicable for the numerical modeling effort, it is important to understand the fuel formation process in order to help guide future work to improve either exhaust signature or ramjet combustion efficiency.

2.2.1.1 Window bomb testing

The window bomb apparatus was constructed to examine the propellant surface, flame front, and ejected solids using a transparent window to allow visual access to propellant samples burning in an inert argon atmosphere. The test apparatus is shown in Figure 2.2.1-1. A propellant strand 0.25 in. by 0.25 in. in cross section is ignited and a video camera is used to record the propellant burning surface while visible through the window. A single frame of a representative video is shown in Figure 2.2.1-2. A hot ammonium perchlorate flame zone is seen as well as particles combusting, which are likely magnesium. The polystyrene beads are clearly identifiable in the photo, both on the propellant surface as well as in the flame front as they begin to react. The video clearly shows long strings of beads forming and reacting as they are carried from the propellant surface. This was a significant finding, as the clumping of beads is not in the direction of assuring complete reaction prior to introduction to the combustion chamber, and may be in part responsible for the unreacted carbon seen in the ramjet exhaust.

Image property of Aerojet Corporation

Figure 2.2.1-1 Window Bomb Apparatus

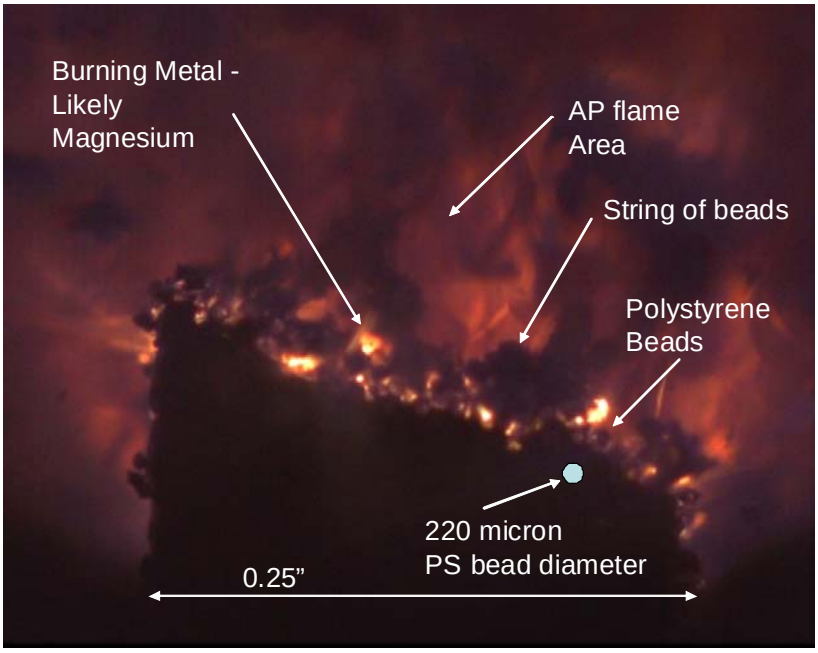

Image property of Aerojet Corporation

Figure 2.2.1-2 Window Bomb Image of Flame Front

2.2.1.1 Particle Collection tests

The window bomb collection tests provide a qualitative indication of the surface reactions, but little other data. For this reason, a series of particle collection tests was conducted.

The particle collection bomb shown in Figure 2.2.1-3 consists of an internal stainless steel cylinder which spins with a layer of alcohol coating the internal surface. The propellant sample is mounted just above the alcohol layer. The particle bomb is filled with argon and the propellant is ignited. Particles coming off the propellant are quenched in the cold alcohol, and the alcohol containing the sample is sent to the analytical lab for analysis.

Image property of Aerojet Corporation

Figure 2.2.1-3 Particle Collection Bomb

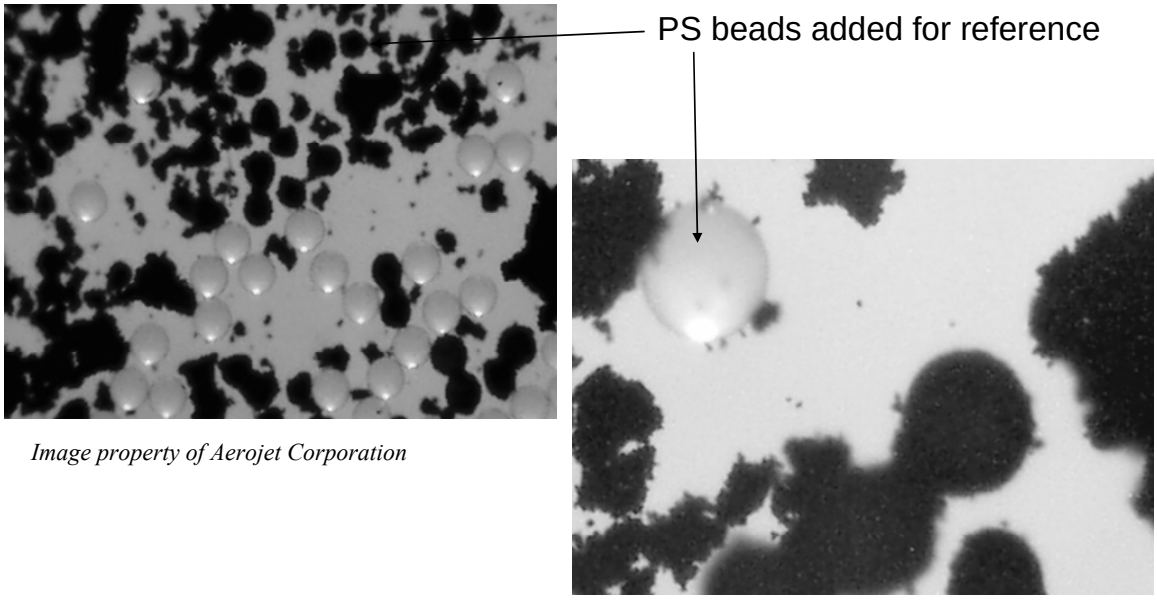

Image property of Aerojet Corporation

Image property of Aerojet Corporation

Figure 2.2.1-4 Particle Collection Bomb Results

The particle collection bomb procedure results in particles collected very close to the burning surface of the propellant. For many standard propellant problems this may provide valuable data, but for these fuel rich propellants under marginal combustion conditions such a low residence time prior to collection, it provides only basic knowledge that the combustion process is underway. The preliminary surface reactions result in particles that are far from the state at which the fuel exhaust is injected, as illustrated in the following sections. The most useful information from these tests is that the polystyrene has begun to react very close to the surface, as seen visually in the window bomb experiments. Figure 2.2.1-4 shows the particle bomb residue along with neat polystyrene beads to illustrate the particle sizes obtained. Data collected from laboratory analysis indicated that 40-50% of the insoluble material collected was charred polystyrene beads. These findings also support the analytical conclusion that the polystyrene reacts quickly in the gas generator under sustained heating, and can be excluded from the particle fraction used to represent the fuel exhaust for the numerical modeling effort.

2.2.2 Gas Generator Exhaust Particle Testing

There exists a wealth of prior research in particle collection from rocket exhausts as described aptly by Sambamurthi[11]. The primary obstacle encountered in particle collection is reliably obtaining measurements over a wide range of particle diameters. Some methods lend themselves to fine fractions and misrepresent the larger fraction, and some demonstrate the opposite trend. After reviewing past research in particle collection and size characterization including optical diagnostics, the copper tape method developed by Sambamurthi was adapted to the test hardware employed for this project.

The method described in that paper was developed to collect aluminum oxide particles, but appeared readily usable for boron and carbon collection. In personal correspondence with the author on 2/23/06, Dr. Sambamurthi (NASA Marshall) endorsed the method for collection of other rocket motor particulate exhaust, and indicated it was currently being employed to collect turbine exhaust particulates.

For the SSST fuel collection, double-sided adhesive copper tape (3M® Code 1182) was placed on three one-inch diameter steel rods. These rods were placed downstream of the exhaust of a gas generator firing using SSST propellant (no mixing with air). The test setup is shown schematically in Figure 2.2.2-1.

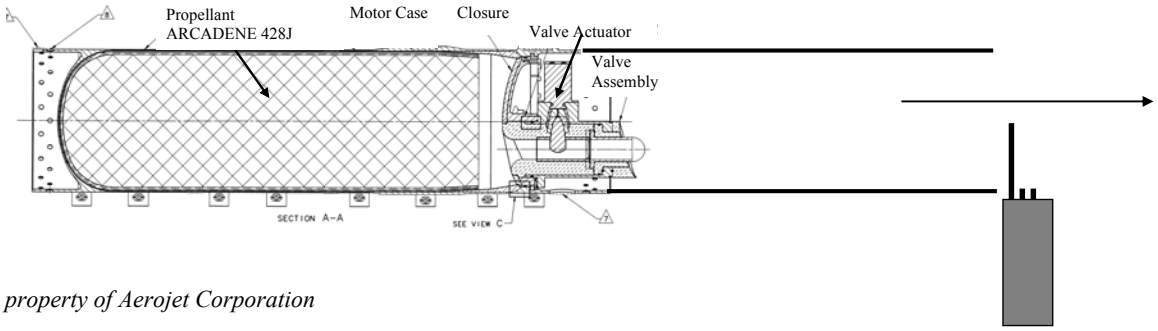

Image property of Aerojet Corporation

Figure 2.2.2-1 Gas Generator Exhaust Sampling Test Setup

During the motor firing, the rods were extended using a hydraulic ram and left exposed to the motor exhaust for a period of one second. Sampling was conducted at 0-1 sec (retract at 1 sec), 2 sec, and 10 sec.

The three copper tape tubes immersed during firing at time intervals were submitted to the lab for analysis. Scanning Electron Microscopy and Energy Dispersive Spectrometer (SEM/EDS), was used to determine inorganic material, and Fourier Transform Infrared Spectroscopy (FTIR) was used to identify any organic material present. The SEM/EDS samples were prepared by collecting residue that fell off the tubes onto a stub then coated with palladium. The FTIR samples were prepared by cutting a piece of the copper tape away from the metal rod then extracting in methylene chloride. The samples were then filtered and spotted onto a prepared KBr plate for analysis.

FTIRs indicated only the presence of the adhesive material used on the copper tape. This verifies the assumption that the polystyrene is reacting in the gas generator. SEM/EDS detected the presence of magnesium, silicon, chlorine, titanium, and iron. Scanned photomicrographs at 100x, 200x, and 500x (top to bottom) are shown in Figure 2.2.2-2 for 0, 2, and 10 second samples. The photos exhibit very irregular non-spherical particle geometry.

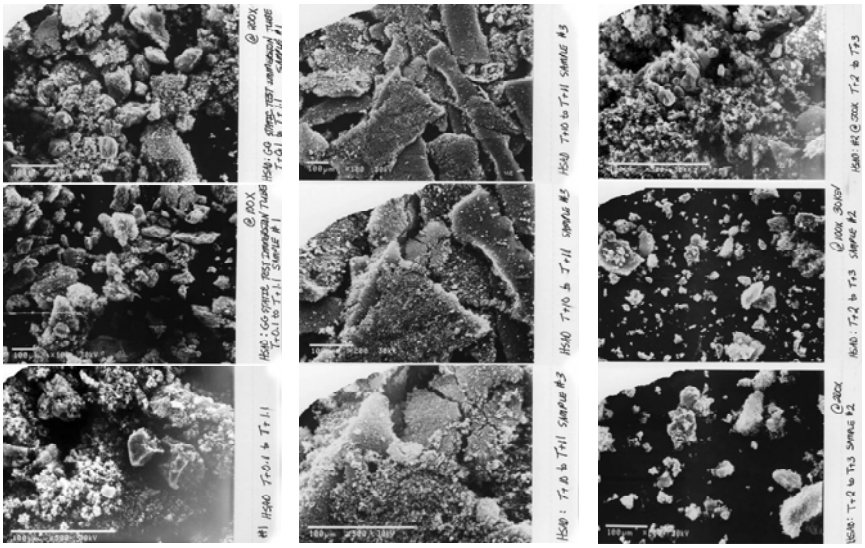

Image property of Aerojet Corporation

Figure 2.2.2-2 Gas Generator Exhaust Particle Photomicrographs

The laboratory analysis of the particles collected attempted to determine the chemical composition and particle sizes. Table 2.2.2-1 presents equilibrium composition of solid and liquid exhaust products for SSST propellant as a percentage of the total exhaust and as a percentage of the particulates.

Table 2.2.2-1 SSST Propellant Equilibrium Exhaust Solids

Compound	Mass fraction of exhaust (%)	Mass fraction of particulates
Solid Boron Nitride	0.5	0.7
Solid Magnesium Oxide	4.5	6.7
Solid Carbon	45.	67.
Solid Boron Oxide	17.	25.

The laboratory analysis technique used does not distinguish between elemental boron and boron oxide, only the total elemental amount of boron present. Table 2.2.2-2 presents the analysis results for boron. The question to be answered is whether the boron is reacting in the gas generator, or is injected without reacting, as assumed based on experience expressed in the literature.

Table 2.2.2-2 Boron Analysis Results

Sample Time (sec)	Boron % if B_2O_3	Boron % if B
T + 0.1 to T + 1.1	37.7	5.85
T + 2 to T + 3	17.5	2.71
T + 10 to T + 11	20.9	3.24

Since the 38% boron oxide level calculated exceeds even the equilibrium value, it is apparent that early in the firing all the boron is likely not in oxide form. However, as the values decrease for later samples it is possible that the boron is reacting more than thought in the gas generator. Future testing and analysis would be required to better characterize the form of boron particles, but for the SSST propellant at low levels of boron, the assumption that the boron is unreacted when injected appears a reasonable simplification.

Probably more pertinent to the present research are the particle sizes obtained from the photomicrographs. Each photograph section was used to determine individual particle volumes and express them as an effective spherical volume, assuming the particle width is equal to the depth. The results are shown in Figures 2.2.2-3 through 2.2.2-5.

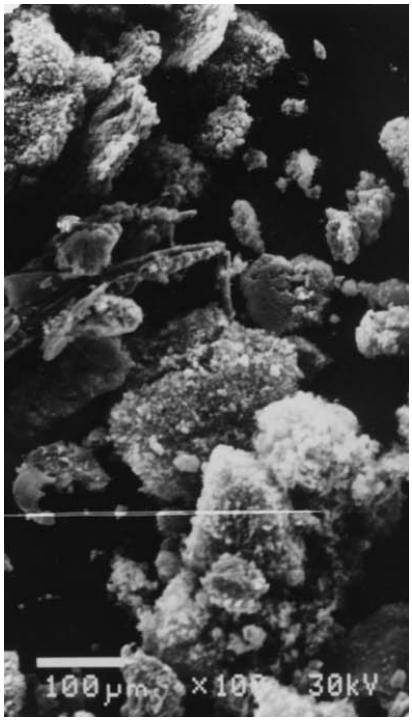

Image property of Aerojet Corporation

0-1 sec	
Mean	50.16350435
Standard Error	5.149346911
Median	33.31184589
Mode	12.0828555
Standard Deviation	43.99603929
Sample Variance	1935.651473
Kurtosis	2.485395842
Skewness	1.689180561
Range	192.9836471
Minimum	7.702820382
Maximum	200.6864675
Sum	3661.935817
Count	73
Confidence Level(95.0%)	10.26503532

Gas Generator Exhaust Sampling Data

Figure 2.2.2-3 Gas Generator Particle Sizes, 0-1 Second Sample

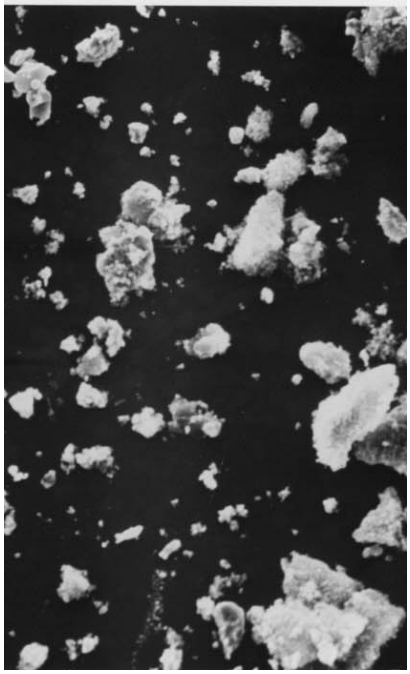

Image property of Aerojet Corporation

2 sec

Mean	18.96073349
Standard Error	1.278773804
Median	13.03698637
Mode	6.796606219
Standard Deviation	18.70684802
Sample Variance	349.9461628
Kurtosis	8.588922736
Skewness	2.681164836
Range	115.9225476
Minimum	4.8331422
Maximum	120.7556898
Sum	4057.596967
Count	214
Confidence Level(95.0%)	2.520672678

Figure 2.2.2-4 Gas Generator Particle Sizes, 2-3 Second Sample

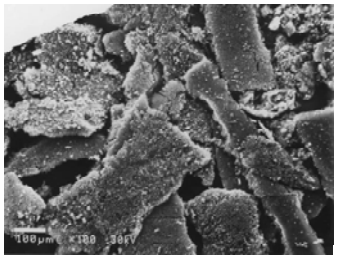

10 sec

x500

Image property of Aerojet Corporation

Figure 2.2.2-5 Gas Generator Particle Sizes, 10-11 Second Sample

The 10-11 second sample does not exhibit distinct particles, but represents more of a "caking". This may be a result of fine particles coating the tape during the 10 sec period prior to insertion, preventing a representative sample to be obtained. There is also a significant drop in mean particle diameter from the first to second samples, indicating that there is a time-dependent component to the exhaust properties. The 2-3 second results however would be most representative of the 1 to 20 second period used to calibrate the CFD model with ramjet ground test data.

2.2.3 Combustor Exit Exhaust Characterization

As a final experimental method, the exhaust of the ramjet combustor was sampled during a ramjet ground test. The test setup shown in Figures 2.2.3-1 and 2.2.3-2 is similar to the arrangement used for the fuel exhaust testing discussed in Section 2.2.2.

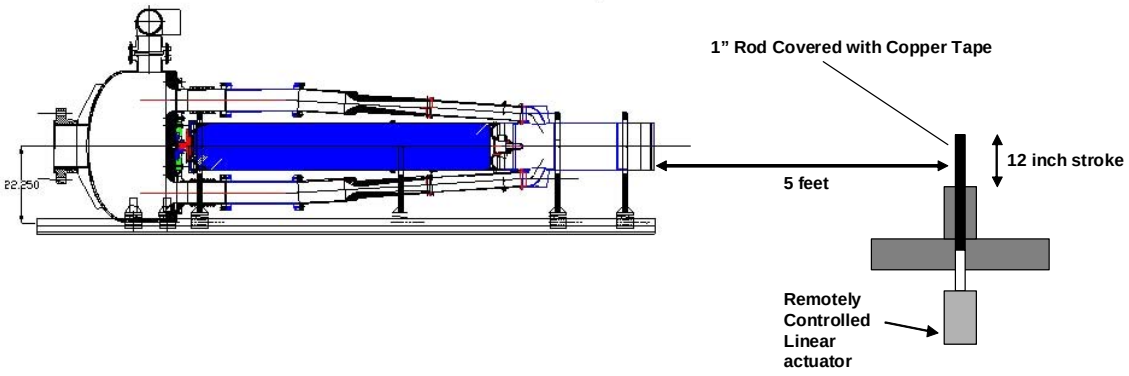

Figure 2.2.3-1 Ramjet Exhaust Sampling Test Schematic

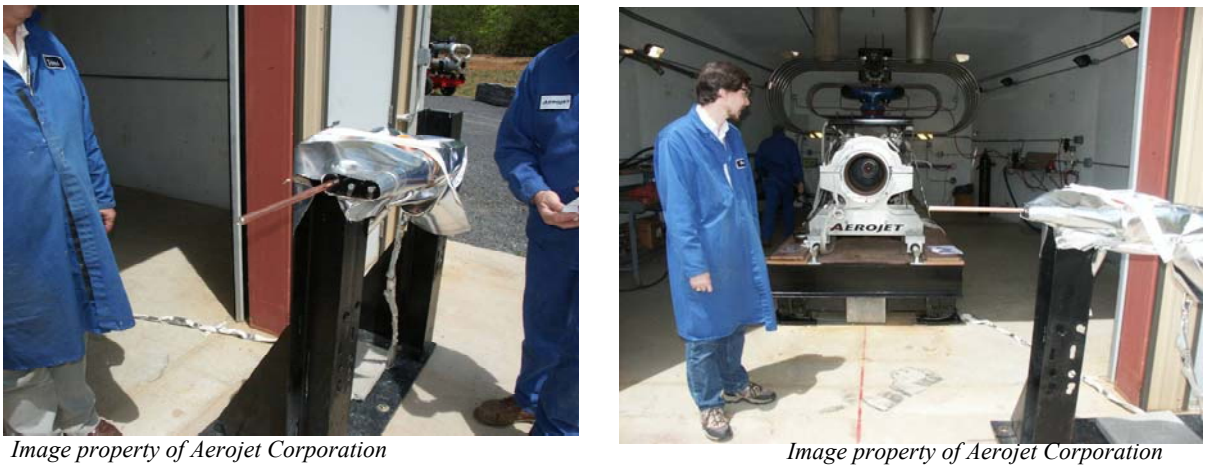

Image property of Aerojet Corporation *Image property of Aerojet Corporation*

Figure 2.2.3-2 Ramjet Exhaust Sampling Test Setup

For this testing, the sampling probes were located 5 feet downstream due to the higher temperatures experienced at the nozzle exit. Video coverage verified that when extended, the rods were immersed in the motor exhaust. In this case, the rods were inserted at 2, 10, and 60 seconds, with a 1 second dwell time for each case. The rod ends following the test are shown in Figure 2.2.3-3.

Image property of Aerojet Corporation

Figure 2.2.3-3 Ramjet Exhaust Samples

An extraction was performed to remove particles from some strips in a solvent. They were easily removed and the copper base foil was left clean. The mixture was sonicated to separate agglomerated particles and a FTIR was used to identify organic materials. Again, the adhesive was detected, but there was no unreacted polystyrene present. An SEM/EDS was used to identify metals. Magnesium and copper were detected, likely copper from the tape, and Mg from the fuel. No boron was detected. Carbon was not detected by SEM/EDS due to the lab's type of detector. As was the case with the propellant surface combustion particles collected, the ramjet exhaust particles serve more to help with a general understanding of the combustion process. The most directly pertinent data were obtained with the gas generator exhaust sampling, as these data address the condition of the fuel particles injected in the CFD model discussed in subsequent sections.

CHAPTER 3 – Ramjet Verification Tests

3.1 SSST Program Direct Connect Tests

3.1.1 Validation Ramjet Test Description

The first three ramjet direct-connect tests conducted under the Supersonic Sea-Skimming Target (SSST) program at Aerojet were conducted in heavy-weight hardware with the intention of optimizing the fuel injector configuration and identifying any thermal issues with the combustor design. A convergent-only exit nozzle was used in order to obtain more accurate thrust data without considering the losses associated with flow divergence or separation in the expansion cone.

For the tests, vitiated air was supplied by a specially constructed facility designed to deliver air at a desired mass flow rate and temperature. The air is heated through combustion of oxygen and propane, with excess oxygen added to ensure 21% mole fraction when delivered to the ramjet combustor. The result of vitiated heating becomes higher amounts of water and CO_2 in the "air" mixture, which is then accounted for in the equilibrium thermochemistry calculations. The ramjet engine is mounted on a stand allowed to freely translate axially for measurement of thrust. The Aerojet facility is shown schematically in Figure 3.1.1-1. An ejector is shown downstream of the combustor exit for tests where low base pressures simulating high altitude flight are required. The SSST direct-connect hardware is shown installed in the facility in Figure 3.1.1-2. An on-stand vitiator was fabricated for SSST to minimize the run-up time required to achieve the desired test condition. The curved feed lines supply required gases and liquids to the vitiator without inducing excessive thrust tares.

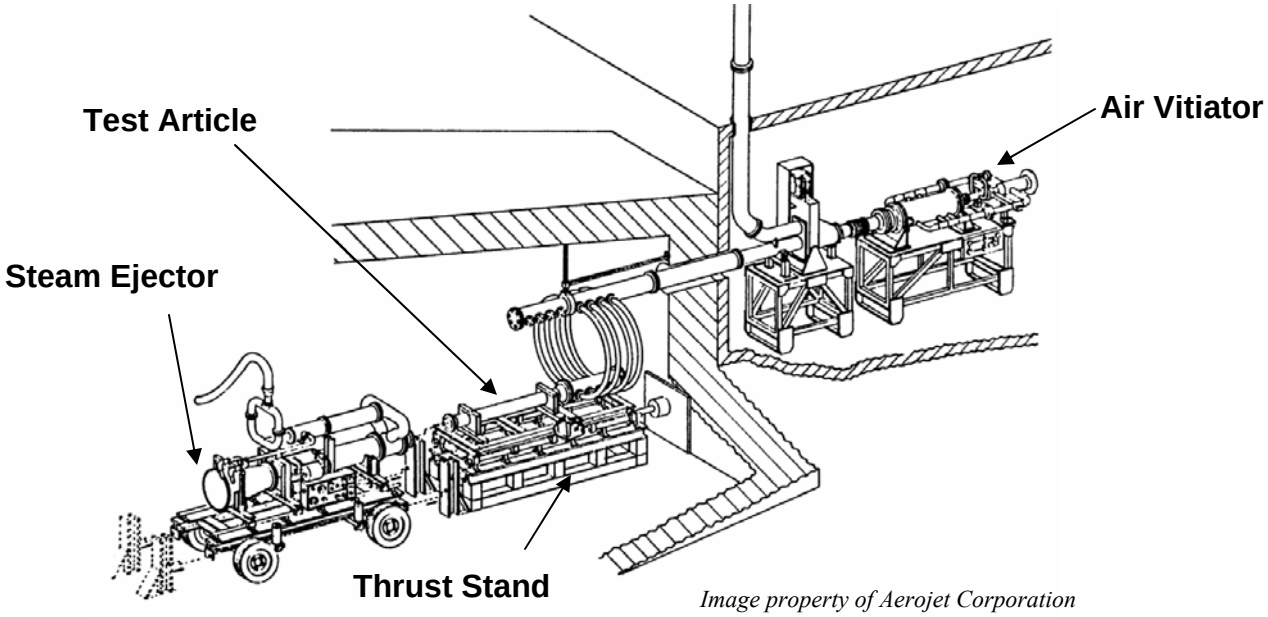

Image property of Aerojet Corporation

Figure 3.1.1-1 Aerojet Ramjet Test Facility

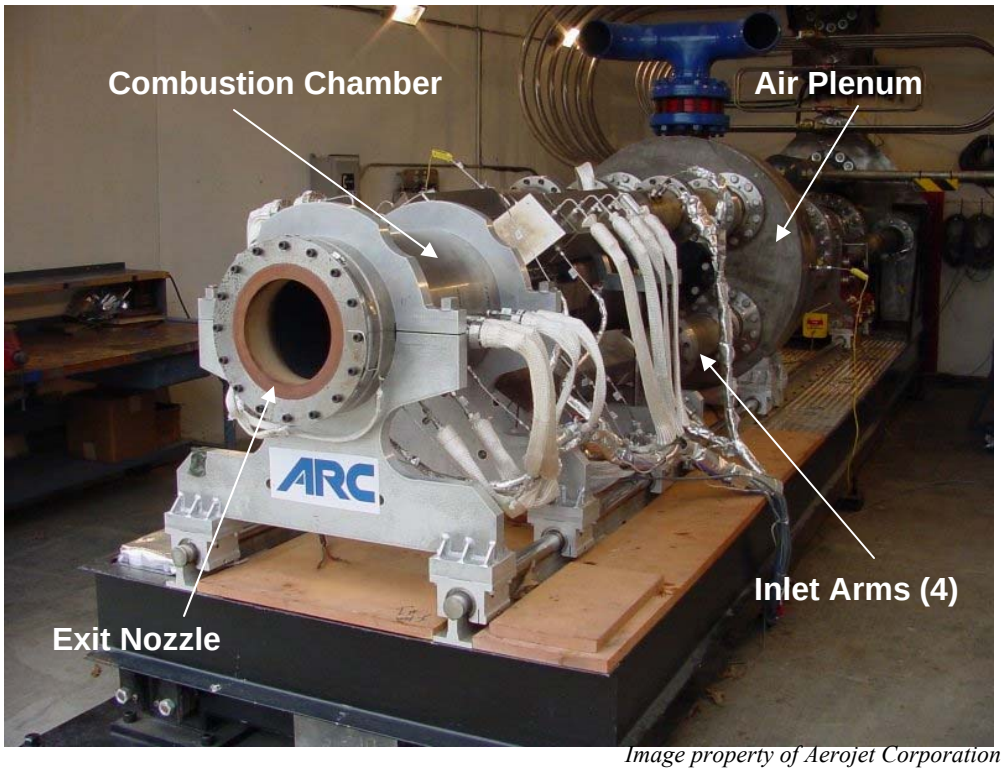

Image property of Aerojet Corporation

Figure 3.1.1-2 SSST Heavywall Direct-Connect Installation

The SSST heavywall test hardware is shown in Figure 3.1.1-3. The inlet arms include a sonic point to isolate upstream flow influences and to act as a metering point to determine air flowrate for the tests. The internal gas generator fuel delivery system flowpath and combustor geometry was simulated by the test hardware.

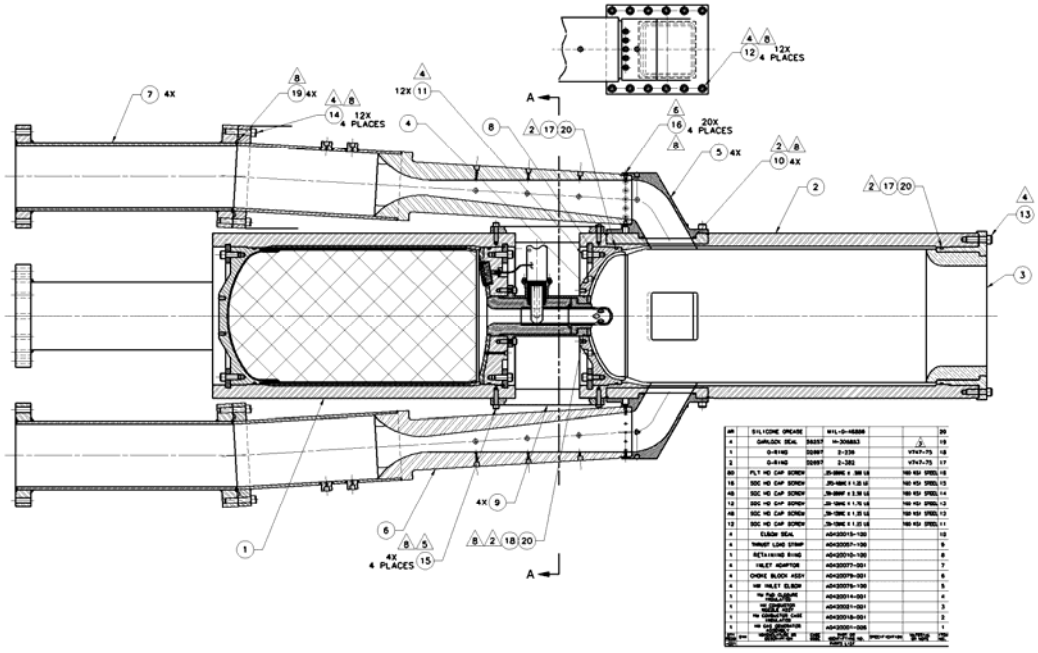

Image property of Aerojet Corporation

Figure 3.1.1-3 SSST Heavywall Test Hardware

A different fuel injector geometry was evaluated for each of the tests denoted DC-1, DC-2, and DC-3. The three injectors are shown in Figure 3.1.1-4. The first test DC-1 used a split of axial injection and radial fuel injection. Based on the observance of unburned carbon the in exhaust, test DC-2 eliminated the axial fuel port in an attempt to improve fuel residence time in the combustor. As the exhaust signature remained unchanged, a move to a showerhead type injector was made for DC-3.

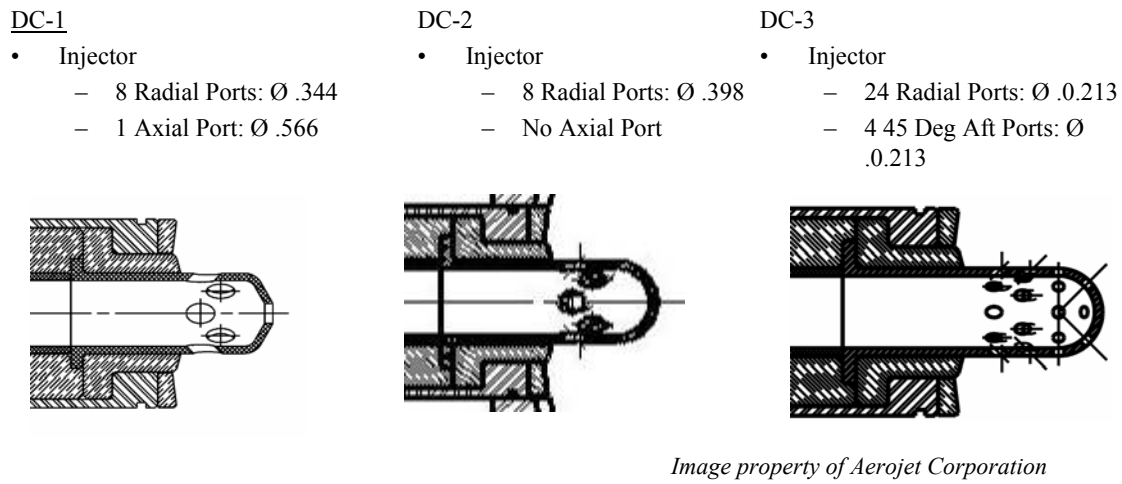

Image property of Aerojet Corporation

Figure 3.1.1-4 SSST Heavywall Fuel Injectors

These three fuel injectors and the associated direct-connect test data were used to validate the numerical model developed in the present research.

Pertinent hardware flow areas are presented in Table 3.1.1-1

Table 3.1.1-1 Heavywall Test Hardware Flow Areas

Parameter		Value	**D**rawing or **M**easured
ACBE	Choke Block Entrance Area	120.57 in^2	D
ACB*	Choke Block Throat Area	26.796 in^2	M
A1.5	Diffuser Area	69.806 in^2	D
A3	Fwd Combustor Area	132.73 in^2	D
A4	Aft Combustor Area	132.73 in^2	D
A5	Ramjet Nozzle Throat Area	40.42 in^2	M
A6	Ramjet Nozzle Exit Area	40.42 in^2	M

3.1.2 Test Data

The raw test data presented in this section were used to calculate the combustion efficiency of the ducted rocket for each test. In each case, the raw data were smoothed with a 10-point rolling averaging technique. Low speed data obtained using a PSI, Inc. multiplexed pressure scanner measurement system are reported, at nominally a 10 Hz data rate.

The test facility air flow rate actually consists of the component flows of air, oxygen, and propane. Each quantity is redundantly measured at the metering point and in the process building. In order to accommodate transients in air delivery during a test, the total flow is also measured just upstream of the test article at a sonic flow point, referred to as the inlet "choke block". This flow point is calibrated using steady-state facility flow data from immediately prior to the actual test. The facility air flow rates for the three tests are shown in Figure 3.1.2-1, with time zero being onset of facility air flow. All three tests were run at constant air conditions corresponding to Mach 2.5 at sea level, with a desired value of 83.4 lbm/sec.

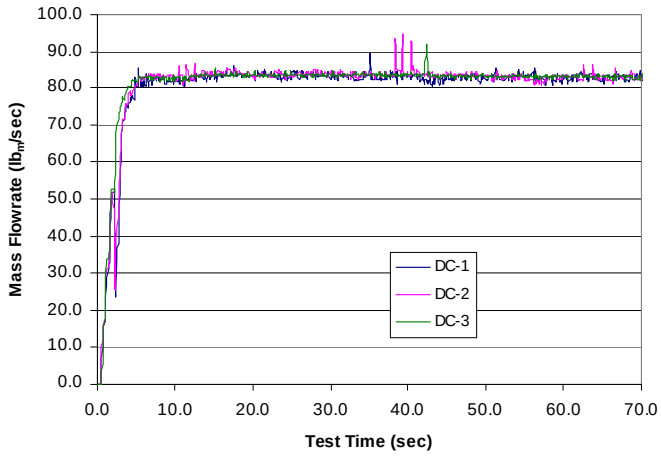

Figure 3.1.2-1 Direct-Connect Vitiated Air Mass Flowrates

The air temperature is computer controlled to a given set point by choosing the flows of propane and oxygen to the air vitiator. The ratio of oxygen to propane is kept constant in order to deliver 21% oxygen mole fraction in the inlet air. The desired inlet operating point for simulating sea level air is 1172°R. The facility was able to hold this value closely for all three tests as shown in Figure 3.1.2-2.

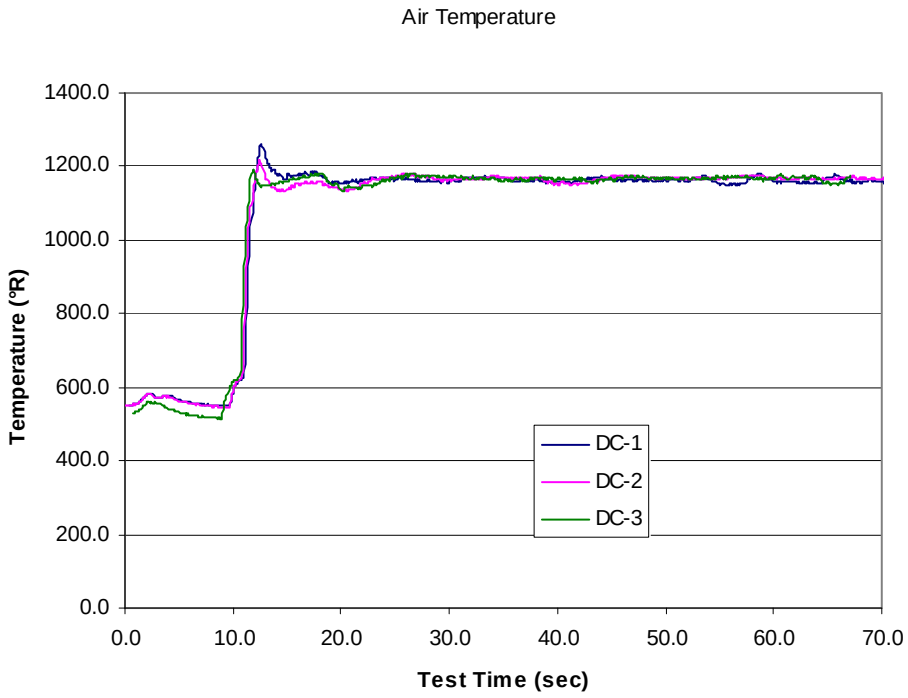

Figure 3.1.2-2 Direct-Connect Air Temperature

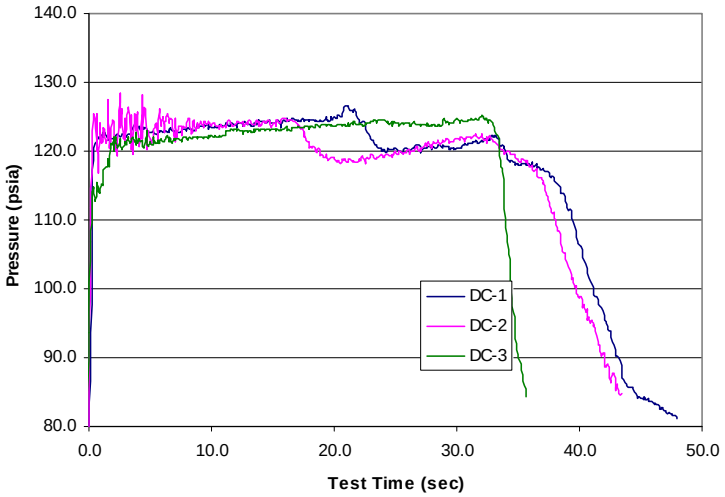

Figure 3.1.2-3 Direct-Connect Ramburner Static Pressures

The combustor static pressure is measured from several radial positions and axial stations for use in calculating the combustor total pressure. Averaged data from a station upstream of the ramburner exit nozzle are shown in Figure 3.1.2-3. In general, the three tests demonstrate good agreement. The time scale is shown in which zero is gas generator ignition. The fuel flowrates were varied in tests DC-1 and DC-2, and a corresponding change in combustor pressure is seen in each case. Figure 3.1.2-4 shows the gas generator internal operating pressure and Figure 3.1.2-5 shows the corresponding change in calculated fuel flowrate. Figure 3.1.2-6 shows the delivered gross thrust.

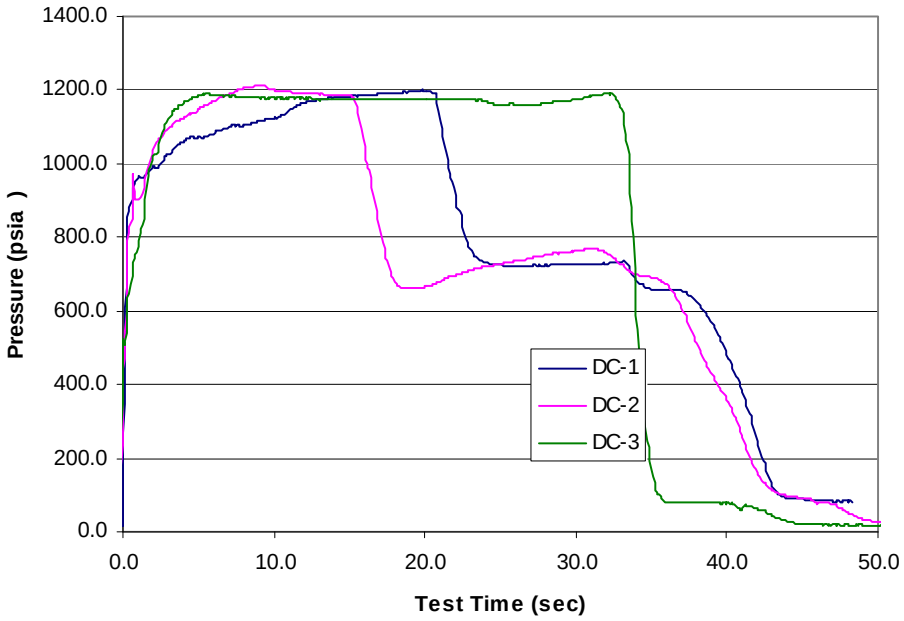

Figure 3.1.2-4 Direct-Connect Gas Generator Chamber Pressures

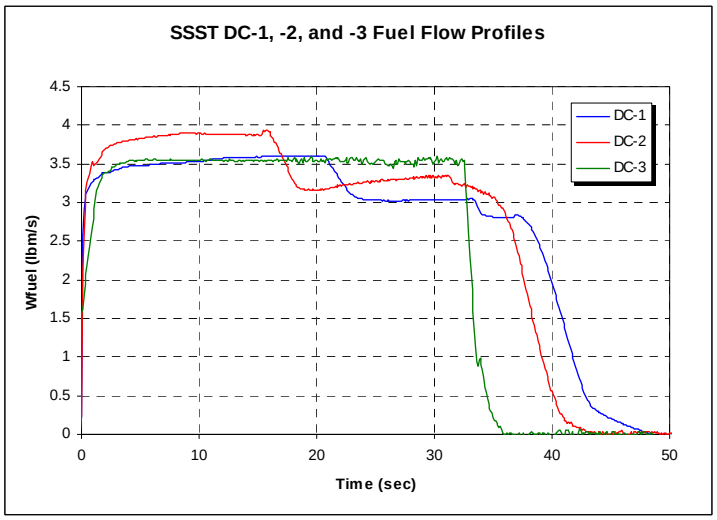

Figure 3.1.2-5 Direct-Connect Fuel Flowrates

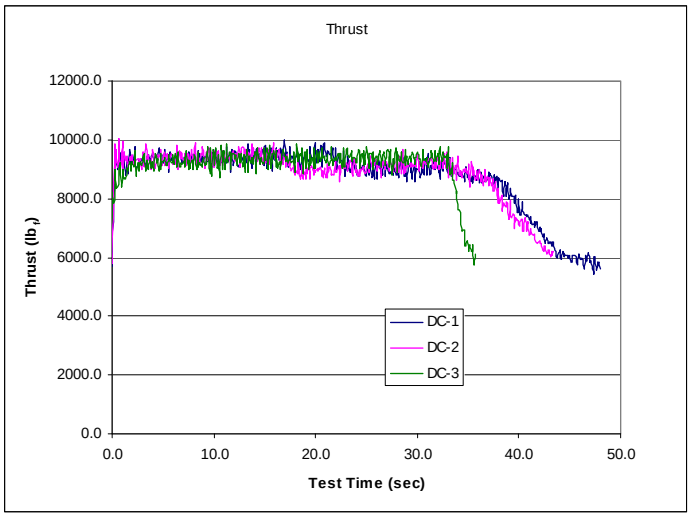

Figure 3.1.2-6 Direct-Connect Gross Thrust

3.2 Data Reduction Procedures

In order to calculate engine performance from ground test data, a procedure was developed as outlined below. These steps were programmed in FORTRAN in a routine called ARCEFF. This program was used to reduce the test data from the three SSST validation cases as described in Section 3.3. The ramjet station nomenclature used is illustrated in Figure 3.2-1. For engine ground testing, there is no capture station c, and inlet arm total temperature is used as station 0. Some features are not applicable to the test data examined, but the entire process is described for posterity and future reference.

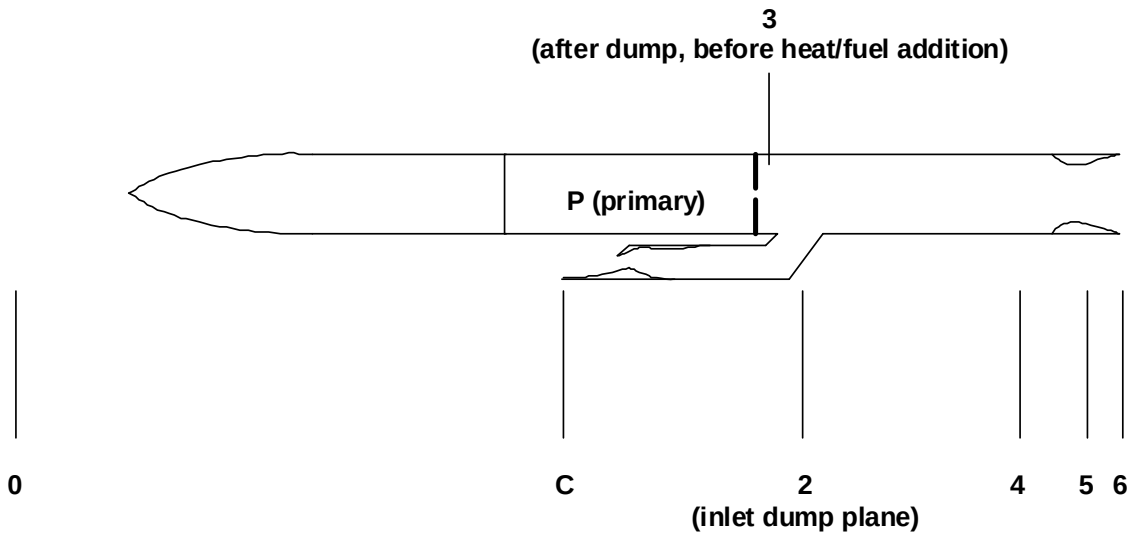

Figure 3.2-1 Ramjet Engine Station Nomenclature

The following flow functions are defined here for reference, as they are utilized in the data reduction procedures.

The X function calculates flow Mach / area relations:

$$X(\gamma, M) = \frac{\sqrt{\gamma}\, M}{(1+\frac{\gamma-1}{2}M^2)^{\frac{\gamma+1}{2(\gamma-1)}}} \text{ where } X_2 = X_1\left(\frac{A_1}{A_2}\right)$$

The Y function is used for mixing and heat addition:

$$Y(\gamma, M) = \frac{M\sqrt{\gamma(1+\frac{\gamma-1}{2}M^2)}}{1+\gamma M^2}$$

The Z function is used in stream thrust relations:

$$Z(\gamma, M) = \frac{1+\gamma M^2}{(1+\frac{\gamma-1}{2}M^2)^{\frac{\gamma}{\gamma-1}}} \text{ where } \overline{F_1} = P_{T_1} A_1 Z_1$$

3.2.1 Thermochemistry

The theoretical equilibrium values for the process gamma, gas constant, total temperature, and vacuum specific impulse are determined using vitiated air (combustion of propane, air and make-up oxygen in these cases). Process gamma is that calculated by equilibrium thermochemistry for isentropic flow between the stations indicated. The table of properties is generated accounting for the correct amounts of propane and oxygen added to reach the desired inlet total temperature. The analysis includes a constant temperature drop reflecting the difference between measured vitiator temperature and inlet arm temperature to determine the proper vitiator products; however, the reported properties are at the inlet arm temperature. The data are calculated as a function of inlet arm total temperature, combustor total pressure, and Air/Fuel ratio.

Vitiated air properties are also determined for use in pre- and post-test air-only calculations.

3.2.2 Air Mass Flow Measurement

The values used for air mass flow in post-test analysis for all tests are calculated from measured inlet arm temperatures and pressures. The discharge coefficient of the sonic area of the inlet was measured during the period of constant airflow immediately preceding the test using facility-based air flow measurements. All subsequent data calculations used the inlet-based air flowrate to account for air flow transients during the test.

3.2.3 Flow Areas

Pre- and post-test measurements of ramburner I.D. (sta. 4), nozzle throat (sta. 5), nozzle exit (sta. 6), and base area were taken and the associated flow areas are normally varied linearly between the ignition time and gas generator burnout. For the data reduction performed herein, constant values were used, as determined from pre-test measurements.

3.2.4 Ramburner Nozzle Discharge Coefficient:

In order to support the calculation of pressure-based combustion efficiency, the exit nozzle discharge coefficient was determined during a time of constant airflow and temperature (nozzle sonic) preceding the test. The choke-block entrance total temperature, station 4 static pressures, and choke block airflow were used in the calculations with vitiated air properties.

Discharge Coefficient Equations:

$$X_4 = \left(\frac{C_D * A_5}{A_4} \right) * X_5; \; Defines \; M_4$$

$$\dot{w}_a = \frac{P_{T_5} C_{D_5} A_5 X_5 * \sqrt{\frac{g_c}{R}}}{T_{T_0}}$$

$$P_{T_4} = P_4 * \left(1 + \frac{(\gamma - 1)}{2} M_4^{\,2} \right)^{\frac{\gamma}{\gamma - 1}}$$

3.2.5 Pressure-Based Combustion Efficiency

The data used in the calculation are measured P_4, choke-block total temperature, choke-block air flowrate, and post-test fuel flow calculations resulting from a separate analysis. Theoretical T_{T4}, Process Gamma, and gas constant are looked up as a function of T_{T0}, fuel/air ratio, and Combustor Total Pressure.

$$X_4 = \left(\frac{C_D * A_5}{A_4} \right) * X_5 ; \; Defines \; M_4$$

$$\dot{w}_a + \dot{w}_f = \frac{P_{T_5} C_{D_5} A_5 X_5 * \sqrt{\frac{g_c}{R_4}}}{T_{T_4}}$$

$$P_{T_{4,P}} = P_4 * \left(1 + \frac{\left(\gamma_{4-5} - 1 \right)}{2} M_4{}^2 \right)^{\frac{\gamma_{4-5}}{\gamma_{4-5}-1}}$$

$$\eta_{c,\Delta T,P} = \frac{T_{T_{4,P}} - T_{T_0}}{T_{T_{4,Th}} - T_{T_0}} * 100.$$

3.2.6 Thrust-Based Combustion Efficiency

The following procedure was followed:

1) Correct the measured thrust for the thrust stand tares. For the Aerojet test stand a linear spring constant is used:

$$F_{corr} = \frac{F_{meas}}{0.9865}$$

2) Correct for base pressure forces

For tests using an ejector to lower the exit pressure, a base pressure correction should be made –

$$F_x = F_{corr} + A_{base}\left(P_a - P_{base}\right); \quad where\ A_{base} = A_{case} - A_6$$

For these tests there was no ejector installed, so $F_x = F_{corr}$

3) Correct For Nozzle Divergence

For tests using convergent-divergent nozzles, a correction should be made to the momentum term in the thrust equation to account for measurement of only the axial component of thrust. The SSST tests utilized a convergent-only nozzle so no divergence losses were seen and $F_g = F_x$.

$$F_g = \frac{\left[F_x - \left(P_6 - P_{atm}\right)A_6\right]}{\frac{\left(1+\cos\theta\right)}{2}} + \left(P_6 - P_{atm}\right)A_6$$

where theta is the nozzle half-angle.

$$P_6 = P_{T_{6,F}} / \left(1 + \frac{\left(\gamma_{4-5} - 1\right)}{2} M_6{}^2\right)^{\frac{\gamma_{4-5}}{\gamma_{4-5}-1}}; \quad P_{T_{6F}} \text{ determined below}$$

$$X_6 = \left(\frac{C_{d_5} A_5}{A_6}\right) * X_5\ ; \quad \text{Defines } M_6, Z_6$$

4) Determine the nozzle stream thrust efficiency before the test during air flow only, after reaching equilibrium. Combustor Mach number, total pressure, and total

temperature were determined in the C_d calculations. For the SSST tests the nozzle efficiency was calculated for the 10 seconds immediately preceding gas generator ignition.

Stream thrust based on measured thrust; $\bar{F}_6 = F_g + P_{atm} A_6$

$$P_{T_{6,F}} = \frac{\bar{F}_6}{A_6 Z_6}$$

$$\eta_n = \frac{P_{T_{6,F}}}{P_{T_{4,P}}}$$

5) Calculate Thrust-Based Efficiency

The nozzle stream thrust efficiency can be varied linearly between pre- and post-test values, however the constant pre-test value was used. The efficiency calculation procedure is the same except P_{T4F} and T_{T4F} are not known.

$$\bar{F}_6 = F_g + P_{atm} A_6$$

$$P_{T_{6,F}} = \bar{F}_6 A_6 Z_6$$

$$P_{T_{4,F}} = \frac{P_{T_{6,F}}}{\eta_n}$$

$$P_{T4F} = \frac{P_{T6F}}{\eta_n}$$

$$\dot{w}_a + \dot{w}_f = \frac{P_{T_{5,F}} C_{D_5} A_5 X_5 * \sqrt{\frac{g_c}{R_4}}}{T_{T_{4,F}}}$$

$$\eta_{c,\Delta T,F} = \frac{T_{T_{4,F}} - T_{T_0}}{T_{T_{4,Th}} - T_{T_0}} * 100.$$

6) Burner Pressure Recovery

Pressure recovery is reported as the ratio of ramburner total pressure ($P_{T4,P}$, based on pressure) to inlet diffuser total pressure based on the inlet static pressure measurements at station 1.5. The ratio is plotted as a function of modified heat addition parameter MHAP as defined below.

$$MHAP = \frac{S_A^*}{\sqrt{T_{T_0}}} * \phi = \frac{P_{T_{4,P}} A_5 Z_5}{\dot{w}_a \sqrt{T_{T_0}}} * \phi$$

3.3 Baseline Verification Test Results

3.3.1 Equilibrium Combustion

The ARCEFF program was used to process the test data for tests DC-1, 2, and 3. As the results are normalized at ignition with pre-test cold flow coefficients, the most accurate time for obtaining accurate ramburner performance is soon after gas generator ignition. For this reason, only the first twenty seconds of data are presented here. All three tests are near the same throttle setting and fuel flowrate during this time so the effects of equivalence ratio are removed and the differences in combustion efficiency reduce to injector design.

Base pressures were measured for each test; however, the change in pressure from zero flow to ignition was 0.09 psi, or roughly 10 lb_f out of 9500 lb_f. Since this is 0.1%, and the effect is normalized by utilizing a cold flow stream thrust coefficient, base pressures were not included in the analysis.

Input files for ARCEFF were created for the fuel thermochemistry, test data, and fuel flow rate which is separately calculated. The coefficients determined for each test during the pre-ignition cold flow averaging are shown in Table 3.3.1-1.

Table 3.3.1-1 Ramjet Test Data Coefficients

Test Number	C_{d_0}	C_{d_5}	η_n
DC-1	1.0058	.9929	.9770
DC-2	1.0269	1.014	.9767
DC-3	1.0096	.9914	.9747

Tests one and three are consistent in terms of coefficients obtained; however, the test 2 discharge coefficients appear out of family. This discrepancy could be due to errors in instrumentation channels or facility parameters affecting airflow measurements. The calculated temperature rise combustion efficiencies for each test for the first 20 seconds are shown in Figures 3.3.1-1 through 3.3.1-3. The red line is thrust-based in all cases.

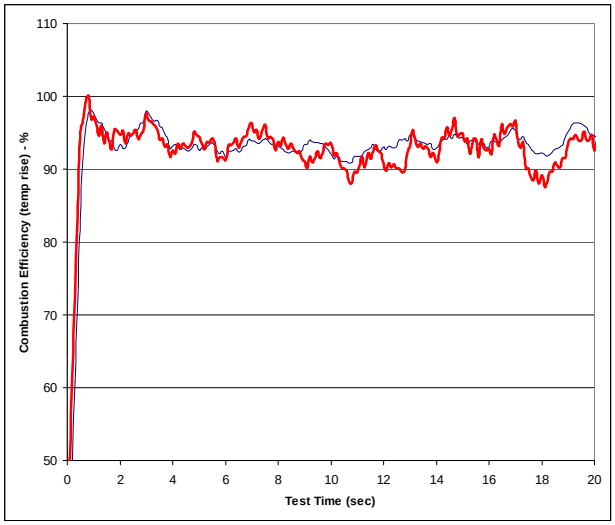

Figure 3.3.1-1 DC-1 Temperature Rise Combustion Efficiency

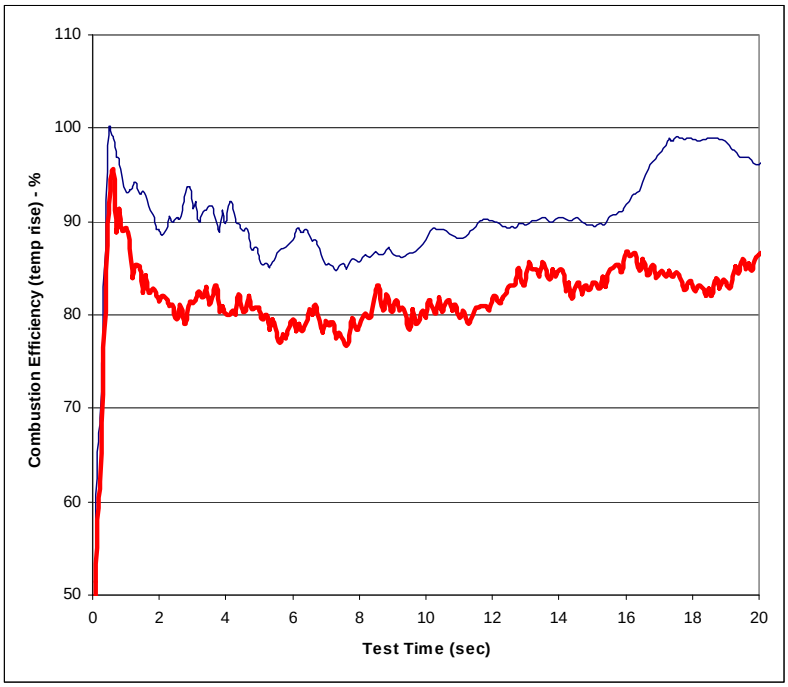

Figure 3.3.1-2 DC-2 Temperature Rise Combustion Efficiency

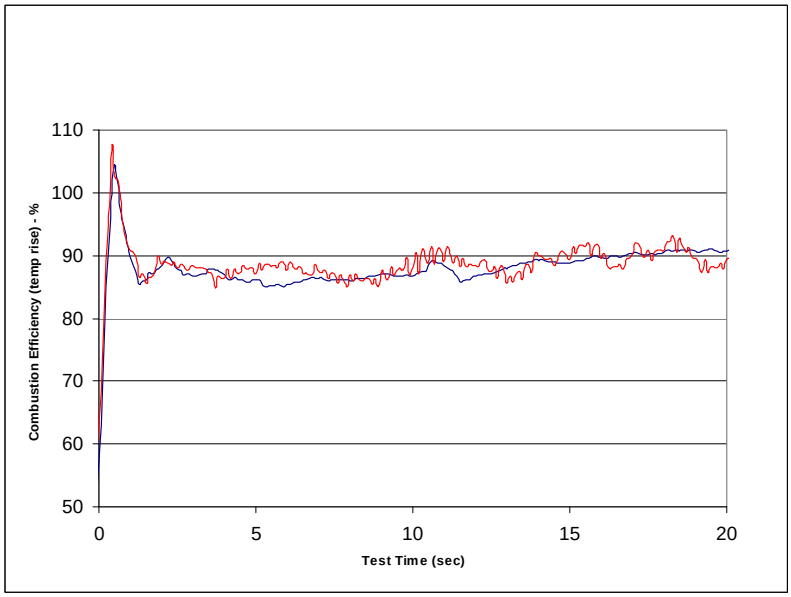

Figure 3.3.1-3 DC-3 Temperature Rise Combustion Efficiency

Both DC-1 and DC-3 exhibit extremely good agreement between pressure-based and thrust-based combustion efficiencies. The disagreement between the two on test DC-2 casts some doubt on the absolute levels for either. The pressure-based efficiencies for the three tests are shown together in Figure 3.3.1-4 for comparison. The effects of injector geometry for the three tests is clearly defined, with the DC-1 injector yielding the highest efficiency. These results were used to gauge the effectiveness of the numerical FLUENT model and the ability to correctly predict injector effects.

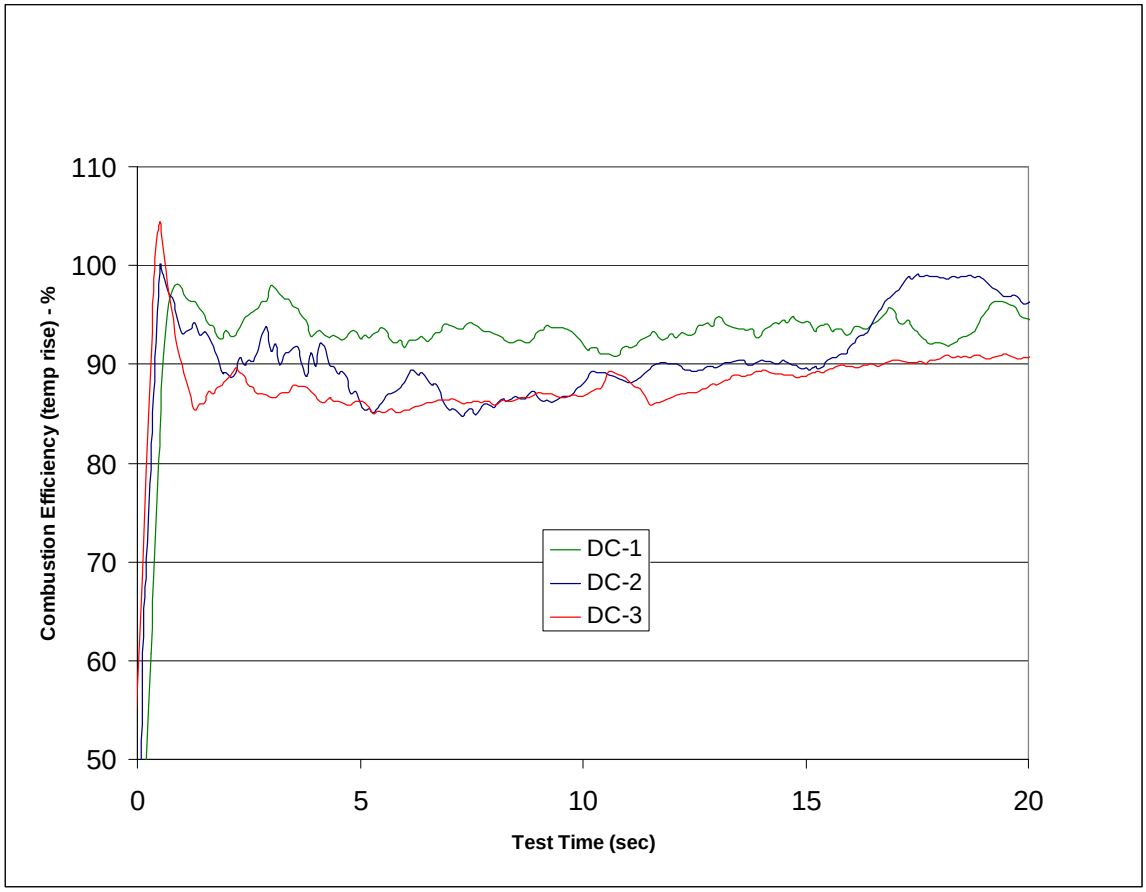

Figure 3.3.1-4 Pressure-Based Temperature Rise Combustion Efficiency

An alternate method of calculating combustion efficiency uses the fuel/air definition shown in Figure 3.3.1-5. As in the case of temperature rise efficiency, the temperature at station 4 is calculated; however, for this definition an "effective" fuel/air ratio is found corresponding to the calculated temperature. The ratio of effective to operating

efficiency forms the fuel/air efficiency. Although not entirely accurate since non-equilibrium intermediate reactions can be the source of reduced total temperature, the value provides a rough indication of unburned fuel at the exit. The data based on a temperature calculated from the measured pressure are provided in Figure 3.3.1-6, again for comparison to the FLUENT predictions.

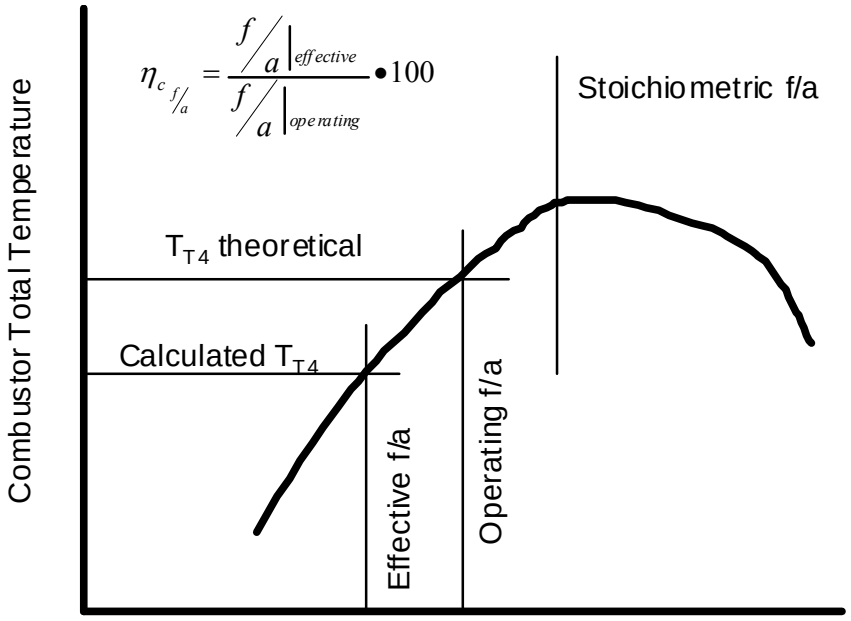

Figure 3.3.1-5 Fuel/Air Combustion Efficiency Definition

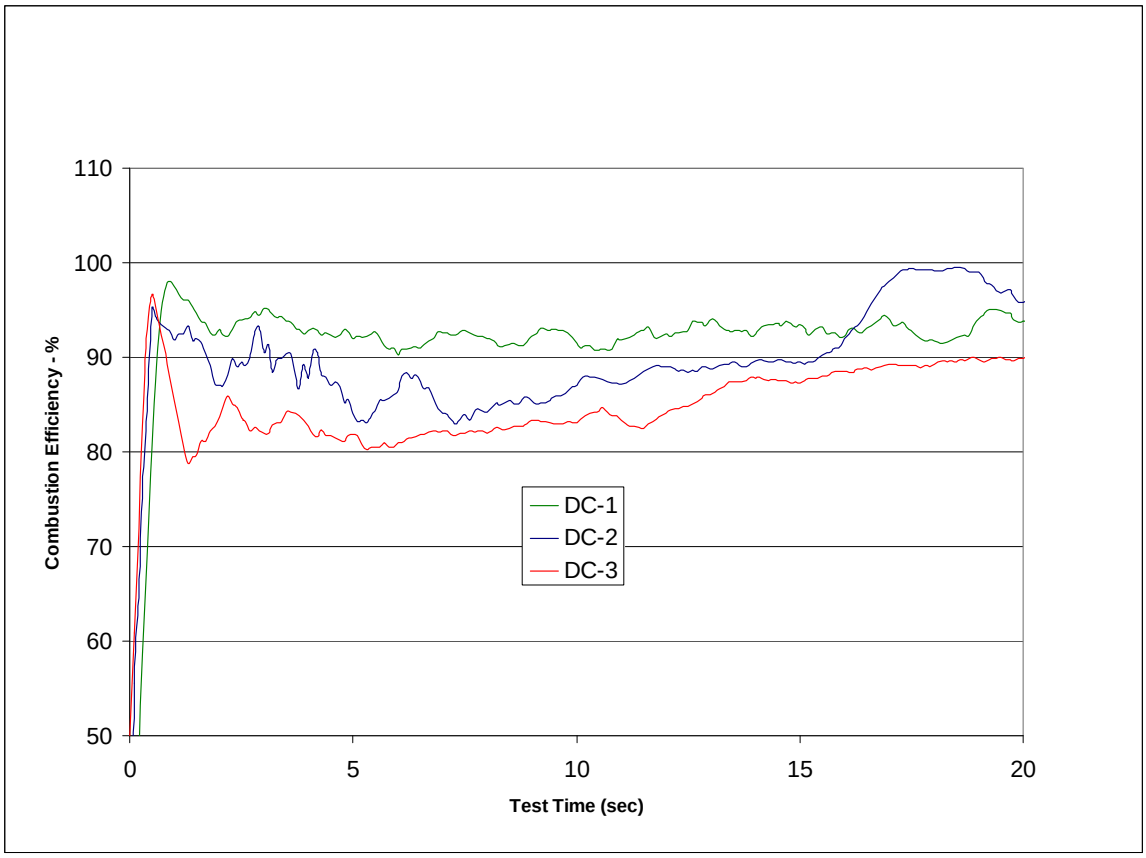

Figure 3.3.1-6 Fuel/Air Combustion Efficiency – Based on Pressure

The burner pressure loss for each test is shown in Figure 3.3.1-7 as a function of Modified Heat Addition Parameter (MHAP). As there is little change in test conditions and MHAP between tests, the data are centered at a value of approximately 1.18. The pressure loss for tests DC-1 and DC-3 is consistent at 0.875. Test DC-2 is again out of family at over 0.92.

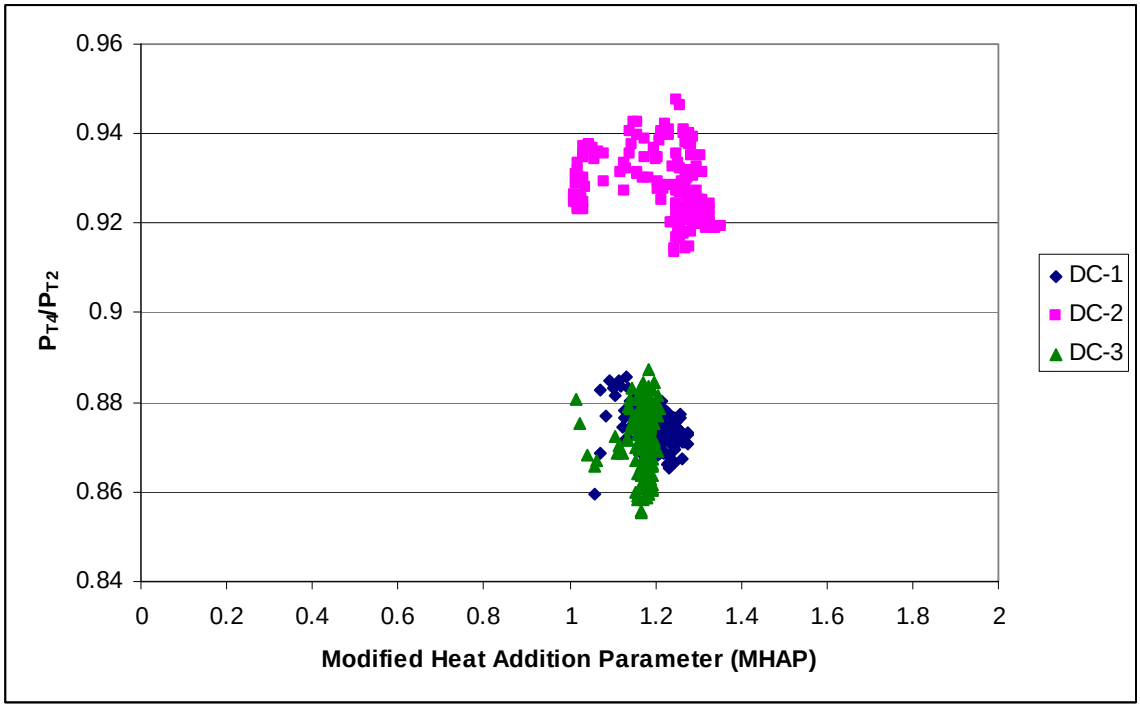

Figure 3.3.1-7 Ramburner Pressure Losses

3.3.2 Test Data Used for CFD Analysis

Since the DC-2 test rendered results that appear corrupted, the tests DC-1 and DC-3 were used to validate the FLUENT combustor model. These tests represent two distinctly different injector configurations and present the opportunity to evaluate the model capability to distinguish between the two flowfields.

A nineteen second average was calculated for the tests for use in correlating the CFD models. Transient effects are apparent during the first second and, later in the test, uncertainties are introduced such as flow area changes, instrumentation drift, and fuel flowrate accuracy as the grain face may deviate from a flat surface. The temperature rise efficiencies and corresponding total combustion temperatures were determined as:

Test DC-1

$\eta c = 93.6\%$, $T_{T4} = 1352.6$ °K (2434.7 °R)

Test DC-3

$\eta c = 87.9\%$, $T_{T4} = 1309.7$ °K (2357.5 °R)

This data analysis determines total combustion temperatures assuming that boron contributes to the combustion process. The final FLUENT modeling neglected boron in the modeling; therefore, these temperature results require modification to serve as a basis for modeling. Figure 3.3.2-1 illustrates the effect of boron combustion on the equilibrium total temperature as a function of fuel/air ratio.

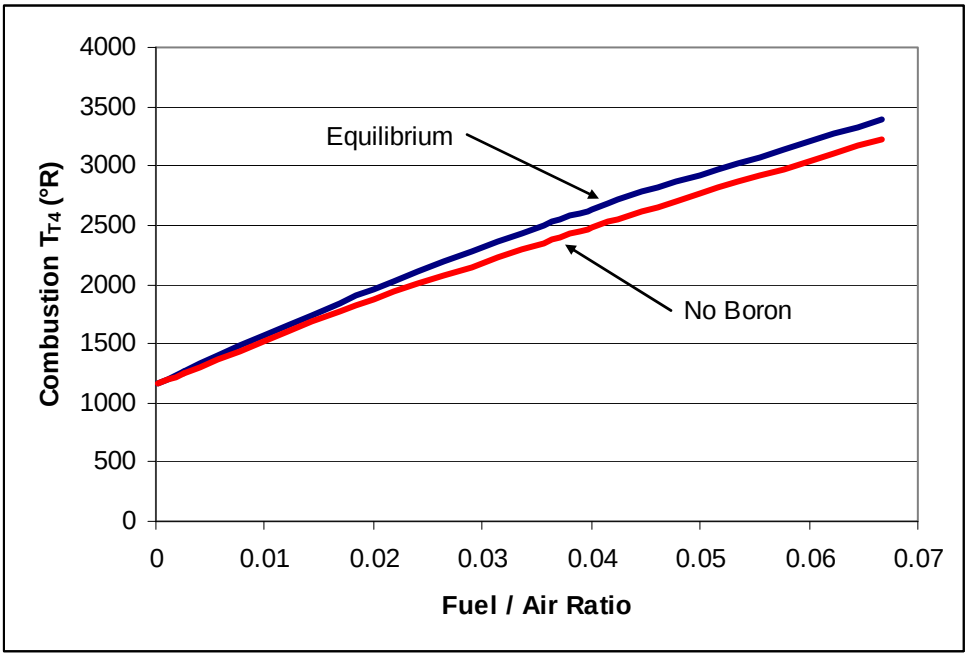

Figure 3.3.2-1 Effect of Boron Combustion on Ramjet Flame Temperature

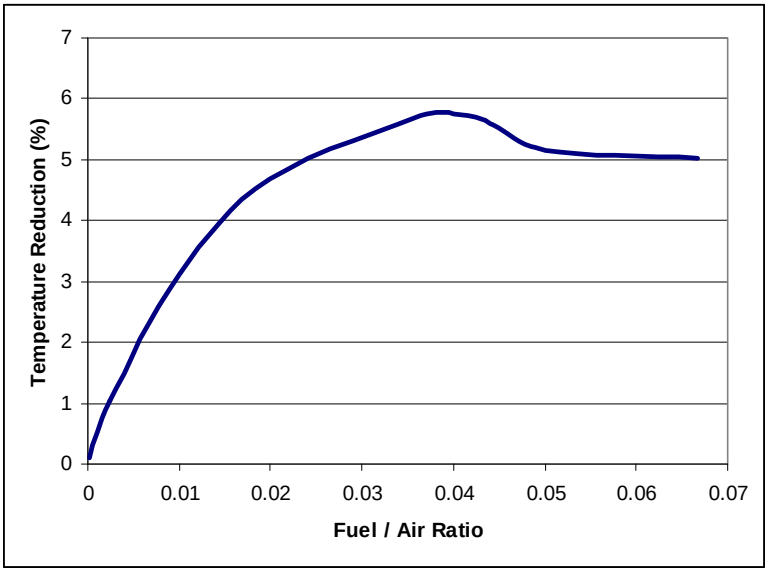

Figure 3.3.2-2 Temperature Decrease by Neglecting Boron

In the region of interest for the FLUENT modeling, the fuel/air ratio is .042, and the corresponding decrease in combustion temperature by neglecting boron is 5.7%. The corresponding total temperature basis for the FLUENT model then becomes:

Test DC-1, T_{T4} = 1279.7 °K (2303.4 °R)
Test DC-3, T_{T4} = 1239.1 °K (2230.3 °R)

Perhaps a better indication of model accuracy would be that under a given set of assumptions, the DC-1 case shows higher combustion efficiency, on the order of a 6% improvement. This is the case in which a significant portion of the fuel is injected axially through a center port in the injector. This distinguishing feature proved significant in the development of the FLUENT model in the following chapter.

CHAPTER 4 – Computational Fluid Dynamics Modeling

With the fuel exhaust characterization experiments, theoretical thermochemical calculations, and validation test data reduction complete, a numerical CFD model of the SSST heavywall combustor was constructed using GAMBIT for grid generation and FLUENT Version 6.2 to solve the steady flow equations for continuity, momentum, and energy. Models were developed with increasing complexity, starting with reacting gas phase only, then adding particle combustion using built-in FLUENT algorithms following the theory described in Section 1.3.3.

4.1 Grid Development

A solid model of the SSST heavywall combustor test hardware was used to create a ¼-slice and imported into GAMBIT to form the vertex and line structure for the combustor inlet, wall, and nozzle. The initial nominal grid spacing was .05 inches, which corresponds to 0.6% of the inlet flow area minimum dimension, 0.8% of the combustor flow area radius, and 1.4% of the nozzle internal radius. A baseline grid was created in this geometry as shown in Figure 4.1-1. Details for a mapped grid are shown in Figures 4.1-2, 4.1-3, and 4.1-4. The models include a total of 783,116 cells for the DC1 configuration, and 730,775 cells for the DC3 configuration, with the differences being mostly in the fuel injector region. The maximum cell skewness is 0.968 for both the DC1 and DC3 cases. Edge boundary conditions were defined for the inlet and combustor walls, inlet flow, and outlet flow as shown in Figure 4.1-1.

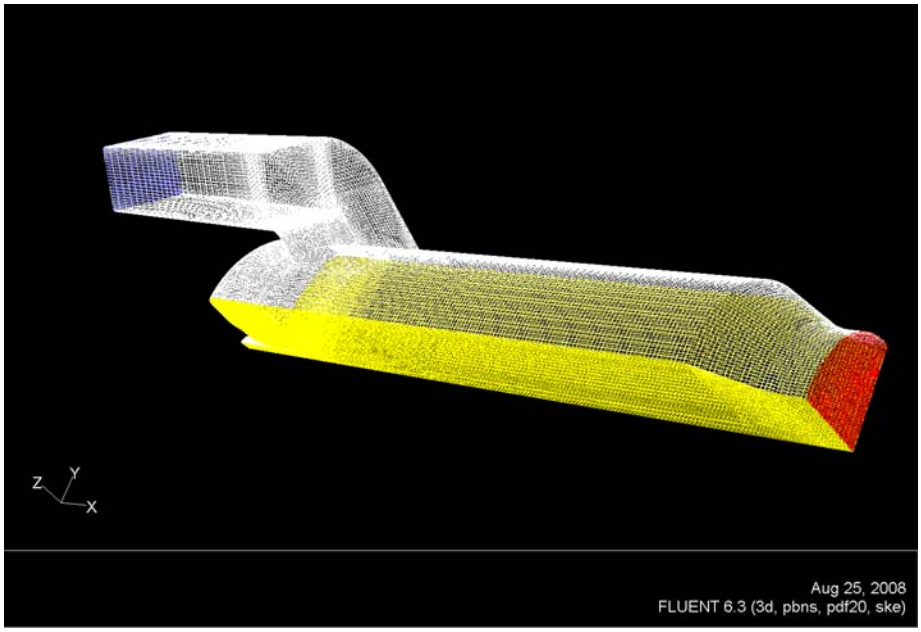

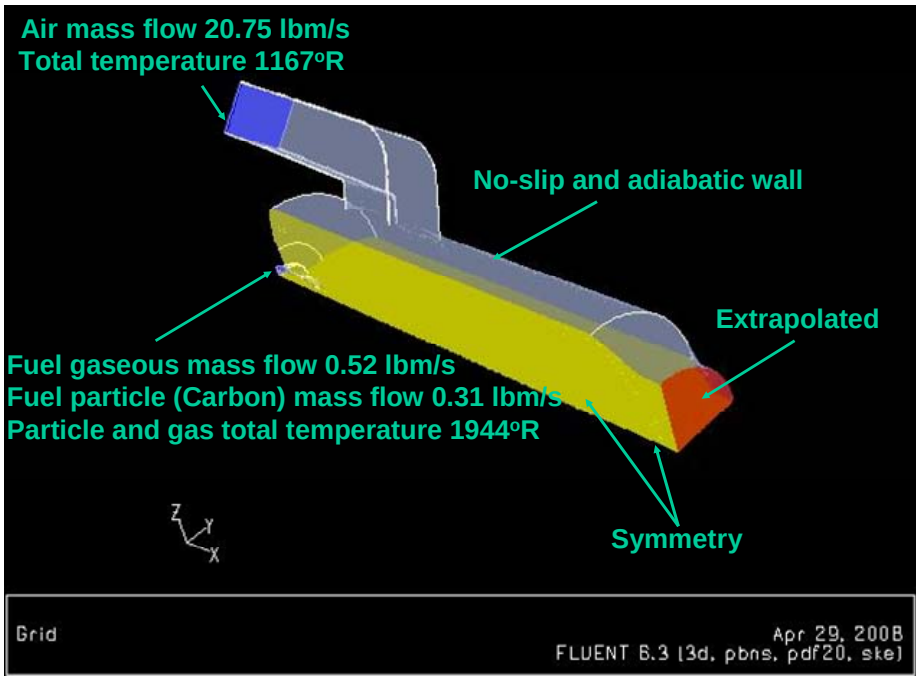

Figure 4.1-1 Baseline Grid and Edge Boundary Condition Designations

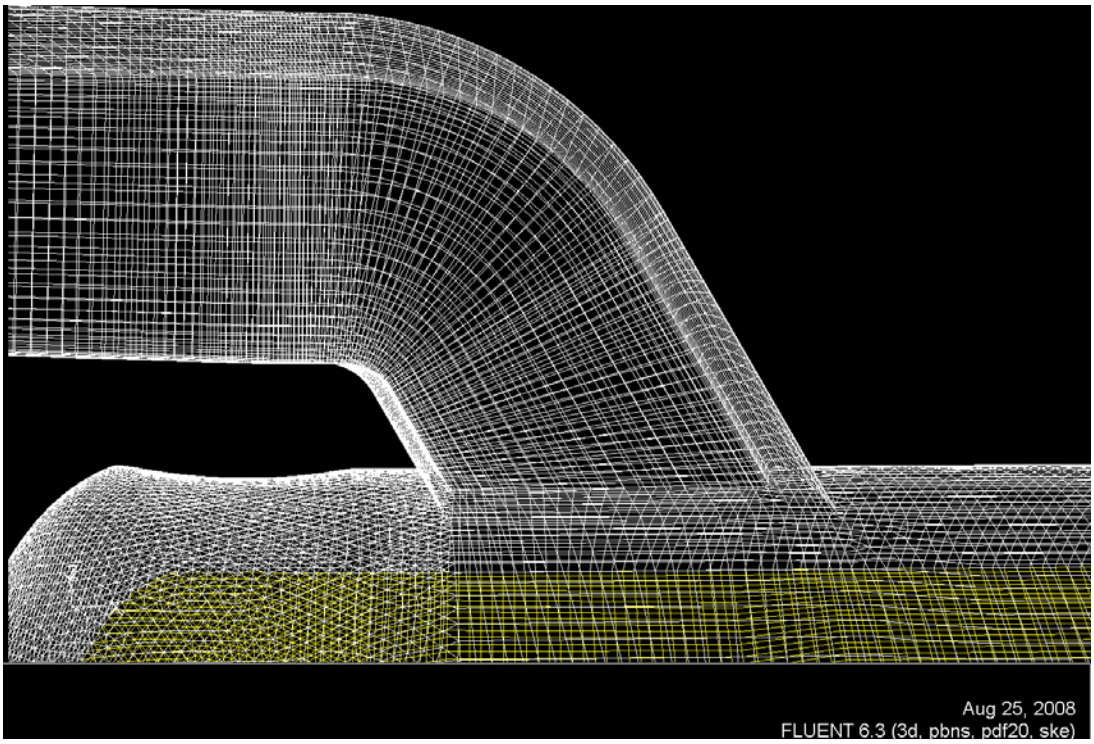

Figure 4.1-2 Baseline .05 in. Nominal Grid – Dump Region

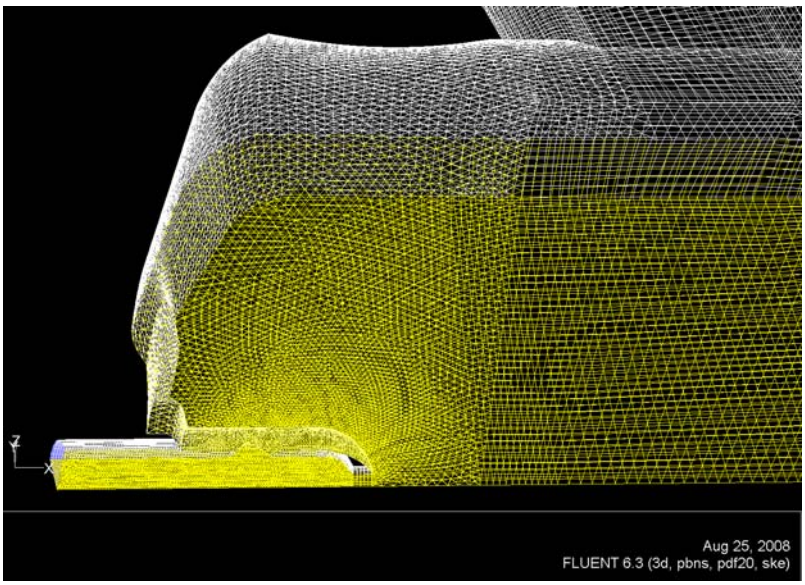

Figure 4.1-3 Baseline .05 in. Nominal Grid – Dome Region

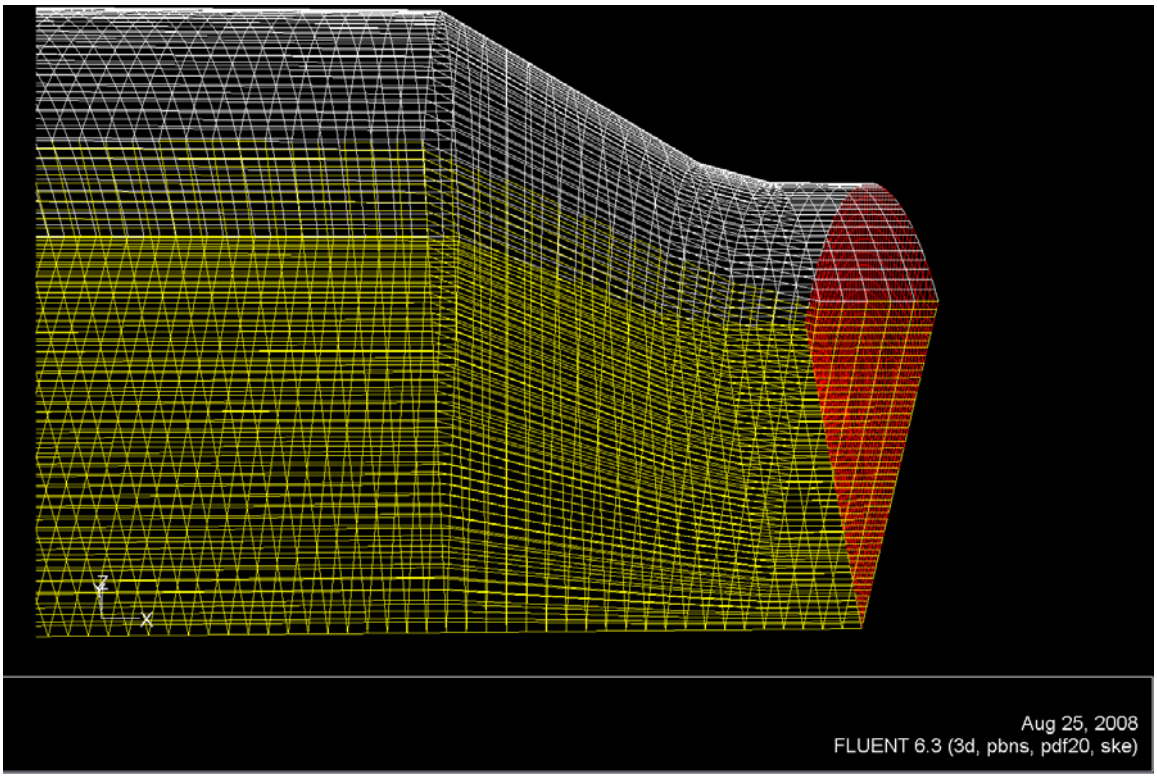

Figure 4.1-4- Baseline .05 in. Nominal Grid – Nozzle Region

4.2 Turbulence Modeling

The turbulence modeling options available in FLUENT 6.2[44] are summarized below:

Spalart-Allmaras model

This is a one equation model that solves a modeled transport equation for the kinematic eddy (turbulent) viscosity. It is not recommended where flow changes abruptly from a wall-bounded to a free shear flow. Turbulent dispersion of particles cannot be included.

k-ε models

Standard k-ε model

This is a two-equation model in which the solution of two separate transport equations allows the turbulent velocity and length scales to be considered. It is known for its robustness, economy, and reasonable accuracy for a wide range of turbulent flows.

Renormalization-group (RNG) k-ε model

The analytical derivation results in a model with constants different from those in the standard k- ε model, and additional terms and functions in the transport equations for k and ε. The RNG model is more responsive to the effects of rapid strain and streamline curvature than the standard k- ε model, which explains the superior performance of the RNG model for certain classes of flows.

Realizable k-ε model

The term "realizable" means that the model satisfies certain mathematical constraints on the normal stresses, consistent with the physics of turbulent flows. A weakness of the standard k- ε model or other traditional k- ε models lies with the modeled equation for the dissipation rate (ε). The well-known round-jet anomaly (named based on the finding that the spreading rate in planar jets is predicted reasonably well, but prediction of the spreading rate for axi-symmetric jets is unexpectedly poor) is considered to be mainly due to the modeled dissipation equation. The realizable k-ε model was intended to address these deficiencies of traditional k-ε models, and was extensively validated for a wide range of flows, including rotating homogeneous shear flows, free flows including jets and mixing layers, channel and boundary layer flows, and separated flows. For all these cases, the performance of the model has been found to be substantially better than that of the standard k- ε model.

<u>k-ω models</u>

Standard k-ω model

This is an empirical model based on model transport equations for the turbulence kinetic energy (k) and the specific dissipation rate (ω). A gradual change from the standard k-ω model in the inner region of the boundary layer to a high-Reynolds-number version of the k- ε model in the outer part of the boundary layer is made. A modified turbulent viscosity formulation is used to account for the transport effects of the principal turbulent shear stress.

Shear-stress transport (SST) k-ω model

Turbulent viscosity is modified to account for the transport of the principal turbulent shear stress.

<u>Reynolds stress model (RSM)</u>

This method solves transport equations for each of the terms in the Reynolds stress tensor. It is good for highly swirling flows and stress driven secondary flows, but 7 additional transport equations are introduced.

Detached eddy simulation (DES) model

RANS modeling with LES for applications in which classical LES is not affordable.

Large eddy simulation (LES) model

The CPU time is prohibitive for complicated flows.

The standard k-ε model was selected here for the baseline calculations. Sensitivity to turbulence model selection was also considered.

4.3 Gas Phase Model

As a first step in the CFD analysis, a gas-phase only FLUENT model was developed for the DC-1 and DC-3 test cases. In order to define the fuel constituents, a simplified representation of the fuel was created. Equilibrium thermochemistry calculations were performed with non-reacting boron to identify the major gas phase fuel compounds to be methane, hydrogen, carbon monoxide, hydrochloric acid, nitrogen, and water as shown in Table 4.3-1.

Table 4.3-1 Gas Generator Throat Products for Non-Reacting Boron

THROAT MASS FRACTIONS AT EQUILIBRIUM CONDITIONS (non-reacting boron)

(BOF)3	0.00001	(FECL2)2	0.00149	(HOBO)3	0.00269
(MGCL2)2	0.00000	B2O3	0.00000	BF3	0.00003
BHF2	0.00000	BOCL	0.00000	BOF	0.00003
BOHF	0.00000	BOHF2	0.00009	**CH4**	**0.05566**
CL	0.00000	CL2	0.00000	**CO**	**0.21625**
CO2	0.01725	FE	0.00000	FECL	0.00000
FECL2	0.01878	FECL3	0.00001	FEF3	0.00000
FEH2O2	0.00000	FEOH	0.00000	H	0.00000
H2	**0.04015**	**H2O**	**0.03115**	H3BO3	0.00184
HBO	0.00000	HOBO	0.00015	**HCL**	**0.09360**
HCN	0.00003	HF	0.00168	MG(OH)2	0.00000
MG<NR>	0.00023	MGCL	0.00000	MGCL2	0.00032
MGCLF	0.00000	MGF2	0.00000	**N2**	**0.04129**
NH3	0.00026	OH	0.00000	**B$<NR>**	**0.05003**
B4C$	0.00000	BN$	0.00000	**C$**	**0.35567**
FE$	0.00000	FE2O3$	0.00000	FE2O3$	0.00000
FE3C$	0.00541	FE3O4$	0.00000	FE3O4$	0.00000
MG$<NR>	0.00000	MGF2$	0.00426	MGO$	0.04685
B*<NR>	0.00000	B2O3*	0.01479	FE3C*	0.00000
FEO*	0.00000	MGO*	0.00000		

These major gaseous products, as well as the solid carbon and boron were extracted and the major inert species were adjusted to account for the neglected products as shown in Table 4.3-2.

Table 4.3-2 Adjusted Throat Mass Fractions

Simplified "Fuel" Mass Fractions		Unaccounted Lumped into Major Gaseous Inerts (CO, N2, HCL)			
Gas Phase		**Gas Phase**		**Total Gas**	**Mass Flow (.875 lb/sec total)** (lbm/sec)
CH4	0.05566	CH4	0.05566		
H2	0.04015	H2	0.04015		
CO	0.21625	CO	0.21625	0.5944	0.52
N2	0.04129	N2	0.06774		
HCL	0.09360	HCL	0.15355		
H2O	0.03115	H2O	0.06100		
Solid Phase		**Solid Phase**			
C	0.35567	C	0.35567	0.4057	0.35
B	0.05003	B	0.05003		
Unaccounted	0.11620				

Thus, with gaseous fuel used as the only injectant, the resulting mass fractions for the major products are shown in Table 4.3-3.

Table 4.3-3 Gaseous Fuel Only Mass Fractions

Gaseous Fuel Mass Fractions	
CH4	0.09365
H2	0.06755
CO	0.36384
N2	0.11397
HCL	0.25835
H2O	0.10263

These fuel ingredients were used as the injectant in a FLUENT model, in addition to vitiated air including appropriate amounts of CO_2 and water. For air heated to 1167°R with propane and makeup oxygen added to reach 21% mole fraction the oxidizer mass fractions are: N2 – 0.737, O2 – 0.233, CO2 – 0.02, H2O – 0.01.

In order to check the results of the FLUENT case, special thermochemistry calculations were required to arrive at a predicted equilibrium combustion temperature with these fuel ingredients and vitiated air ingredients. In order to accomplish this, the heats of formation were calculated using NIST data[44] for each ingredient at the temperature that they are introduced (1944°R for the fuel, and 1166°R for the air). The resulting equilibrium combustion total temperature is shown in Figure 4.3-1, and is expressed in terms of temperature rise combustion efficiency in Figure 4.3-2.

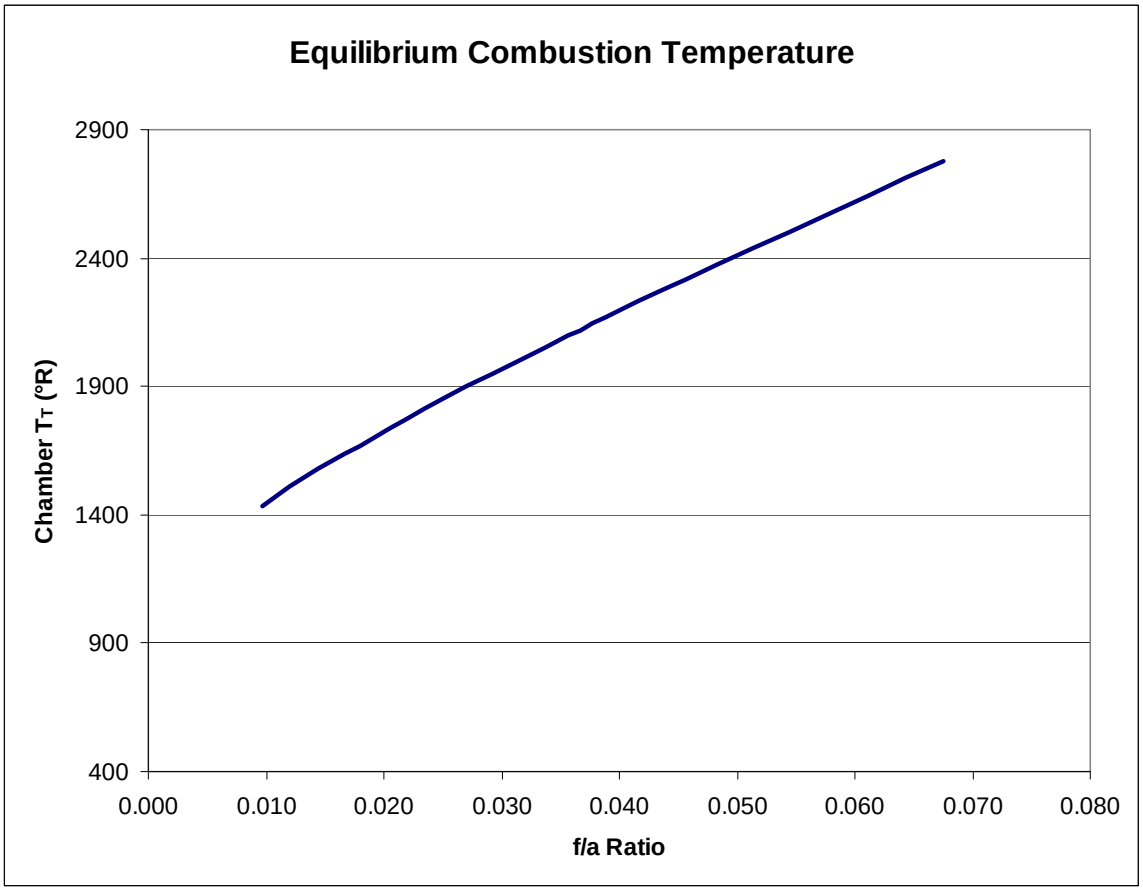

Figure 4.3-1 Combustion Total Temperature for Simplified Gaseous Fuel

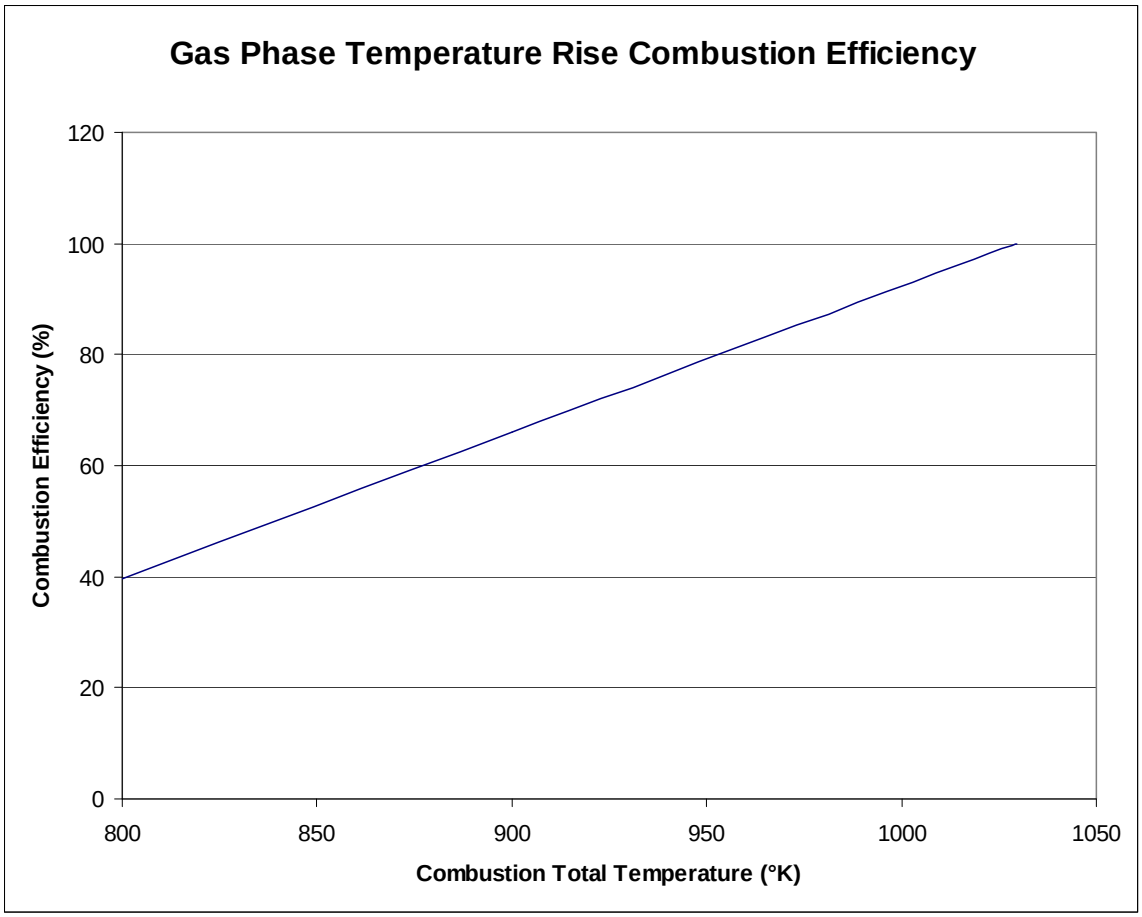

Figure 4.3-2 Combustion Efficiency for Simplified Gaseous Fuel

For the baseline fuel/air ratio of 0.025, the corresponding combustion temperature is 1853 °R.

Non – premixed combustion FLUENT cases were run for test DC-3 with air as the inlet gas and the fuel ingredients as shown in Table 4.3-3. The mass flowrates of 20.75 lbm/sec of air and 0.52 lbm/sec of fuel represent approximately one-fourth of the full scale test mass flowrates. Important options selected for the solver and controls are provided below for the baseline case:

DC3 Case (-102 Injector Configuration):
Mass flow inlet – 20.75 lbm/s
Fuel Inlet boundary condition temperature: 1944R

Fuel Mass Flow: 0.52 lbm/sec (gaseous portion of 0.875 lbm/sec GG fuel flow)

3-D model & grid

Pressure based implicit

K-epsilon turbulence model

Combustion modeling:

- Non-premixed Combustion (Mixture Fractions)
- Radiation Model – P1

Operating Pressure 120psi

Pressure outlet Boundary Condition @ throat (-119 psi)

Solver Options

- Coupled solver
- Initial Courant number of 1, increased to 10, then 50
- Under relaxation factors: Energy 0.5, Mean mixture fraction 0.9, mixture fraction variation 0.9
- First order upwind

Predicted contours of static temperatures are shown in Figure 4.3-3. The contours illustrate that for the gas phase reactions, the majority of the combustion takes place in hot zones in the combustor head end and immediately downstream of the inlet arms. The temperature profile has nearly stabilized by the time the nozzle is reached. This should point to a reasonably high value for combustion efficiency.

Contours of mean fuel mixture fraction are shown in Figure 4.3-4. These contours illustrate again that there is very little unreacted gaseous fuel at the nozzle exit.

The mass-weighted average total temperature calculated for this case at the nozzle exit was 1018.7 °K. Using the thermochemical calculations above, this equates to a combustion efficiency of 97.2%. This indicates that at least the gaseous phase of the fuel injectant should be readily combusting in the ramjet engine. This case also served to validate the thermochemical inputs to the FLUENT model, as they closely matched an independent analysis method.

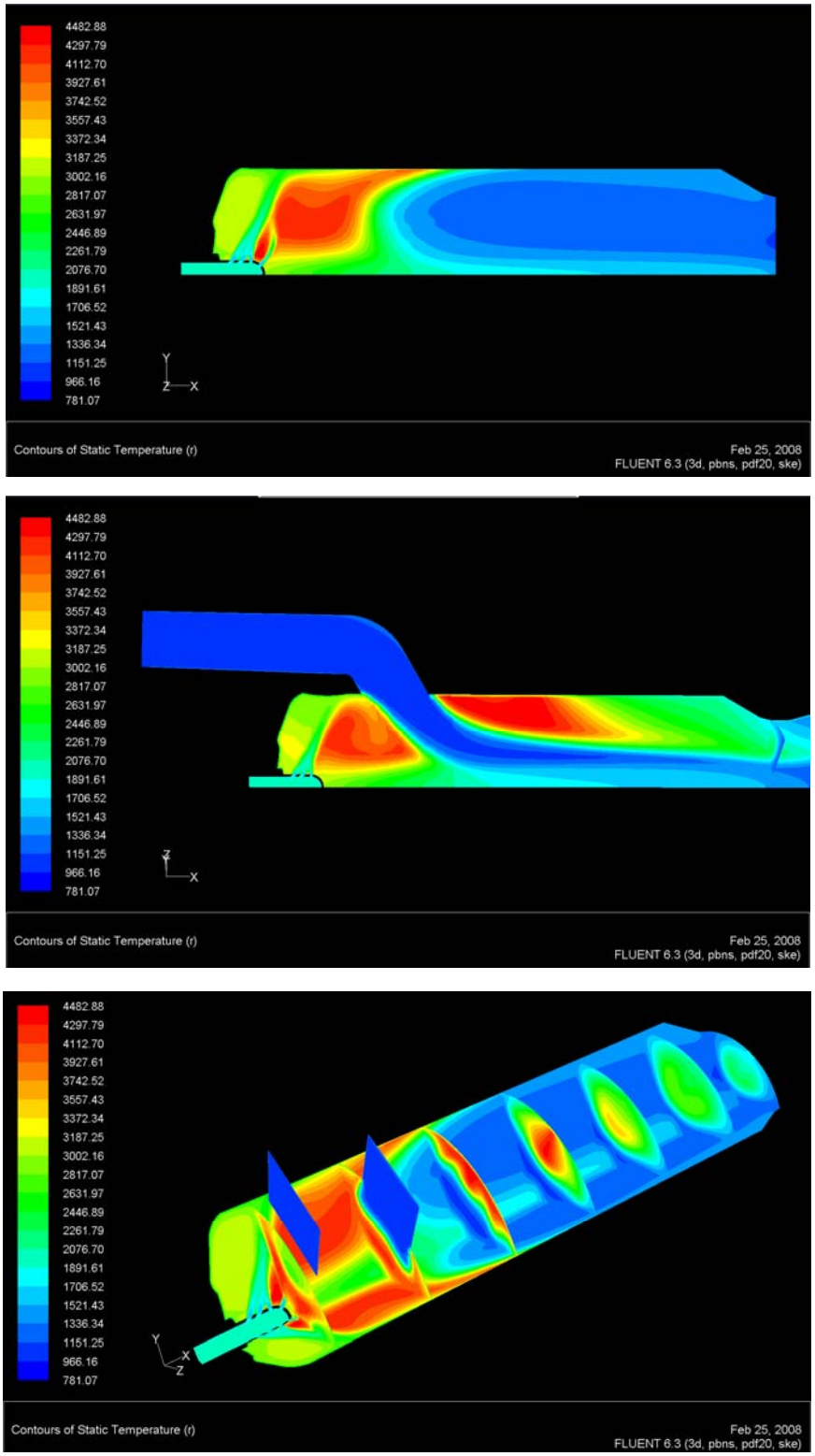

Figure 4.3-3 Predicted Contours of Static Temperatures for Case DC-3 – Gas Phase Only

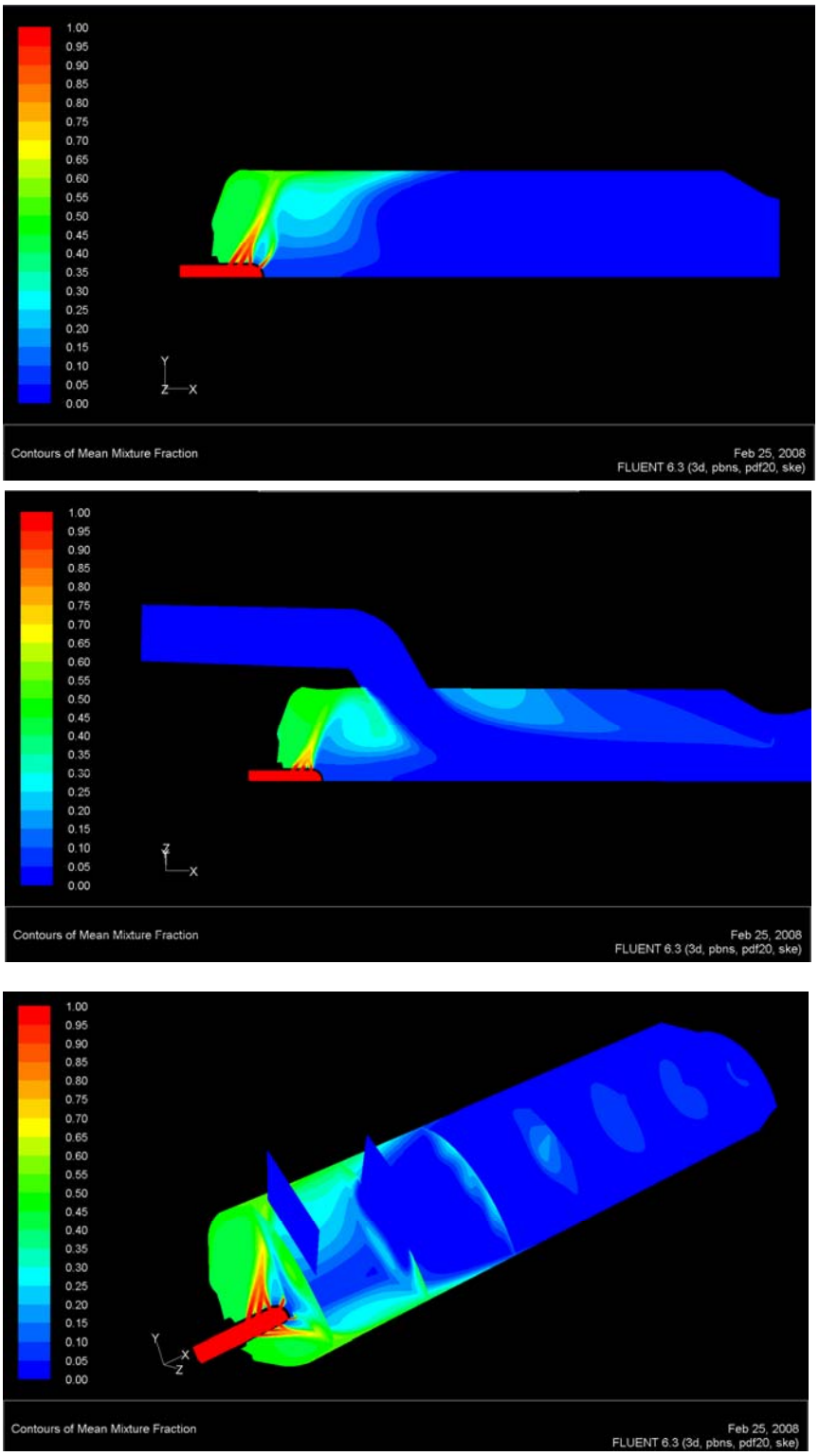

Figure 4.3-4 Predicted Contours of Fuel Mixture Fraction for Case DC-3 – Gas Phase Only

4.4 Particle Combustion Modeling

The next step in the modeling effort was to introduce solid particles as part of the fuel stream. A module is built into the FLUENT code based on pulverized coal particle combustion. The solid phase carbon fuel exhaust was added to the CFD model using this option, using a 20 micron particle diameter based on the collection data, and a mass flowrate based on equilibrium thermochemistry calculations. The small amount of boron present in the fuel was neglected for these studies. Important options selected for the solver and controls are provided below for the particle combustion cases:

Pure C(s) added as a secondary fuel stream to the pdf
- Temperature = 1944R
- Rich Flammability Limit
  - 0.8 for primary stream (gaseous fuels phi=~3)
  - 0.2 for secondary stream (C<s>, stoich = 0.086)

Set up Discrete Phase Model:
Interaction with Continuous Phase
- 10 Continuous Phase Iterations per DPM iteration
- Max # Steps = 10,000, Step Length Factor = 5
- Spherical Drag Law
- Particle Radiation Interaction

Injection Properties:
- Injection Type = Surface, released from "fuel_inlet"
- Particle Type = Combusting
- Material = "carbon-kin/dif-limit" (Fluent Database carbon, with kinetic/diffusion-limited combustion enabled)
  - Diameter Distribution = uniform
  - Oxidizing Species = O2
  - Devolatilizing Stream = secondary
  - Char Stream = secondary
- Point Properties
  - Diameter = 0.0007874 inch = 20 um
  - Temperature = 1944R
  - Velocity Magnitude = 1500 ft/s (matches velocity at "fuel_inlet" surface; this was important to prevent incomplete particle tracking)
  - Total Flow Rate = 0.3112 lbm/s (mdot of solid carbon; solid boron mdot not included)
  - Injected using face normal direction
- Turbulent Dispersion
  - Stochastic Tracking (in the stochastic tracking approach, FLUENT predicts the turbulent dispersion of particles by integrating the trajectory equations for individual particles, using the instantaneous fluid velocity along the particle path

during the integration. By computing the trajectory in this manner for a sufficient number of representative particles (termed the number of “tries"), the random effects of turbulence on the particle dispersion may be accounted for. In FLUENT, the Discrete Random Walk (DRW) model is used. In this model, the fluctuating velocity components are discrete piecewise constant functions of time. Their random value is kept constant over an interval of time given by the characteristic lifetime of the eddies)

Discrete Random Walk Model
# of tries = 10 (default)
Time Scale Constant = 0.15 (default)

Material Properties for Combusting Particle:

Selected “carbon” from the Fluent Database
Density = 124.8517 lbm/ft3
Cp (Btu/lb-R) = 0.2913997
Thermal Conductivity (btu/h-ft-R) = 0.02623823
Latent Heat (btu/lbm) = 0
Vaporization Temperature = 1944R
Volatile Fraction = 0%
Binary Diffusivity (ft2/s) = 0.0004305564
Particle emissivity = 0.9
Particle Scattering Factor = 0
Swelling Coefficient = 1 (stays constant diameter)
Burnout Stoichiometric Ratio = 2.67
Combustible Fraction = 100%
Devolatilization Model (1/s) = 0
Combustion Model = kinetics/diffusion-limited

Additional manual equilibrium calculations were again made for the fuel mixture including particulate carbon and boron as shown in Figure 4.4-1. For the case of gaseous fuel and carbon (no boron), at a fuel/air ratio of .04, the total temperature is 1401°K. Also shown is a traditional equilibrium thermochemistry calculation performed the traditional way using fuel raw ingredients as the ingredients. The results are very close to the piece-wise technique required due to the simplified fuel chemical modeling.

air	20.75	lb/sec		a/f
fuel	0.52	lb/sec		24.9639
boron	0	lb/sec	0.044	
carbon	0.3112	lb/sec		
total fuel	0.8312	lb/sec		

		MF	mass	tot MF
fuel (1080K	CO	0.36387	0.189212	0.2276
	CH4	0.093656	0.048701	0.0586
	N2	0.11398	0.05927	0.0713
	H2	0.067558	0.03513	0.0423
	HCL	0.25839	0.134363	0.1616
	H2O	0.10256	0.053331	0.0642
	B	1	0	0.0000
	C	1	0.3112	0.3744
			total	1.0000

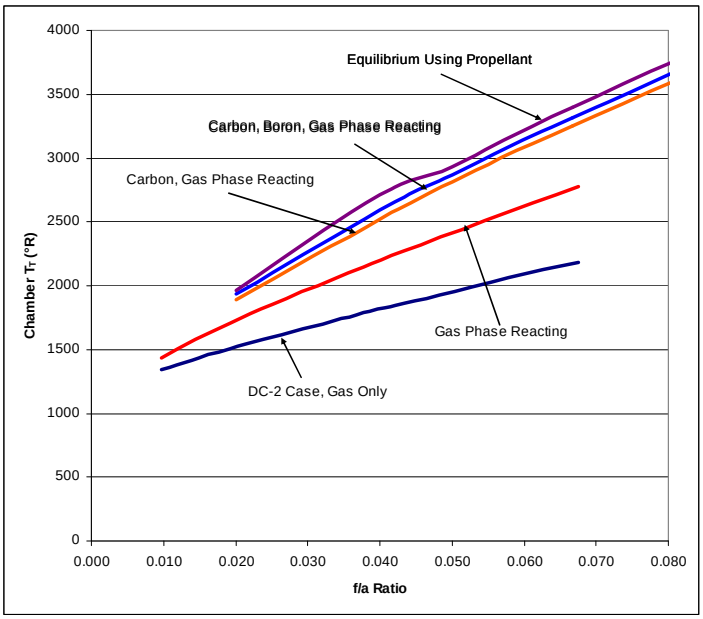

Figure 4.4-1 Thermochemistry for Gas Phase and Carbon Particles

The initial results indicated that any axial particles in this size range injected axially would bypass the significant combustion zones and exit the combustor unreacted. Figure 4.4-2 shows the carbon particle mixture fraction for a representative case, and Figure 4.4-3 shows the particle traces for test DC-1, in which the axially injected particles are predicted to essentially pass through most of the combustor unreacted.

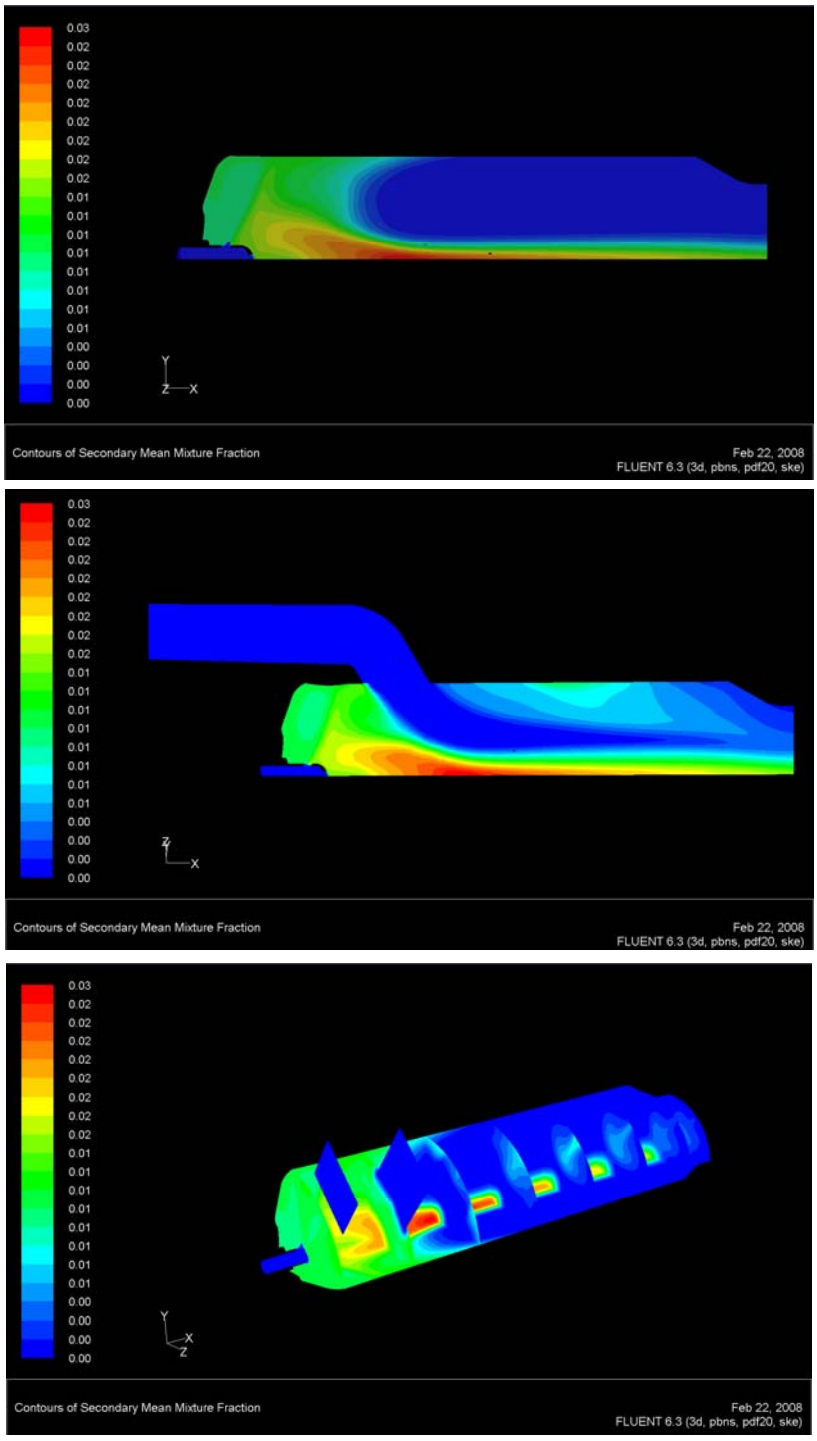

Figure 4.4-2 Predicted Mixture Fraction for Carbon Particle Fuel for Case DC-3

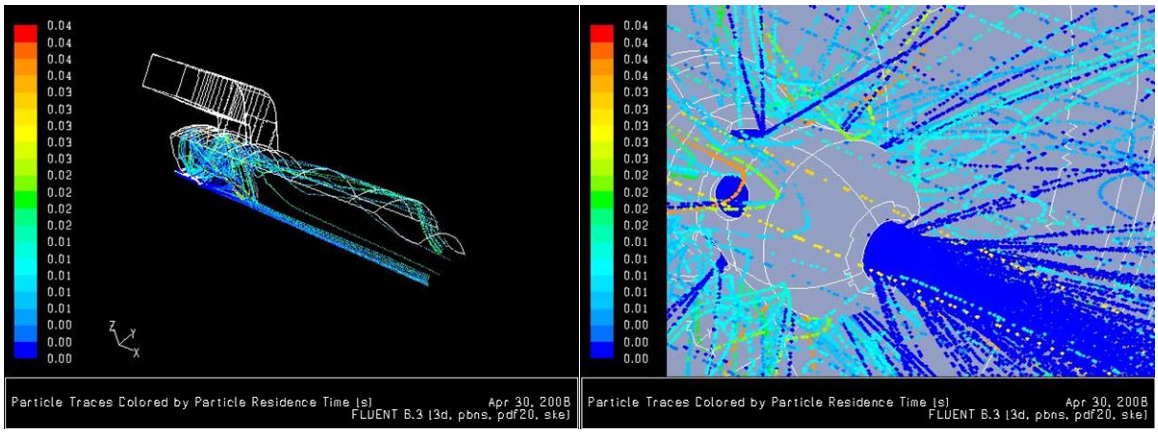

Figure 4.4-3 Predicted Case DC-1 Particle Traces

Another concern with the initial particle combustion runs was that the DC-3 combustor configuration (with all radial fuel injection) showed higher mean total temperatures at the nozzle exit. This is in direct contradiction to the ground test results. Representative temperature profiles for tests DC-1 and DC-3 are shown in Figure 4.4-4, illustrating the higher temperatures at the nozzle exit.

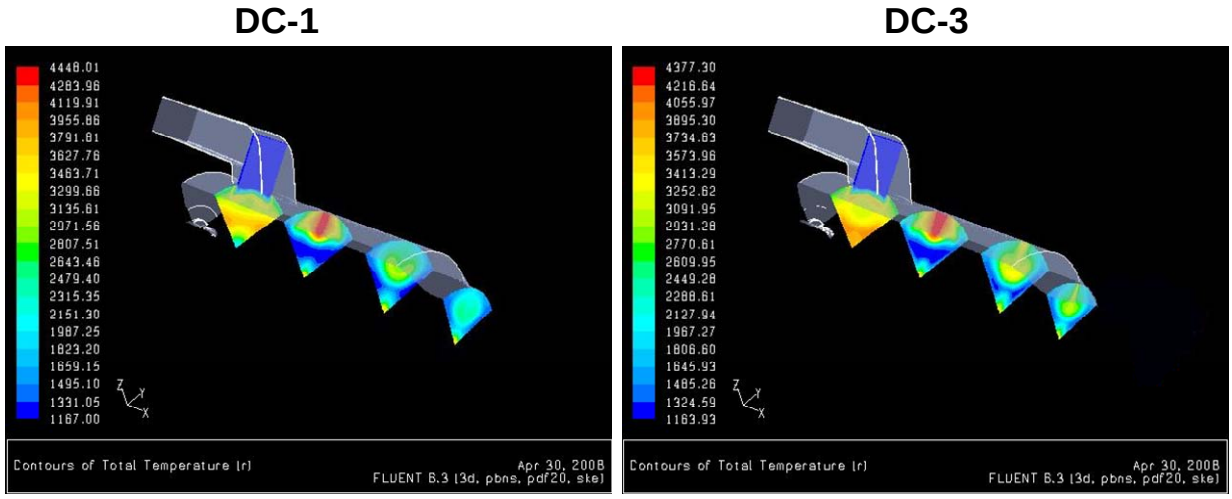

Figure 4.4-4 Predicted Temperature Profiles for Tests DC-1 and DC-3

The conclusions drawn from the initial FLUENT runs for both DC-1 and DC-3 were that:

1) If using a pulverized coal carbon combustion model and particle diameters obtained from ground testing for the solid phase, insufficient particle combustion would take place to match test temperature rise results

2) Axial carbon particle injection such as DC-1 results in lower combustion efficiency as the particles pass through unreacted, in direct contrast to the test results, wherein DC-1 presented higher performance

Options available to numerically increase solid phase particle combustion consist of:

- Arbitrarily decrease mean particle size

- Utilize a particle size distribution (test data exist), as the smaller particles react and provide a heat source to accelerate the combustion of larger particles

- Arbitrarily increase the reaction rate coefficient. No data exist for solid ducted rocket carbon reaction rates

- Decrease the injected particle velocity relative to the fuel gas phase to reduce axial momentum and enhance mixing. The baseline cases were run with particle velocity matching the gas phase.

A series of FLUENT cases were run to help determine trends for these various assumptions. The results are shown in Table 4.4-1.

Table 4.4-1 Carbon Combustion Parametric Results

	Fraction of Carbon Burned lbm/s	Total Temperature at Exit oR
DC-3 with nozzle		
Gas only, Tf=1944oR	n/a	
Baseline reaction rate	0.143	2107
Double reaction rate	0.196	2231
10X reaction rate	0.311	2374
Injection velocity 10 fps	0.136	2013
Particle size 2 microns	0.311	2288

Test data - 2358 R

The parametric FLUENT particle results show that simply adding a particle size distribution or increasing reaction rate will improve combustion, but not show improved DC-1 combustion over DC-3. The demonstrated temperature rise can be achieved in the FLUENT model if all carbon is forced to react (10X rate case). The conclusions drawn from these parametric runs were:

Carbon reaction rate -> strong effect
Particle size -> strong effect
Particle initial velocity -> little or none
Turbulence dispersion -> strong effect with small particles, less effect with large particles (for large particles on the order of 20 microns there is less interaction with the gas flow and particle dispersion effects are minimal).

Interestingly enough, runs made with just the gas phase reacting for DC-1 and DC-3 show improved performance for DC-1, in better agreement with the test data. Representative temperature profiles for the two cases are shown in Figure 4.4-5. Since the gas phase only FLUENT runs indicate that DC-1 has higher performance, the

conclusion can be reached that the fuel solid phase likely contains a large fraction of sub-micron carbon particles that follow the gas flow and react quickly, or less carbon is produced than equilibrium calculations would predict. The remaining carbon would likely be in the form of higher molecular weight gases that do not fully react in the gas generator and are introduced to the combustion process as part of the fuel gas phase. In either case, the FLUENT model must be adjusted to account for a large portion of the fuel particulates that are more closely coupled to gas phase reactions than the particle combustion model.

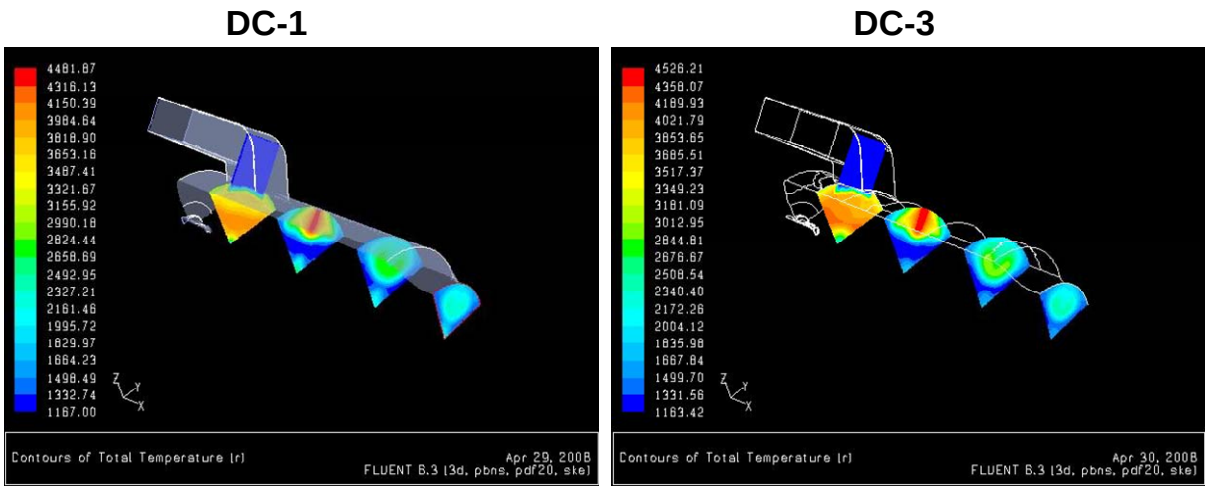

Figure 4.4-5 Predicted Gas Phase Combustion Profiles for Tests DC-1 and DC-3

The next, and final, series of runs in model development were undertaken to replace a fraction of particulate carbon in the fuel with gaseous fuel constituents. This was done to test the hypothesis that all the carbon in the fuel was not introduced as 20 micron particles as the particle collection tests would lead one to believe. Although visible in the exhaust, they may actually only make up a small percentage of the mass flow, and may in fact represent agglomerates of much finer soot particles.

Table 4.4-2 shows the matrix of runs made with the fraction of solid carbon in the fuel varying from 100% down to 3.2%, with the resulting mass fractions of gaseous species.

Table 4.4-2 Fuel Solid Phase Substitution

Percent of C in solid phase	100% C is solid	3.2% is solid	20.0% is solid	40.0% is solid	60.0% is solid
CH4	0.0937	0.0593	0.0633	0.0689	0.0756
H2	0.0676	0.0428	0.0457	0.0497	0.0545
N2	0.1140	0.0722	0.0771	0.0839	0.0920
H2O	0.1026	0.0649	0.0694	0.0755	0.0828
HCL	0.2584	0.1636	0.1747	0.1901	0.2085
CO	0.3639	0.2304	0.2461	0.2677	0.2936
C	0.0000	0.3668	0.3238	0.2642	0.1931
SUM	1.0000	1.0000	1.0000	1.0000	1.0000
Fraction of C in particle form		0.0321	0.2000	0.4000	0.6000
Fraction of C in "gaseous" form		0.9679	0.8000	0.6000	0.4000
Gaseous fuel flow rate, lbm/s	0.52	0.52	0.52	0.52	0.52
Particle carbon flow rate, lbm/s	0.3112	0.0100	0.0622	0.1245	0.1867
"Gaseous" carbon flow rate, lbm/s	0	0.3012	0.2490	0.1867	0.1245
SUM	0.8312	0.8312	0.8312	0.8312	0.8312
Gaseous fuel and "gaseous" C flow rate, lbm/s	0.5200	0.8212	0.7690	0.7067	0.6445

As the validation ground tests were conducted with fuel containing boron, an adjustment is required to compare results of the FLUENT calculations in which the boron is ignored. For the specific case with an air temperature of 1167°R, a combustion pressure of 125 psia, and fuel/air ratio of .04, the theoretical combustion total temperature is 2553 °R. The combustion efficiencies obtained from the validation tests as discussed in Section 3.3.2 are restated below:

Test DC-1 ηc = 93.6%, T_{T4} = 1279.7 °K (2303.4 °R), boron neglected

Test DC-3 ηc = 87.9%, T_{T4} = 1239.1 °K (2230.3 °R), boron neglected

The FLUENT model results for cases varying the fraction of fine/large carbon particles are shown in Figure 4.4-6. The curves labeled DC-1 and DC-2 represent the

baseline CFD results for the two configurations, and the curves labeled DC-1 Test and DC-3 Test are the average values of combustion efficiency reported for the first twenty seconds of the ramjet direct-connect test. As the 20 micron particles are replaced with gaseous species, the absolute levels of combustion efficiency increase, and approach the magnitudes seen in the validation direct-connect testing. Initially DC-3 shows improved performance over DC-1, but as the gaseous fraction increases, DC-1 is predicted to show 5-6% better combustion efficiency. This behavior is in good agreement with the performance levels and trends observed in testing. These results confirm the hypothesis that a large portion of the carbon soot predicted by equilibrium thermochemistry is in fact sub-micron in size and/or is actually still in the form of gaseous hydrocarbons. With these results in hand, the baseline model development was considered complete.

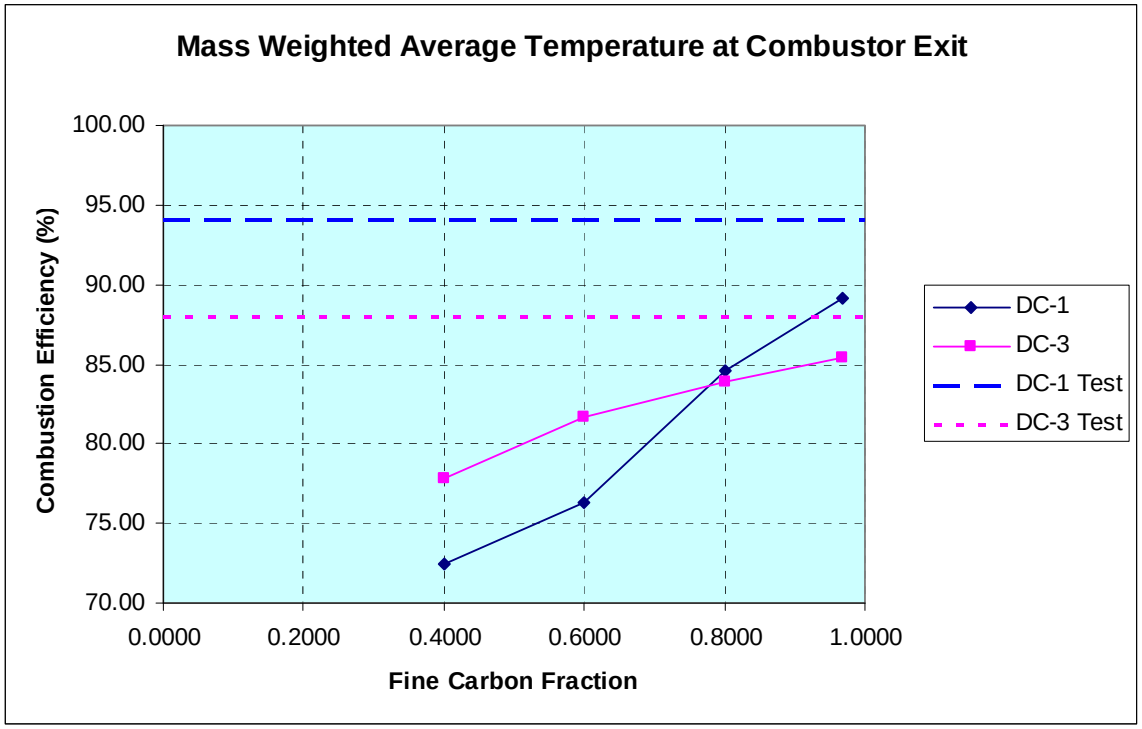

Figure 4.4-6 Combustion Efficiency as a Function of Fine Carbon

4.5 Model Parametrics

Additional FLUENT runs were conducted to evaluate the sensitivity of the model results to select modeling parameters. The results indicated that there is little variation in solutions such that the baseline case assumptions remained valid.

4.5.1 Turbulence Model

The realizable k-ε model was chosen as the most applicable scheme to compare to the baseline model results as discussed in Section 4.2. Figure 4.5.1-1 presents the baseline model data compared to the realizable turbulence model. The curves labeled DC-1 and DC-2 represent the baseline CFD results for the two configurations, and the curves labeled DC-1 Realizable and DC-3 Realizable are the values of combustion efficiency obtained with the realizable turbulence model. All other parameters were left unchanged in the analysis. As seen, the levels of combustion efficiency for the two models compare favorably at all levels of gaseous fuel fraction, validating the use of the standard k-ε model for all other analysis.

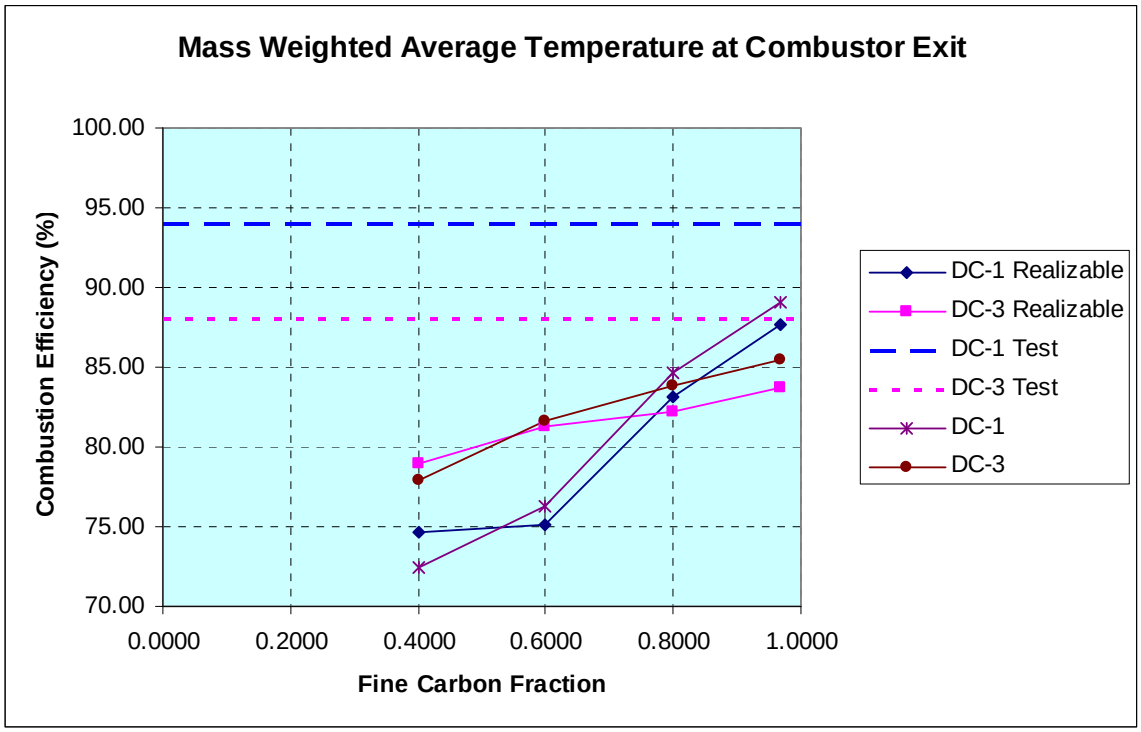

Figure 4.5.1-1 Model Results for Realizable k-ε Model

4.5.2 Higher Order Calculations

As another check on model sensitivity, a second order upwind analysis was made. While the first-order upwind discretization generally yields better convergence than the second-order scheme, it generally will yield less accurate results, especially in situations in which the flow is not aligned with the cell face. A comparison of second order discretization compared to the first order baseline computations is shown in Figure 4.5.2-1. Again in this case very good agreement is seen with the baseline analysis.

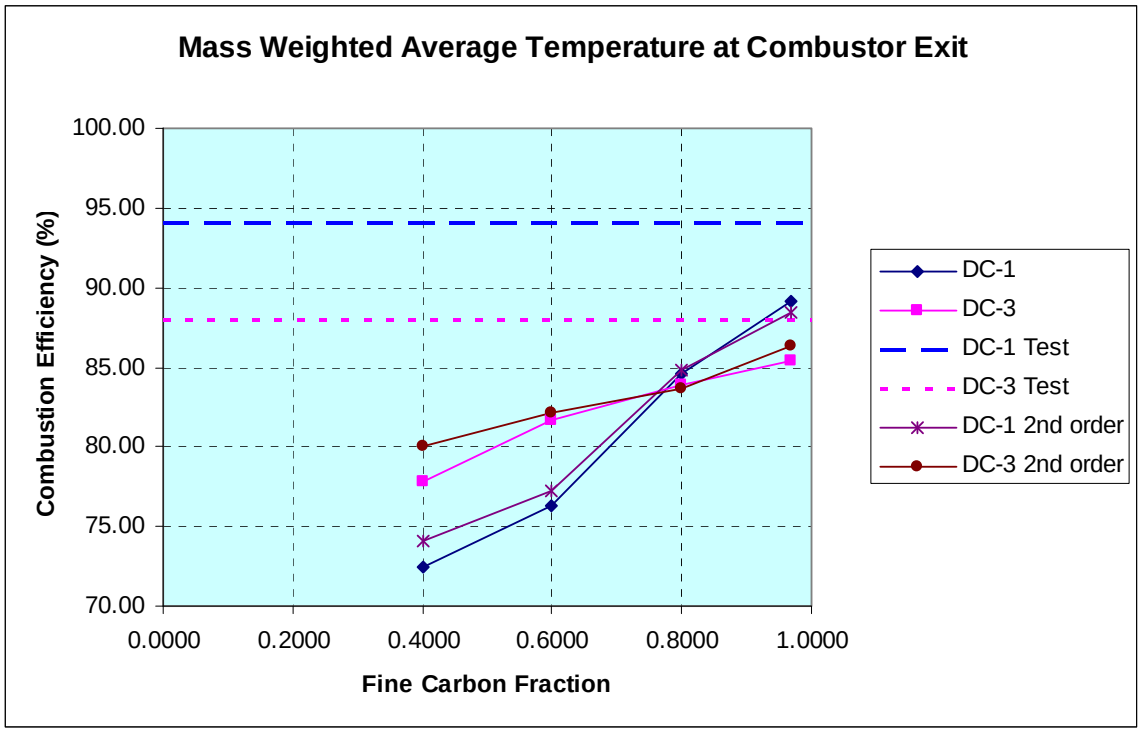

Figure 4.5.2-1 Second Order Model Results

4.5.3 Grid Dependency

In order to evaluate the effects of grid size on model accuracy, a finer grid was created by bisecting each edge of the baseline grid for the DC-1 case. DC-1 was used for the grid dependency analysis as it was felt to present a more complex flow environment due to the strong axial component of particulate fuel injection. The number of cells increased from 783,000 to 6,290,000. A dramatic increase in computation time was observed for each iteration. The mass-averaged exit flow temperature history is shown in Figure 4.5.3-1 as the iterations proceeded over a period of 10 days using sixteen CPUs. Although a decrease in exit temperature of over 50 degrees is seen, it was unclear whether a larger amplitude sinusoidal pattern would result with continued computations, and where the solution would eventually converge. In order to more aggressively approach the solution the momentum under-relaxation factor was increased from 0.1 to 0.3, and the Courant Number was increased from 20 to 50. The resulting temperature convergence history is seen in figure 4.5.3-2.

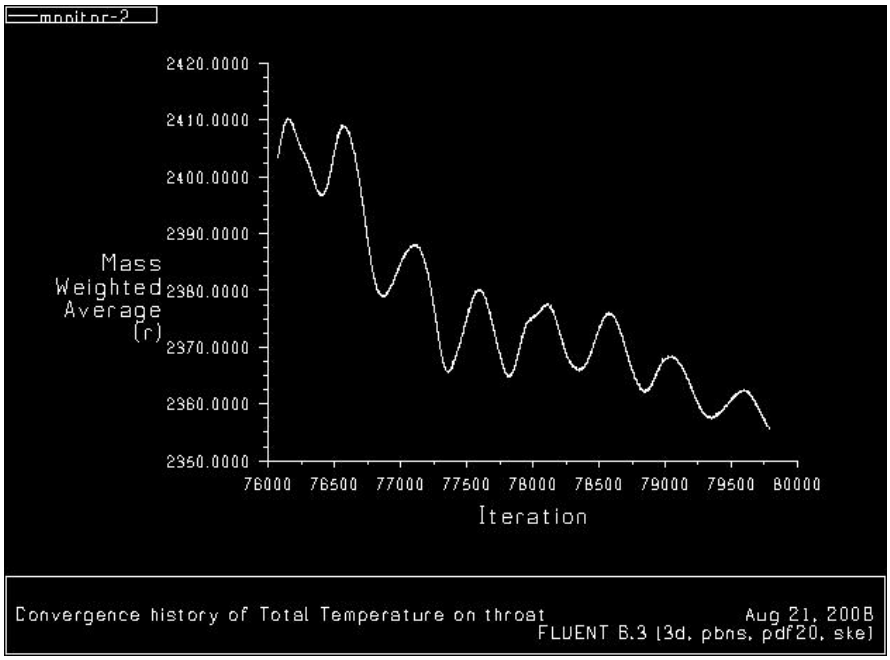

Figure 4.5.3-1 Fine Grid Convergence History – Baseline Under-Relaxation

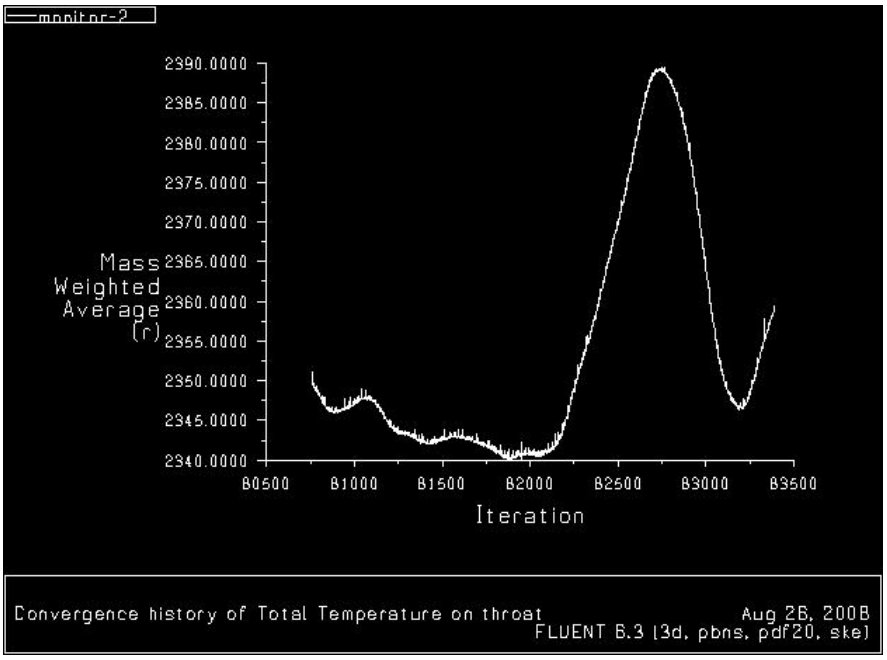

Figure 4.5.3-2 Fine Grid Convergence History – Aggressive Under-Relaxation

With the more aggressive under-relaxation the expected sinusoidal behavior was observed but the required computation time required to reach convergence again was prohibitive.

A simpler case using gas phase fuel combustion only for case DC-1 was then used to examine the effect of a finer grid. This appeared a reasonable approach since the CFD results had shown that test data matched predicted model temperatures more closely when the majority of fuel was included in the gaseous phase. In this case the fine grid converged much more quickly and demonstrated good agreement with the baseline grid. The mass-averaged total temperature at the throat was 2397°R for the baseline grid, and 2407°R for the fine grid.

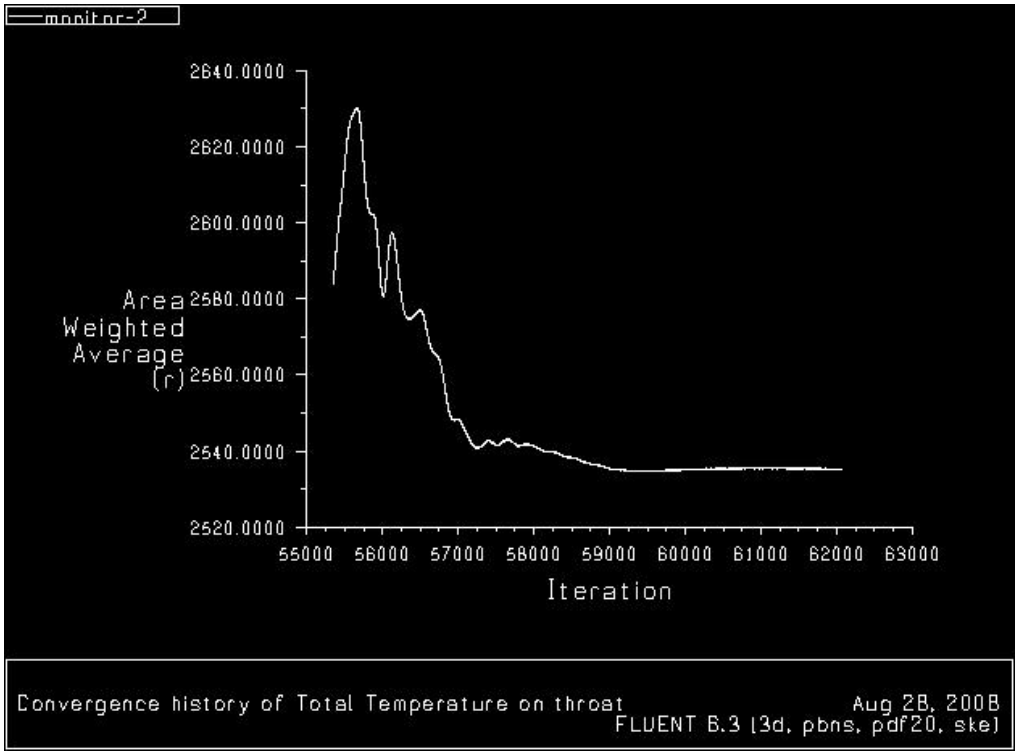

Figure 4.5.3-3 Fine Grid Convergence History – Gas Phase Combustion Only

The basic flow structure for the fine grid and baseline grid compared well, as shown in Figure 4.5.3-4. There was little change in internal flow patterns, with the exception of very near the nozzle exit, where slightly higher Mach numbers are seen. If greater resolution is desired in this nozzle for other applications it would prove wise to transition to a finer mesh in the nozzle, while maintaining the baseline grid sizing to speed computations. For the present research the baseline grid was judged to be sufficiently accurate, and offered reasonable computation times for convergence.

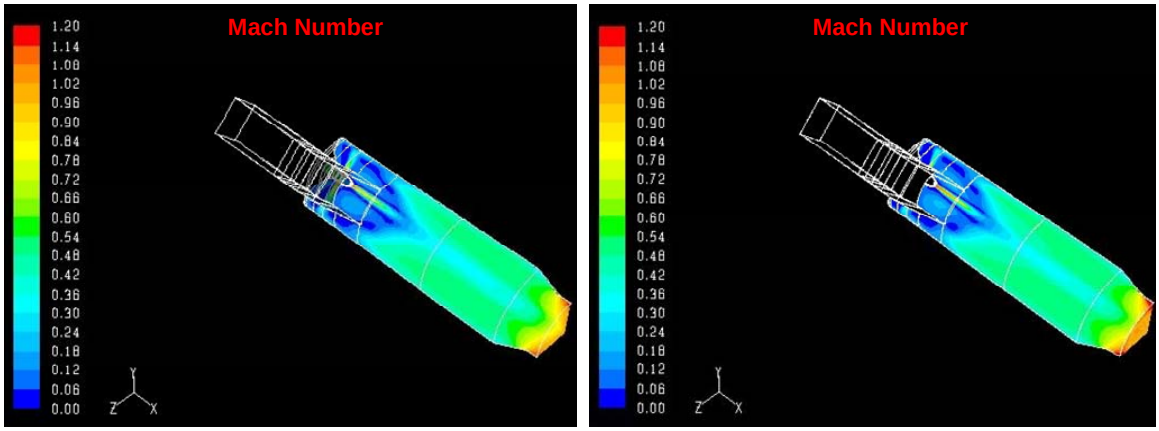

Baseline Mesh **Fine Mesh**

Figure 4.5.3-4 Fine Grid Convergence History – Gas Phase Combustion Only

CHAPTER 5 - Conclusions and Recommendations

The present research was undertaken to numerically model a very complex combustion flow problem, including multi-phase fuel injection with momentum and temperature through a ported injector into a highly turbulent combustor flowfield. This type of flow is found in practice in pulverized coal combustors and ducted rocket ramjets, for example. The approach taken was to develop an understanding of a baseline ducted rocket combustion case, primarily focused on characterization of the fuel properties, followed by the development of a numerical model and comparison to combustion test data for the baseline case.

The ducted rocket engine used as a basis for computational model development was the MARC-R282, developed by Aerojet for the SSST missile target. This is a four-inlet side-dump combustion chamber with no flameholding devices. The solid fuel is partially combusted to produce a fuel rich mixture containing combustible gases and carbon soot that are injected into the main airstream in the combustor.

The first step in the investigation was to develop a better understanding of the gas generator exhaust properties. This process included conducting experiments to investigate the propellant burning surface (window bomb and particle collection tests), the gas generator exhaust prior to mixing with air (static motor firings with exhaust sampling), and the flow exiting the combustor exit nozzle (direct-connect ramjet tests with exhaust sampling). Important conclusions drawn from these experiments were: 1) the polystyrene used as a fuel ingredient was shown to begin reacting very close to the propellant surface and with reactions completed prior to injection into the combustion chamber, 2) the boron fuel ingredient was shown to be incompletely reacted exiting the gas generator early in the firing, and 3) the particles collected from the gas generator exhaust were not spherical, but highly irregular with a wide range of sizes, and were found to have a mean effective particle diameter of 20 microns.

In order to formulate a set of test data to validate a computation model, a series of ground test ramjet test data was collected and analyzed for different fuel injector geometries in the MARC-R282 engine. Two distinct injector geometries formed the basis for the comparison; one with a large axial component to the injector flow, and one

with nearly all injectant directed radially. The combustion efficiency for the version with axial fuel injection was shown to be roughly 6% higher than the radial injector. This difference in performance caused by injector geometry was used to test the predictive capability of the model developed in this project.

A computational model was developed using the FLUENT 6.2 commercial CFD code. First, a simplified "fuel" was developed for the gas-phase components based on equilibrium thermochemistry calculations. This fuel was injected in a CFD model of the MARC-R282 combustor at air flow conditions matching the ground test data. FLUENT predicted temperature-rise combustion efficiencies approaching 100%. The gas-phase model served to validate the thermochemical inputs to the CFD computations, and provided confidence that the combustor flowfield was conducive to efficient combustion if the kinetic limitations inherent in the fuel are not exceeded.

A second simplified "fuel" was then developed for FLUENT modeling adding particulate carbon at a mass fraction predicted by equilibrium thermochemistry for the gas generator exhaust. The built-in routines developed for pulverized coal particles in FLUENT were used, with a mean particle diameter of 20 microns, based on the data collected from the ground test experiments. The solid boron particles contained in the exhaust were neglected for this study due to their low concentration. The model predictions for this particulate-laden fuel for the two validation test cases showed a trend opposite to that seen in ground testing, i.e., the axial injector geometry resulted in lower combustion efficiency than the radial injector. This was shown to be a result of poor dispersion of the solids and incomplete particle combustion.

It was then theorized that potentially some fraction of the particulates were in fact much smaller than those collected, and the actual mass fraction of solids in the exhaust was smaller than equilibrium thermochemistry would predict. To test this hypothesis a series of FLUENT cases was run in which a varying portion of the particulate exhaust was replaced with gaseous fuel. The cases showed that as the solid fuel fraction was reduced, the difference in model predictions narrowed and actually reversed to be consistent with the ground test data. This indicated that the soot particles collected in experiments may actually be a small mass fraction of the total fuel exhaust, and may in fact be agglomerates of much finer soot particles introduced with the fuel. The absolute

combustion efficiencies predicted by the revised FLUENT model were also very close to matching levels seen in ground testing.

These results served to verify the accuracy and predictive capability of the computational model. The robustness of the computational model was also evaluated parametrically by examining the effects of turbulence model, order of discretization, and grid size. Comparable trends and results were seen for all cases examined.

This study clearly demonstrated the usefulness of planning an engineering project combining CFD with complementary experimental data. By simply relying on the laboratory data collected for particle sizes with a single ground test configuration, one could have used the many variables at hand to force the particle combustion to fit the test data and been misled in the process. By considering multiple sets of ground test data, guided by CFD interpretations, a much more complete understanding of the process was reached.

This combustor analysis tool can now be employed for similar flow problems involving particulate-laden fuel injected with high velocity and temperature. For the specific problem investigated, the model was able to help understand particle behavior in a combustion environment, with results correlated to ground test observations. The results show that for the MARC R282 engine it should be possible to use the model to identify hardware changes to manage the fuel and air mixing to improve combustion efficiency, and thereby reduce the amount of visible soot in the exhaust. Indeed, for initial combustor design efforts to improve the MARC R282 combustor it may be possible to neglect the particulate fuel phase altogether until more rigorous modeling is needed. Nonetheless, the framework exists in this modeling approach to investigate future flow problems in which larger particles are present and a more substantial influence on the combustion process.

Additionally, the analytical studies and data collected in this project indicated that the polystyrene is likely the cause of the majority of the soot produced. In addition to flow management to improve combustion efficiency, this also would suggest chemical formulation approaches as a possible avenue to reducing soot in the exhaust. Options could include the use of alternate fuels or the use combustion catalysts in the fuel formulation.

This combustion problem is complex, and there are many assumptions made that further research may be directed toward. Recommended areas to focus future attention on include: 1) actual gas temperature measurements, 2) boron combustion modeling, 3) tests to determine boron combustion levels in the ramjet combustor, and 4) fuel exhaust gas sampling to determine gaseous species and molecular weight.

References

1 Baum, M.M., and Street, P.J., "Predicting the Combustion Behavior of Coal Particles", Combustion Science Technology, Vol 3 pp. 231-243, 1971.

2 Corporan, E., Oppelt, J.B., and Buckley, P.L., "A Ducted Rocket Fuel Injector Evaluation with a Gas Generator Simulator", 1992 JANNAF Propulsion Meeting.

3 Wilson, K.J., Shadow, K.C., Gutmark, E., and Smith, R.A., "Passive Combustion In a Ducted Rocket with Side Mounted Inlets" 1990 JANNAF Propulsion Meeting, Anaheim, CA 3-5 Oct 1990, pp383-396.

4 Magnussen, B.F., and Hjertager, B.H., On Mathematical Modeling of Turbulent Combustion with Special Emphasis on Soot Formation and Combustion", 16th Symposium (International) on Combustion, pp. 719-729, The Combustion Institute, Pittsburgh, 1976.

5 Field, M.A., "Rate of Combustion of Size-Graded Fractions of Char from a Low-Rank Coal between 1200K-200K", Combustion and Flame, 13:237-252, 1969.

6 Peters, A.F. and Weber, R. (1997), Mathematical Modeling of a 2.4 MW Swirling, Pulverized Coal Flame, Combustion Science and Technology, 122, 131.

7 Edelman, R.B., and Harsha, P.T., "Modeling Techniques for the Modeling of Ramjet Combustion Processes" AIAA Journal, Vol. 19, No. 5, May 1981.

8 Lilley, D.G., "Computer Modeling in Ramjet Combustors", AIAA Journal, Vol. 19, No. 12, December 1981.

9 King, M., "Modeling of Effects of Various Aids (Halogens, Metal Coatings, LiF Coatings) on Boron Particle Ignition", JANNAF Paper?

10 Harsha, P.T., and Edelman, R.B., "Computational Hierarchy for the Analysis of Combustion Phenomena in Ramjet Environments", 1984 JANNAF Propulsion Meeting - Specialist Session, Computational Methods, 9 Feb, 1984, New Orleans, LA.

11 Sambamurthi, J.K., "Al2O3 Collection and Sizing from Solid Rocket Motor Plumes", Journal of Propulsion and Power, VOL. 12, NO. 3, May-Jun 1996.

12 Mellor, A.M., "Particulate Matter in the Exhaust of a Boron-Loaded Solid Propellant", AIAA Journal, Vol 9, No. 10, October 1971.

13 Stowe, R.A., et al, "Two Phase Flow Combustion Modelling of a Ducted Rocket" AIAA 2001-3461, 37th AIAA Joint Propulsion Conference, 8 July 2001, Salt Lake City Utah.
14 Buckley, P., et al. "The Use of Swirl for Efficient L/D Combustors", USAF Document 1982.
15 Kim, C.H., El-Leathy, C.M., and Faeth, G.M., "Laminar Soot Processes (LSP) Experiment: Findings from Ground Based Measurements, NASA/CP-2003-212376/REV1
16 Cangialosi, F. et al. "Combustion Reactivity of Unbirned Carbon in Coal Combustion Fly Ashes" Technical University of Bari, Italy.
17 Lewis, D.J, "Numerical Prediction of Ducted Rocket Ramjet Combustor Performance", JANNAF paper 2003-0010G.
18 Turns, S.R., and Faeth, G.M., "A One-Dimensional Model of Carbon-Black Slurry-Fueled Combustor", Journal of Propulsion, Vol 1, No.1, Jan-Feb, 1985.
19 Rodionov, A.V., et al. "Soot Oxidation Modeling in Plumes", AIAA 2001-3858, 37th AIAA Joint Propulsion Conference, 8 July 2001, Salt Lake City Utah.
20 Abbott, S.W., Smoot, L.D., and Schadow, K., "Direct Mixing and Combustion Efficiency Measurements in Ducted, Particle-Laden Jets", AIAA Journal, Vol 12, No. 3, March 1974.
21 Urban, D.L., and Faeth, G.M., "Soot Research in Combustion Science: Introduction and Review of Current Work", AIAA 2001-0322, 39th AIAA Aerospace Sciences Meeting, January 2001, Reno, NV.
22 Waesche, R.H.W.W., Workshop Report - "Ignition and Combustion in Ducted Rocket Combustors" JANNAF Workshop held June 13, 1984, Cincinnati, OH.
23 Carlos G. Rodriguez, C.G.,"ONE-DIMENSIONAL, FINITE-RATE MODEL FOR GAS-TURBINE COMBUSTORS", Dissertation submitted to the Faculty of the Virginia Polytechnic Institute and State University in partial fulfillment of the requirements for the degree of DOCTOR OF PHILOSOPHY in Mechanical Engineering, July 1997.
24 Thomas, M.E. and Leonard, A.D., "AIR-TURBO-ROCKET COMBUSTION", AIAA-95-0813, 33rd Aerospace Sciences Meeting and Exhibit, January 9-12, 1995, Reno, NV.

25 Ristori, A. , and Dufour, E., "Numerical Simulation of Ducted Rocket Motor", AlAA 2001 -3193, 37th AIAA Joint Propulsion Conference, 8 July 2001, Salt Lake City Utah.
26 "Blevins, L.G., ""PARTICULATE MATTER EMITTED FROM AIRCRAFT ENGINES"", AIAA 2003-2764, AIAA/ICAS International Air and Space Symposium and Exposition: The Next 100 Years
Dayton, Ohio, 14 - 17 Jul 2003."
27 "Ogerby, T. ""Literature Review of Turbine Combustor
Modeling and Emissions"", AIAA JOURNAL, VOL. 12, NO. 6, JUNE 1974 "
28 Komar, J.J, and King, M.K., "Diagnostics of Single Particle Boron Combustion", AIAA 80-0070, AlAA 21st Aerospace Sciences Meeting, January 10-13, 1983, Reno, Nevada
29 Vigot, C., Bardelle, L., and Nadaud, L. “Improvement of Boron Combustion in a Solid-Fuel Ramrocket”, AIAA-86-1590, AIAA 22nd Joint Propulsion Conference, June 16-18, 1986, Huntsville, Alabama.
30 Rood, T.J., et al, "Ignition dynamics of boron particles in a shock tube", AIAA-1997-3234, AIAA/ASME/SAE/ASEE Joint Propulsion Conference and Exhibit, 33rd, Seattle, WA, July 6-9, 1997.
31 Odawara, T., et al, “Ignition Characteristics of Boron Particles in Ducted Rockets”, AIAA 2005-4498, 41st AIAA/ASME/SAE/ASEE Joint Propulsion Conference & Exhibit, 10 - 13 July 2005, Tucson, Arizona
32 Gany, A., “Comprehensive Consideration of Boron Combustion in Airbreathing Propulsion”, AIAA 2006-4567, 42nd AIAA/ASME/SAE/ASEE Joint Propulsion Conference & Exhibit, 9 - 12 July 2006, Sacramento, California
33 Schadow, K., "Experimental Investigation of Boron Combustion in Air-Augmented Rockets", AIAA JOURNAL VOL. 7, NO. 10
34 Schadow, K., Study of Gas-Phase Reactions in Particle Laden, Ducted Flows", AIAA JOURNAL VOL. 11, NO. 7
35 Natan, B., and Gany, A., "Ignition and Combustion of Boron Particles in the Flowfield of a Solid Fuel Ramjet", Journal of Propulsion and Power, VOL. 7, NO. 1, JAN.-FEB. 1991, p. 37.

36 Natan, B., and Gany, A., "Combustion Characteristics of a Boron-Fueled Solid Fuel Ramjet with Aft-Burner", JOURNAL OF PROPULSION AND POWER, Vol. 9, No. 5, Sept.-Oct. 1993

37 Mitani, T and Izumikawat, M., "Combustion Efficiencies of Aluminum and Boron in Solid Propellants", Journal of Spacecraft, VOL. 28, NO. 1, JAN.-FEB. 1991, p. 79

38 Schadow, K., "Fuel-Rich Particle-Laden Plume Combustion", AIAA Journal, VOL. 13, NO. 12, DECEMBER 1975, p.1553

39 "Water Flow Tests of a Ducted Rocket Combustor", Virginia Research Associates Final Report to Atlantic Research Corporation, December 1985.

40 King, M.K., "An Explanation for Early Progressivity in DR-PTV Gas Generator Firings", Atlantic Research Corporation Memorandum, April 1981.

41 Dempsey, J.V., et. al., "Ignition and Combustion of Carbon Particles", AIAA Paper AIAA-95-2993, 31st AIAA Joint Propulsion Conference, San Diego CA, July 10-12 1995.

42 FLUENT 6.2 User's Guide, January 2005

43 McAdams, W.H.: "Heat Transmission," 3rd ed. McGraw-Hill Book Co, New York 1954.

44 National Institute of Standards and Technology web site: http://webbook.nist.gov/cgi/cbook.cgi?ID=C630080&Units=SI&Mask=1#Thermo-Gas